Order Number 9303753

Heat flow, thermal structure and thermal evolution of the Paraná Basin, southern Brazil

Hurter, Suzanne Jacqueline, Ph.D.

The University of Michigan, 1992

U·M·I
300 N. Zeeb Rd.
Ann Arbor, MI 48106

HEAT FLOW, THERMAL STRUCTURE AND THERMAL EVOLUTION OF THE PARANÁ BASIN, SOUTHERN BRAZIL

by

Suzanne Jacqueline Hurter

A dissertation submitted in partial fulfillment
of the requirements for the degree of
Doctor of Philosophy
(Geology)
in The University of Michigan
1992

Doctoral Committee:

Professor Henry N. Pollack, Chair
Assistant Professor Michael C. Gurnis
Professor Donald R. Peacor
Associate Professor Ben A. van der Pluijm
Professor John F. Vesecky
Professor Bruce H. Wilkinson

Minha Terra tem palmeiras,
Onde canta o Sabiá;
As aves, que aqui gorjeiam,
Não gorjeiam como lá.

(Gonçalves Dias, 1823-1864)

For Shirley, Tobias and Michel
mother, father and brother

ACKNOWLEDGMENTS

I am most grateful to my thesis advisor Henry Pollack for this important learning experience. Also I wish to thank my committee members, Mike Gurnis, Don Peacor, Ben van der Pluijm, John Vesecky and Bruce Wilkinson, for their assistance. I also thank Linda Abriola who served on my committee during the first three years of this project but was on sabbatical at the time of completion and defense. Our early discussions about fluid flow modeling were much appreciated. The support and encouragement of my parents and my brother throughout this work have been essential.

Many fellow students contributed generously with their time and friendship. I would specially like to mention a few: Todd Wagner for assistance with sample preparation, Weih Teh for assistance with X-ray diffraction techniques and discussions about clay diagenesis, Ed van Hees for helping me in the XRD and SEM laboratories and Art Leibold in helping with SEM. Andy Nyblade and I shared many helpful and enjoyable discussions for which I am grateful.

David S. Chapman, Brian J. McPherson, and Craig Forster gave generously of their time, and provided much assistance and many useful discussions concerning numerical modeling for Chapter IV and Chapter V.

Core samples and most data for this project were obtained from the Brazilian oil company PETROBRÁS. I wish to thank Dr. Milton Romeu Franke and Dr. Antonio Baccoccoli for granting access to the company's archives. The following persons from PETROBRÁS were instrumental in assisting the data and sample collection: Dr. Pedro Zalán, Dr. Hung K. Chang, Dr. Silvio Zenbruski, Dr. Egon Meister, Ms. Frida, Mr. João Bosco and Mr. Magela. I am extremly grateful for their cooperation.

The São Paulo State Foundation for the Support of Research (FAPESP, proc 1063/87) and the Institute of Astronomy and Geophysics of the University of São Paulo provided the principal financial support for this program; additional funding was provided by the Scott Turner Fund and the Department of Geological Sciences of the University of Michigan.

TABLE OF CONTENTS

LIST OF FIGURES

Figure

LIST OF TABLES

Table

APPENDICES

Appendix

CHAPTER I

INTRODUCTION

In this dissertation I investigate the heat flow, thermal structure and thermal evolution of the Paraná Basin in southern Brazil. The observational bases for this study are temperature measurements in deep exploration wells, thermal conductivity measurements on core samples, regional and local stratigraphic data, and characteristics of clay minerals in the sediments. Theoretical and computational aspects of this study address the temperature evolution of basin sediments due both to subsidence and to multiple intruding igneous bodies. In this introduction, I begin by presenting briefly the principal geologic and tectonic aspects of this basin, then follow with a summary of the general structure of the dissertation.

1. THE PARANÁ BASIN: AN OVERVIEW

The Paraná Basin is a large intracratonic basin in southeastern South America covering an area of about 1,400,000 km^2, most of which is in Brazil, but with extension also into Argentina, Paraguay and Uruguay. The location and extent of the Paraná Basin is depicted in the simplified geological map of Figure 2.1. The north-south extent in the Brazilian territory is about 2,000 km, with the major axis of the basin lying in a NNE direction approximately parallel to the Paraná River. The basin contains up to five kilometers of Paleozoic and Mesozoic predominantly clastic sediments in its thickest central part. The depositional history of this Gondwana basin initiated in the Ordovician and came effectively to completion in the Cretaceous following a large volcanic event related to the opening of the South Atlantic, which extruded flood basalts over most of the basin surface up to 1.7 km thick. The basalt today covers about 75% of the basin surface. Associated with this extrusive event ubiquitous sill intrusion occurred, comprising up to 30% of the stratigraphic column in some localities (Zalán et al., 1986). The following geological summary derives from a recent review and discussion of the geological characteristics and the stratigraphic evolution of the Paraná Basin by Zalán et al. (1991) and the references therein.

This basin developed within the Gondwana supercontinent. The crystalline basement beneath the basin is formed of a mosaic of Precambrian nuclei welded together by mobile belts, and has been affected by the Brasiliano orogenic cycle (corresponding to the Pan-African orogeny in Africa). This tectonomagmatic event represents one aspect of the assembly of

Gondwana; it began during the Late Proterozoic, and extended into the Early Ordovician (Cordani et al., 1984; Neves and Cordani, 1991; Zalán et al., 1991). The later Paleozoic tectonic and sedimentary evolution of the Paraná Basin has been strongly influenced by the reactivation of old preexisting basement faults. For the sedimentary contents of the basin we adopt the stratigraphic divisions proposed by Zalán et al. (1991): the stratigraphic column is divided informally into five depositional sequences: Silurian, Devonian, Permo-Carboniferous, Triassic and Juro-Cretaceous Sequences, each bounded by basin scale unconformities. These sequences are named after the period in which most of the sedimentation took place. The Silurian sequence for example also contains sediments of Late Ordovician to Early Devonian in age (Zalán et al., 1991).

The sediments in the Paraná Basin are predominantly siliciclastic. The three Paleozoic sequences record almost complete transgressive-regressive cycles. The last cycle (Permo-Carboniferous sequence) marks the deposition of a characteristic succession of mostly non-marine strata recognized in all other Gondwana basins. Following the Permo-Carboniferous sequence, sedimentation in the Mesozoic and thereafter was entirely of continental character. The Triassic alternating lacustrine, fluvial and eolian sediments give way to extensive Jurassic eolian sand dunes. This desert was covered by voluminous and extensive basalt flows (Serra Geral Formation) dated as Late Jurassic to Early Cretaceous with a peak at 130 Ma. These flows marked the effective end of the depositional history of the Paraná Basin; isolated exceptions include a thin cover of Late Cretaceous sediments deposited in the northern half of the basin, and Tertiary alluvial sediments of only local significance.

The Serra Geral igneous event heralded the opening of the South Atlantic Ocean. The entire southeastern margin of the Paraná Basin was uplifted along a trend inherited from the Brasiliano cycle, forming the Serra do Mar coastal range. According to Zalán et al. (1991) this uplift began in the Upper Cretaceous, with several recurrent pulses in the Tertiary. The resulting topography imparts elevations of 800 m to 1,000 m along the southeastern basin margin, decreasing to 200 m towards the northwest, west and south.

2. STRUCTURE OF THE DISSERTATION

Four chapters form the core of this dissertation. Chapter II describes the assembled thermal and stratigraphic data and presents new heat flow determinations for 56 sites within the Paraná Basin. These data indicate that heat flow in the areas covered by the Serra Geral flood basalts is lower and more uniform than in those areas where the basalt cover is absent, i.e. around the eastern basin margin. In Chapter III several possible causes to explain the heat flow pattern in the Paraná Basin are investigated: lateral thermal conductivity variations in the basin, variable basement heat flow related to subcrustal heterogeneities (radiogenic heat production contrasts, underplating), thermal effects of igneous activity and of subsurface fluid flow. The subsurface

temperature field in this basin then is studied in detail in Chapter IV. A least squares inversion applied to the temperature data yields geothermal gradients in individual formations and regional temperature variations that express departure from the average conditions. Possible sources of temperature variations include regionally varying heat flow and subsurface fluid flow . In Chapter V, I address the thermal evolution of the sedimentary fill. Two time scales play a role in the thermal evolution of this material: the long term subsidence, uplift and erosional history relates to the effects of the geothermal gradient over time periods of the order of hundreds of millions of years, and a shorter term component of the thermal history is associated with igneous activity, such as the extrusion of the Mesozoic Serra Geral flood basalts and the intrusion of sills, with a time scale shorter than one million years. Thermal aspects of the depositional and uplift history of the sedimentary section penetrated by boreholes in different regions of the basin is computed and compared with indicators of paleothermal conditions, such as illite crystallinity and the ratio of mixed-layer illite/smectite.

In summary, this dissertation presents results of the analysis of the present-day thermal field in the Paraná Basin in Chapter II, Chapter III and Chapter IV. Studies on the thermal evolution of the sediments and igneous rocks within the basin appear in Chapter V; a concluding Chapter VI summarizes the dissertation.

CHAPTER II

TERRESTRIAL HEAT FLOW IN THE PARANÁ BASIN, SOUTHERN BRAZIL

ABSTRACT

We present 56 new heat flow values from the region of the intracratonic Paraná Basin in southeastern South America.This large basin is filled with up to 5 km of Paleozoic and Mesozoic sediments. In the Jurassic-Cretaceous a great igneous event capped most of the basin surface with flood basalts up to 1,700 m thick and intruded the sediments with ubiquitous sills. Geothermal gradients computed using 187 Bottom Hole Temperature values from 79 deep exploration boreholes range typically from 20 K km^{-1} to 30 K km^{-1} with the lower gradients generally located within the central part of the basin. Thermal conductivities were determined on 247 core samples. The mean thermal conductivity of the section encountered by the boreholes decreases from 3.0 W $m^{-1}K^{-1}$ at the eastern basin margin to 2.0 W $m^{-1}K^{-1}$ in its central part; this variation is related to the thickening of the basalt cap from the basin margin to the center. Surface heat flow values for the 56 sites range from 40 mW m^{-2} to 75 mW m^{-2}, with larger and more variable values (50-70 mW m^{-2}) occurring along the eastern margin of the basin in the region devoid of basalt cover. The heat flow in the central part of the basin (40-50 mW m^{-2}) is less than that on the basin margin by about 15 %, and is more uniform. A comparison of the heat flow pattern in the Paraná Basin with other interior cratonic basins in the world, especially those with associated flood basalts (Deccan , Karoo) shows marked similarities.

1. INTRODUCTION

Heat flow studies provide information on the thermal state of the Earth's crust and lithosphere, and serve as important constraints in the modeling of tectonic processes such as rifting, uplift and the initiation of basin subsidence. In particular, the study of the thermal structure and thermal evolution of sedimentary basins is of practical significance because of their relevance to the production and maturation of hydrocarbons. Uyeda and Watanabe (1970) provided the first estimate of a geothermal gradient in the Paraná Basin, and Meister (1973) followed with a compilation of numerous geothermal gradients. Both studies made use of Bottom Hole Temperatures (BHTs) in deep petroleum exploration wells. Since these early investigations, geothermal characteristics of the Paraná Basin including a few heat flow measurements have

been addressed in part by Vitorello (1978), Vitorello et al. (1978), Hamza et al. (1978), Vitorello and Pollack (1980), Vitorello et al. (1980), Hamza and Eston (1983) and Santos (1986). Measurements in shallow boreholes (300 m depth) formed the basis for most of these later studies. The conventional method for determining heat flow (i.e. direct temperature measurements as a function of depth combined with thermal conductivity measurements from cores or cuttings) was applied by Vitorello (1978) and Santos (1986) to sites in the Paraná Basin. In the absence of appropriate boreholes for direct temperature measurements, other researchers have attempted to use alternative methods to estimate heat flow such as the 'aquifer method' (Hamza and Eston, 1983: Santos, 1986) and the 'geochemical thermometer method' (Hurter et al., 1983; Hurter, 1987, 1988). We exclude heat flow data obtained from such alternative methods in the regional interpretations presented in this dissertation due to the poor quality of the resulting heat flow values, as pointed out by the investigators in these studies.

The results we present here represent the first comprehensive study of the thermal structure of the Paraná Basin both in terms of amount of data and geographic and depth coverage. We have been able to compile thermal information from 79 deep boreholes in 64 sites within the basin, making use of Bottom Hole Temperature (BHT) measurements and other geological information assembled from the Brazilian oil company PETROBRÁS. Assessment of the data coherence allowed the selection of 56 sites for computing geothermal gradients and heat flow. A summary of the geological characteristics of the Paraná Basin was presented in Chapter I. Here, we begin by describing the data and the procedures to obtain geothermal gradients, thermal conductivities and heat flow. We then compare the heat flow pattern in the Paraná Basin to heat flow in other intracratonic basins, with special focus towards those that have been the locus of continental flood basalt events.

2. DATA DESCRIPTION

The data necessary for the determination of heat flow include stratigraphy, temperature and conductivity observations. We have assembled stratigraphic information on 107 boreholes, BHT measurements from 79 boreholes in 64 sites, and some 247 core samples from 28 boreholes for thermal conductivity measurements. The general characteristics of this data set are summarized in Table 2.1 and the geographic distribution of boreholes yielding thermal information and conductivity samples is displayed in Figure 2.1.

TABLE 2.1. Characterization of the Data Set

Number	Formation Name	Code	Mean Thickness (m)	Number of wells bottoming	Number of wells penetrating	Number of BHTs	Number of conductivity samples
1	Bauru	Ba	24	-	18		-
2	Serra Geral	SG	451	-	46		7
3	sills	sill	240	-	67		5
4	Botucatu	Bo	165	-	52	5	5
5	Rio do Rasto	RR	283	-	56	12	34
6	Teresina	Te	237	1	68	11	27
7	Serra Alta	SA	87	-	64	4	11
8	Irati	Ir	45	-	72	9	10
9	Palermo	Pa	76	-	70	5	12
10	Rio Bonito	RB	138	3	70	14	30
11	Itarare	It	641	21	72	59	78
12	Ponta Grossa	PG	112	6	30	13	12
13	Furnas	Fu	109	16	31	23	15
14	basement	bas	12	30	30	32	-

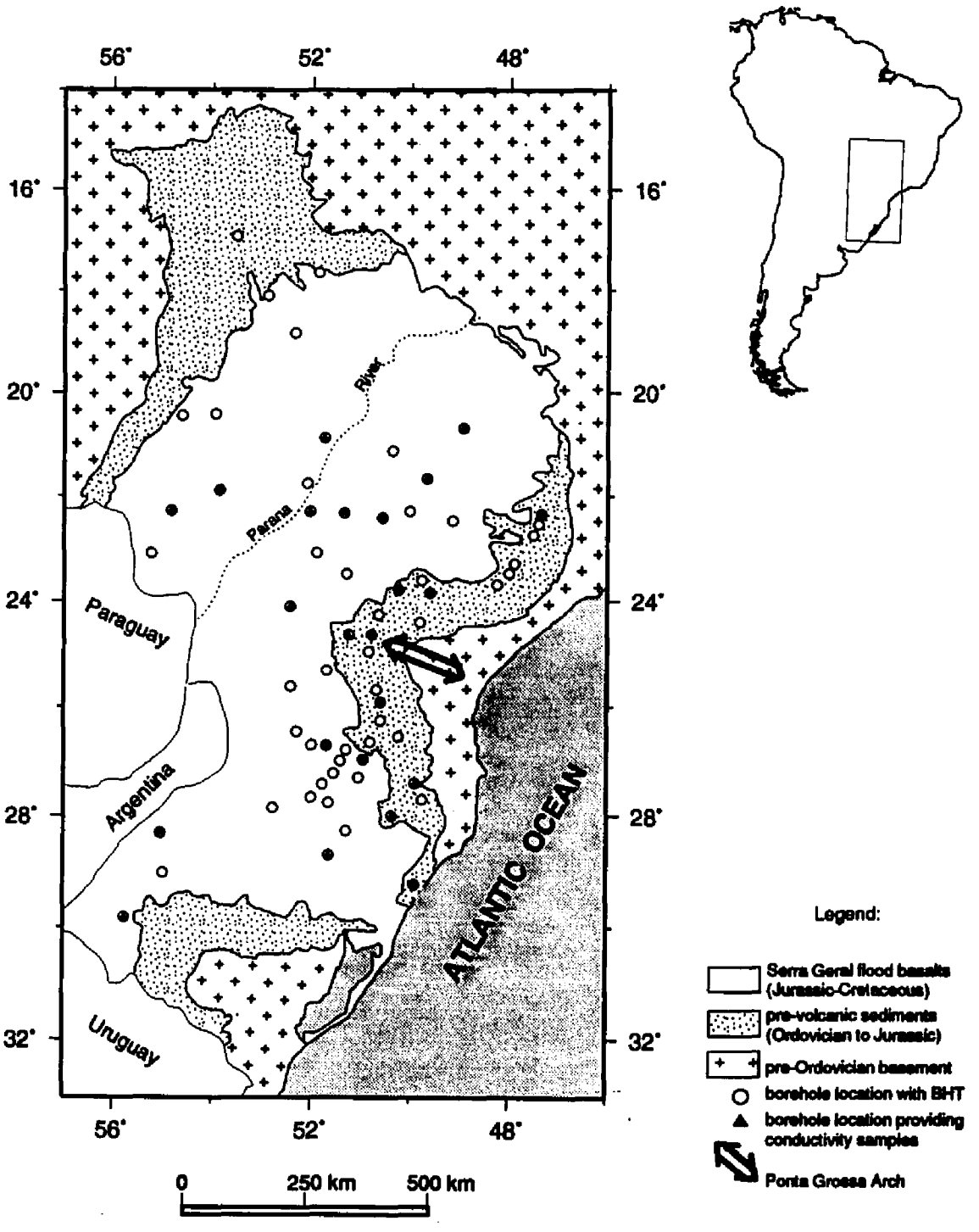

Figure 2.1 Index map of South America (upper right); the box refers to the simplified geologic map (at left) of the Paraná Basin in the Brazilian territory. The 79 boreholes used in this study are distributed among the 64 sites displayed. The Paraná River roughly overlies the basin's major axis, where the flood basalts are thickest. The arrow indicates the direction of the axis of the Ponta Grossa Arch which is perpendicular to the Serra do Mar, a mountain range parallel to the coast.

2.1 Stratigraphy

Fourteen units were selected to represent the stratigraphy of the Paraná Basin, as shown in Table 2.1 and on the stratigraphic column in Figure 2.2. Most boreholes used in this study penetrate one or more sill intrusions with thicknesses varying from a few meters to hundreds of meters. Therefore we have included a separate unit in the stratigraphic column at each site comprising the accumulated sill thickness penetrated. Formal formations and groups plus the sill unit hereafter will all be informally referred to as 'formations'. We have also represented the principal lithologies in each formation based on the information from Zalán et al. (1991). The sedimentary rocks in the Paraná Basin consist predominantly of siliciclastic deposits: sandstones, siltstones and shales. Carbonates are of only local significance in the Irati formation. In Figure 2.2 these formations are displayed to scale by their mean thickness as penetrated by the 79 boreholes included in this study. How well the formations are represented in the data set can be assessed by information provided in Table 2.1, such as the number of wells passing through or bottoming in a given formation. Most boreholes penetrate into the deeper parts of the stratigraphic section, with more than 40 penetrating the complete section down to the Furnas formation and 30 reaching the basement. This indicates a good vertical sampling of the Paraná Basin. The geographic representation of a formation can also be estimated by the number of wells in which the formation is present. For example, the Baurú formation exists only in the northern half of the basin; this limited extent is implicitly expressed in the smaller number of boreholes in which the Baurú formation is present.

2.2 Bottom-hole temperatures

The Bottom Hole Temperature (BHT) data set as originally assembled comprises 187 values in 79 boreholes. Over 30 boreholes individually contain three or more BHT determinations at various depths, taken as the drilling reached those depths. In eight municipalities several boreholes cluster closely together. At these locations data from individual boreholes have been merged and treated as a single site, yielding BHT data sets for 64 sites. Eight among these 64 sites were later excluded on the basis of the large standard deviations resulting from the computation of the geothermal gradient at these sites. The remaining 56 sites are retained for heat flow determinations. They are located mainly in the eastern part of the Paraná Basin, with fewer in the central part and western border (see Figure 2.1). Table 2.1 and Figure 2.2 also show the number of BHTs measured in each formation. Generally, thick and geographically extensive formations contain more BHT measurements: the Itararé formation with average thickness of 641 m and found throughout the basin contains 59 temperature measurements, the most of any formation.

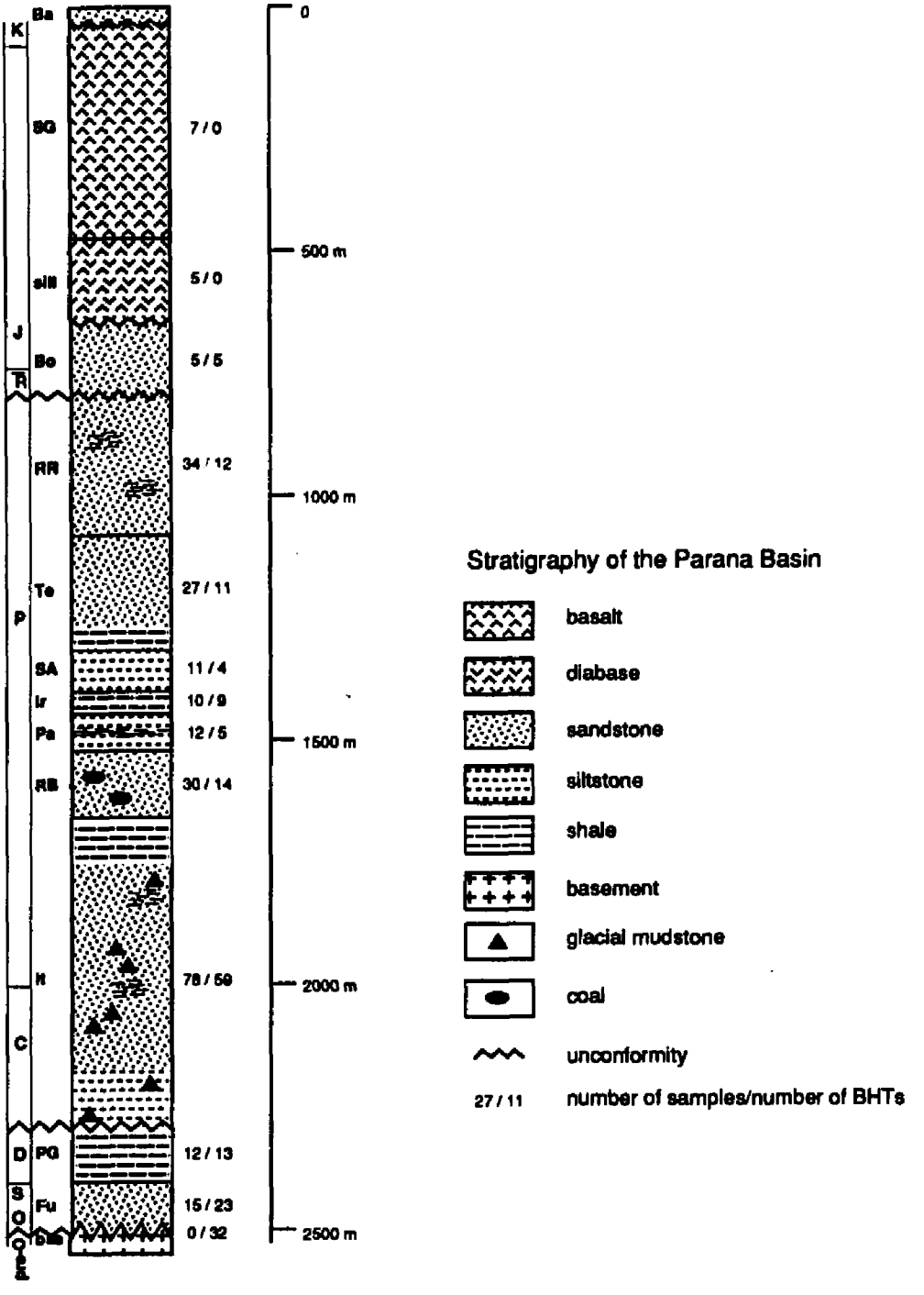

Figure 2.2 Representative stratigraphic column for the Paraná Basin. Formation thicknesses correspond to mean thickness penetrated by the boreholes. The formations displayed are: Ba=Baurú, SG=Serra Geral, Bo=Botucatú, RR=Rio do Rasto, Te=Teresina, SA=Serra Alta, Ir=Irati, Pa=Palermo, RB=Rio Bonito, It=Itararé, PG=Ponta Grossa, Fu=Furnas, bas=basement. Sills are shown collectively beneath the basalt but are distributed throughout the section. Sedimentary lithologies comprise mostly clastic sandstones, siltstones and shales. The number of BHT measurements and core samples from each formation are indicated.

2.2.1 Temperature corrections

BHTs are generally measured during geophysical logging, soon after drilling pauses or ceases. They are affected by the circulation of drilling fluids, and typically are lower than the undisturbed formation temperature. Several methods have been proposed to correct BHTs for this kind of disturbance. There exists an extensive literature on the subject of drilling thermal perturbations and correction methods: we mention the reviews by Luheshi (1983), Shen and Beck (1986) and Cao et al. (1988). Hermanrud et al. (1990) show in a comparison of several methods that more elaborate methods do not result necessarily in improved estimates of undisturbed rock temperatures. The choice of application of a specific method is often constrained by the amount of additional information available, such as mud circulation times, shut-in times (time between cessation of drilling fluid circulation and the time of measurement), and temperature of drilling fluid, among others.

The Horner-plot type correction (Bullard, 1947) is generally acknowledged to be the best because it is based on the physics of the thermal perturbation. The temperature disturbance caused by the circulating drilling fluid is described as a line source of (negative) heat into a homogeneous medium. Its application requires the mud circulation time and shut-in time, and several BHT determinations at the same depth at different times. Unfortunately, most BHT data sets seldom contain enough information to allow the application of such a method. At the other end of the spectrum are empirical corrections such as the AAPG method (AAPG,1976), which is based only on the depth of measurement. This correction is based on a comparison between BHTs and equilibrium temperatures. Its applicability has been extended by the inclusion of a regional correction factor proposed by Speece et al. (1985) that enables the application of this method in different regions from those in which the method was calibrated. Deming and Chapman (1988) devised an 'improved' AAPG temperature correction method (Depth-Time method) based on depth and typical ancillary information such as shut-in time.

Our data set is no exception to the usual paucity of information that would enable the application of the more sophisticated methods: only 11 boreholes allow the Horner method to be applied, and in only 18 boreholes could the Depth-Time method be used. Corrections must be applied uniformly over the data set, i.e. the same method for all BHTs must be used. Otherwise different methods applied to different subsets of data might introduce 'anomalies' due to the mixture of methods. Therefore, BHTs in this study were corrected by the AAPG gradient correction method as described in AAPG (1976), including the regional correction factor of Speece et al. (1985). This method was applied to the 187 BHTs in 64 sites in the Paraná Basin, resulting in corrected temperature values and a mean geothermal gradient for each site.

Assessment of the uncertainty to be attributed to the BHT correction procedure is difficult, but we have attempted to determine the range of correction magnitude by comparing results obtained from the application of different correction methods upon a small subset of our BHT data that allows the application of the Horner-plot type and Depth-Time correction methods, in addition to the AAPG method. This subset included 25 sets of BHTs in 11 boreholes. We interpret the spread in results to be an indication of the uncertainty introduced into the analysis by choosing any particular correction procedure.

The comparison of the results obtained by employing different methods reveals that the AAPG method yields the largest corrections and the Depth-Time method the smallest, at least as applied to this particular subset of BHT data. The AAPG method therefore results in the highest corrected temperatures and gradients. The Depth-Time method yields temperatures and gradients slightly below the Horner corrected values. If the Horner corrected temperatures are assumed to approximate undisturbed rock temperatures best, the choice of the AAPG method results in overestimating geothermal gradients by about 10 % on average, while the Depth-Time method underestimates undisturbed geothermal gradients by about 5 % on average. However we caution against attributing too much significance to these results, obtained from this very sparse data set, which we cannot assume to be representative. What can be extracted from this simple and limited comparison of BHT correction methods is that a choice of any given method can introduce up to 10 % uncertainty in gradients, and that at least in the Paraná Basin the AAPG correction results in corrected temperatures systematically higher than those from other methods. Therefore, the possibility exists that there is a slight upward bias to the heat flow values we report, but no effect on the regional patterns of heat flow variability. Regional patterns from corrected BHTs can be seen equally well from uncorrected BHTs.

To summarize, BHTs in this study have been corrected using the AAPG method with a regional correction factor. Figure 2.3 exhibits both uncorrected and corrected BHTs as a function of depth of measurement. The corrected temperatures range from 30 °C to 160 °C over a depth range of 100 m to 5,500 m. At any given depth, the spread in temperatures is typically 30 - 40 °C. A least squares line through these data indicates a slope of 18.5 K km^{-1} for the uncorrected and 22.4 K km^{-1} for the corrected temperatures, an increase of about 20 %. Individual uncorrected and corrected BHTs are listed in Appendix A.

2.2.2 Geothermal gradients

In order to compute local geothermal gradients at individual sites from corrected BHTs, we have included a surface temperature in the data set at each site. As a proxy for ground surface temperatures we use mean annual air temperatures extracted from climatic maps given by Setzer (1966) and Pereira (1969). Mean annual air temperatures vary between 16 °C and 22 °C over the

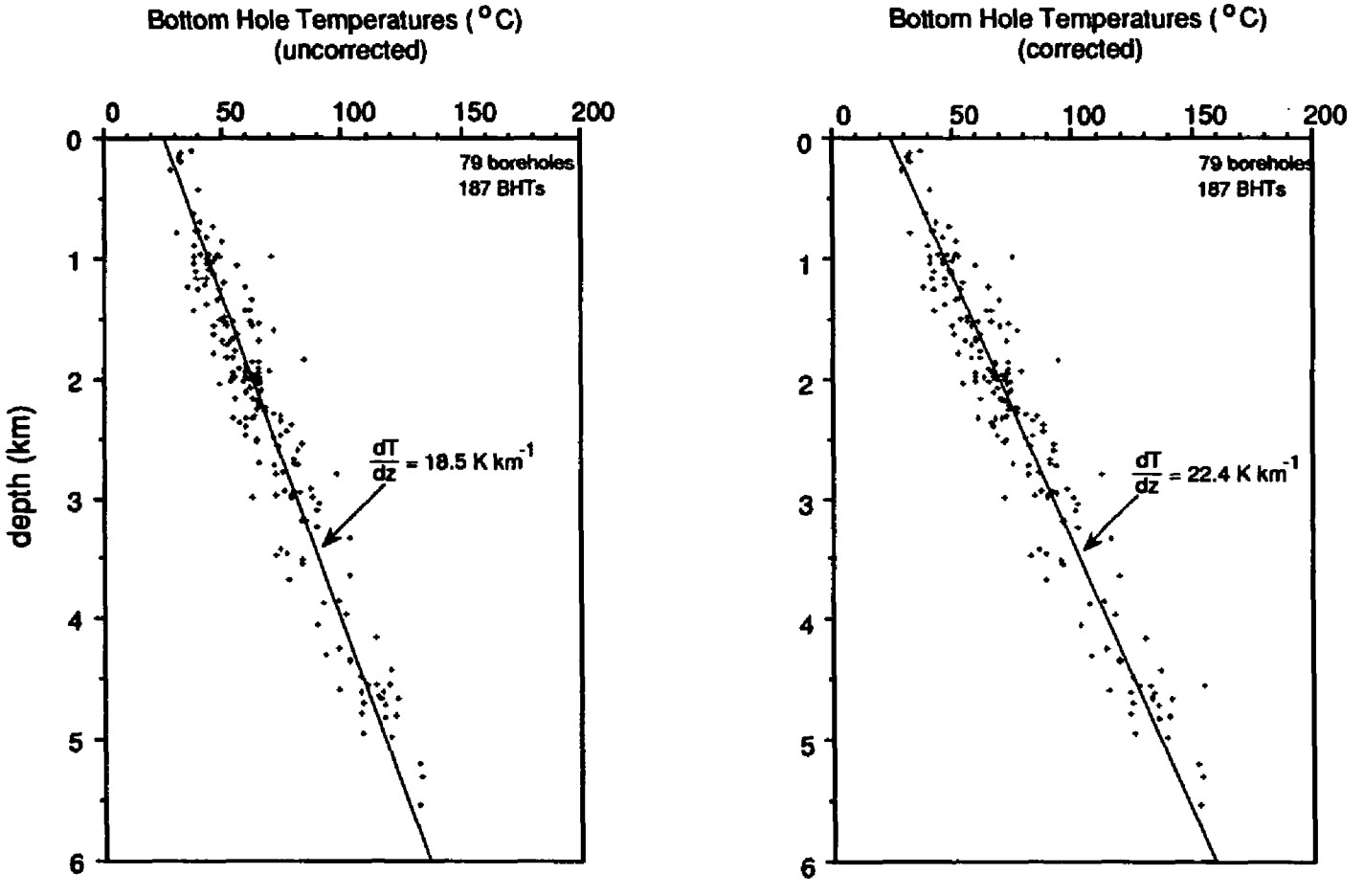

Figure 2.3 Uncorrected and AAPG corrected BHT data as a function of depth of measurement (187 values from 79 boreholes). Lines are least squares fit to the data.

area of the Paraná Basin (see Table 2.3). When two or more BHTs (plus a surface temperature) are available in a borehole, the mean geothermal gradient is computed by a least-squares procedure, along with an estimate of the standard deviation to the mean geothermal gradient. In 18 cases only one BHT and the surface temperature were available, and therefore no estimate of the standard deviation can be made.

The mean geothermal gradient for each borehole is listed in Table 2.3, and their distribution by magnitude shown in Figure 2.4. Most values fall between 20 K km^{-1} and 30 K km^{-1} with a mean near 25 K km^{-1}. Figure 2.4 shows in increasing order each geothermal gradient bounded by its estimated standard deviation. Values without a standard deviation bar refer to those boreholes with only one BHT measurement and a surface temperature. On average, standard deviations of the gradient are of the order of 10 % of the gradient. We have excluded from the subsequent analysis eight sites with standard deviations of the mean geothermal gradient of 5 K km^{-1} or larger, identified with arrows in Figure 2.4. A deviation of 5 K km^{-1} represents about 20 % of the mean of all geothermal gradients. Deviations in geothermal gradients encompass the expression of local conditions and/or measurement errors. In the absence of detailed knowledge on local conditions and measurement procedures, we have chosen to eliminate these data with large deviations prior to developing general regional interpretations. The rejection of these data reduces the number of sites at which heat flow is calculated from 64 to 56.

2.3 Thermal conductivity

Figure 2.1 displays the geographic distribution of the 28 boreholes from which 247 core samples were drawn for thermal conductivity measurements. Other sampling characteristics with respect to (a) depth of origin, (b) stratigraphic unit and (c) lithology are shown in Figure 2.5. The thickest and most extensive formations (such as the Itararé Formation) and the most common rock types (siltstones) are represented by a larger number of samples. Most samples are clastic sediments: sandstones, siltstones and shales, although a few halite and coal samples were included in the collection. Igneous rock samples consist of basalt (Serra Geral formation) and diabase from the sill intrusions within the sediments.

The preparation of samples for thermal conductivity determinations in the laboratory included cutting and polishing cylindrical discs 1.0-1.5 cm thick from the core samples and saturating them in water under vacuum prior to the measurement. The thermal conductivities of the 247 prepared rock discs were measured using a divided bar apparatus (Birch, 1950). Measurements on 104 samples were repeated from 1 to 5 times in order to establish the repeatability of these measurements. On average the deviation is 3.9 ± 0.8 % (95 % confidence interval) of the mean thermal conductivity. We believe most of this variability arises from difficulties

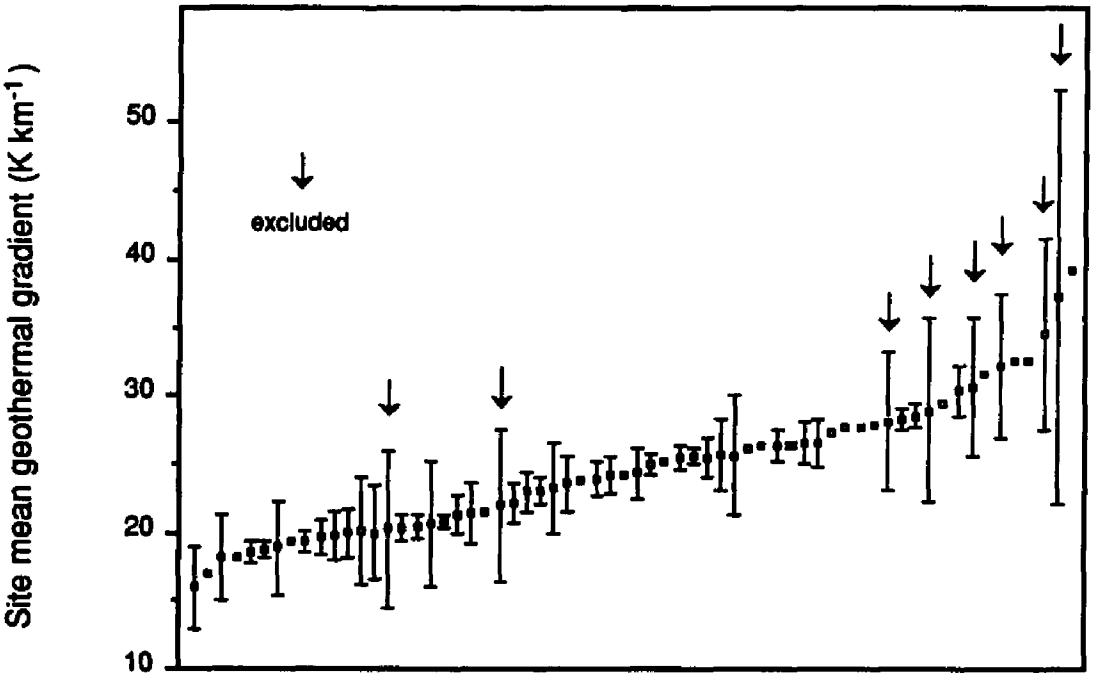

Figure 2.4 Mean geothermal gradients displayed in increasing value from left to right. Bars are the standard deviation of the mean. Points without bars are based on only two temperatures, one BHT and a surface temperature, and thus a standard deviation cannot be determined. Arrows indicate gradients excluded from subsequent analyses because of large standard deviation.

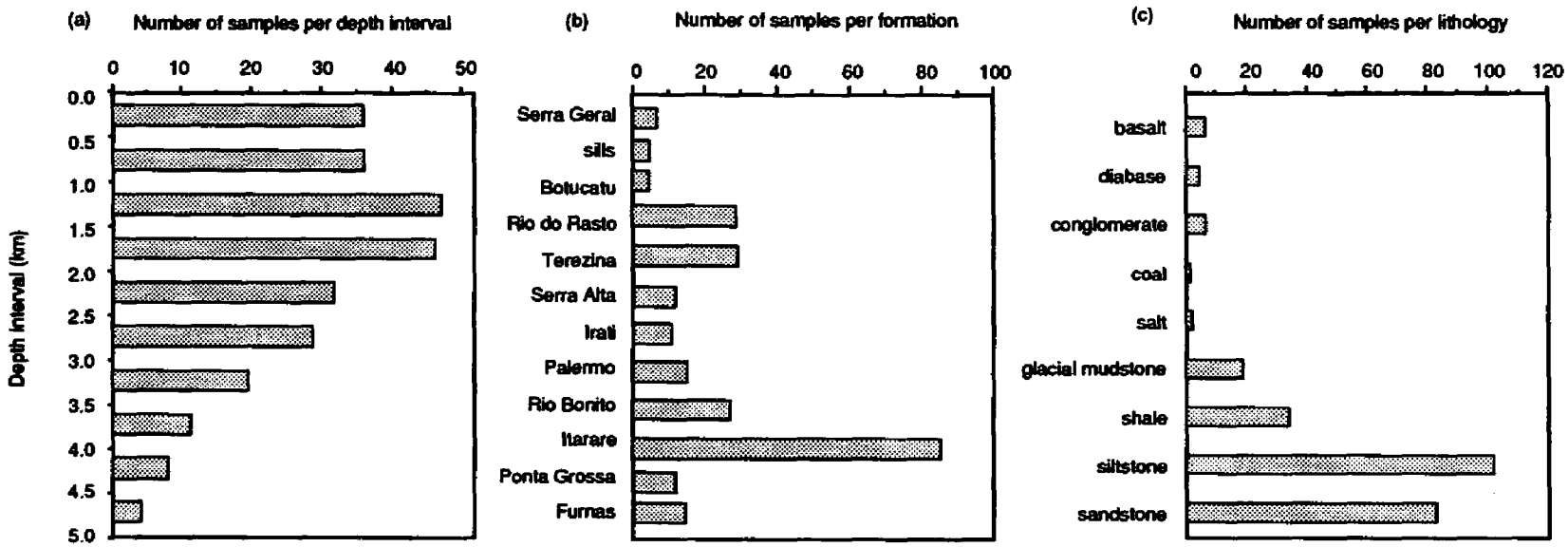

Figure 2.5 General characteristics of thermal conductivity samples: (a) distribution of depth of sample, (b) distribution of samples among stratigraphic units and (c) distribution by lithology.

in attaining repeatedly the same saturation level. Repeated measurements of fused silica standards with zero porosity yielded thermal conductivity values within 2 %. We assess the accuracy at 2 % and repeatability at 4 % for the thermal conductivity measurements of the rock samples. The Appendix B contains the individual thermal conductivity measurements and related information about each sample.

Table 2.2 shows the mean thermal conductivity for each formation and lithology, along with the respective standard errors of the mean and the number of samples used in determining the mean. Figure 2.6 depicts the distribution of thermal conductivities obtained, including mean values for each formation and lithology, along with the standard error of the mean. Individual sample thermal conductivities lie between 0.33 - 6.26 $W\,m^{-1}K^{-1}$. The lowest value corresponds to a coal sample from the Rio Bonito formation and the maximum value to a sandstone sample from the Furnas formation. The standard errors of the mean thermal conductivity for each of the formations reflect lithologic heterogeneity within each formation. The Serra Geral formation comprising the flood basalts shows great uniformity ($k=1.86 \pm 0.10\ W\,m^{-1}K^{-1}$) while other units such as the Palermo, Rio Bonito, and Ponta Grossa formations appear more heterogeneous. As expected, the mean thermal conductivities for lithologic types have smaller relative standard errors than the means for formations. The standard error represents less than 5 % of the mean for every lithology, whereas in the formation groupings, with lithologic variability, the standard error is larger. The highest relative standard error for formations is 15 % for the Palermo formation.

For each borehole a mean geometric thermal conductivity $(\bar{k})$ was computed based on the total thermal resistance of the stratigraphic section penetrated by it. This is expressed as:

$$\bar{k} = z_t \left\{ \sum_{i=1}^{n} \left[\frac{z_i}{k_i} \right] \right\}^{-1} \qquad (2.1)$$

where z_i/k_i is the thermal resistance of the i-th formation of thickness z_i and conductivity k_i, and z_t is the total thickness of rock penetrated by the borehole.

Thermal conductivity of common rock types generally decreases with increasing temperature. We have corrected the thermal conductivities for the effect of elevated temperatures in deep wells, before computing the total thermal resistance at each site. Over the temperature range of interest thermal conductivity varies approximately with the reciprocal of temperature, according to the expression $k(T) = k_{20}\,[293/(T+273)]$, where all numbers are in °C (Chapman et al., 1984). Within the stratigraphic column at each site, the mean thermal conductivity of each formation was corrected to the temperature at the mean depth of occurrence. This procedure was also applied to each individual sill in its proper depth interval of occurrence. The

TABLE 2.2. Mean Thermal conductivity

Number	Formations	Number of samples	Thermal conductivity ($W m^{-1} K^{-1}$)	Standard error of the mean ($W m^{-1} K^{-1}$)
1	Bauru	-	-	-
2	Serra Geral	7	1.86	0.10
3	sills	5	2.19	0.12
4	Botucatu	5	2.76	0.29
5	Rio do Rasto	34	2.27	0.09
6	Teresina	11	2.04	0.14
7	Serra Alta	27	2.33	0.12
8	Irati	10	2.20	0.34
9	Palermo	12	2.62	0.38
10	Rio Bonito	30	2.87	0.16
11	Itarare	78	3.37	0.12
12	Ponta Grossa	12	2.57	0.26
13	Furnas	15	5.15	0.33
14	basement	-	-	-
	Lithology			
1	basalt	7	1.86	0.10
2	conglomerate	6	4.32	0.23
3	coal	1	0.33	-
4	diabase	5	2.19	0.12
5	glacial mudstone	19	3.17	0.15
6	salt	2	4.87	-
7	sandstone	74	3.94	0.14
8	siltstone	102	2.39	0.06
9	shale	30	1.93	0.10

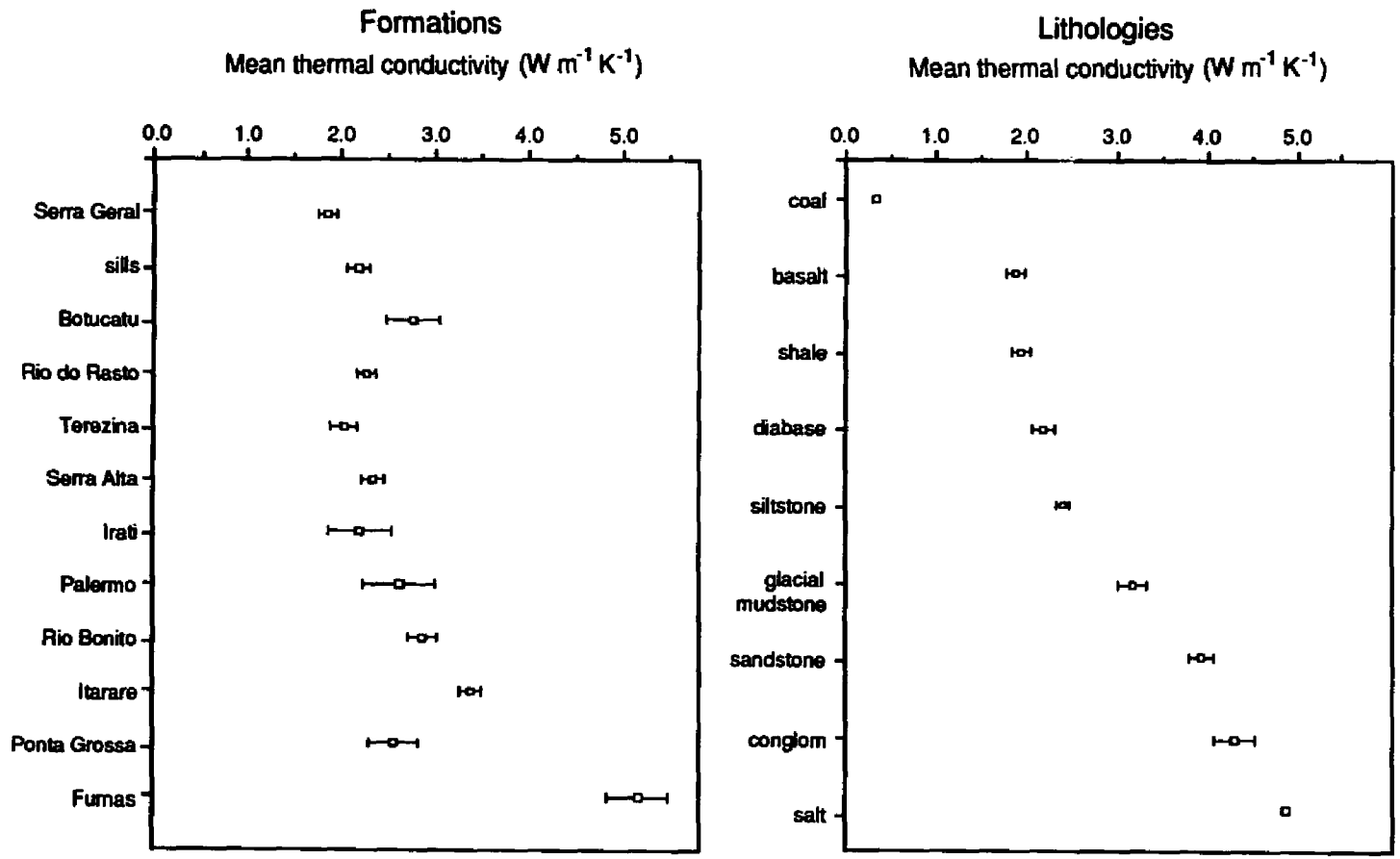

Figure 2.6 Arithmetic mean thermal conductivity of formations and lithologies. Bars represent standard error of the mean. Thermal conductivities refer to laboratory conditions.

temperature at depth was computed taking the surface temperature at the respective site and assuming a mean geothermal gradient of 25 K km^{-1} for the Paraná Basin.

Unfortunately no samples were available for the Baurú formation and the basement. We adopted for the basement a value of 3.0 W $m^{-1}K^{-1}$, and as the Baurú formation is composed mainly of fluvial sandstones we used the same mean thermal conductivity as determined for the Botucatú formation.

We have computed $\bar{k}$ with both formation and lithologic averages. The choice of lithologic or formation units makes no significant difference in computing the mean thermal conductivity of the stratigraphic section for each borehole; this difference is less than the standard deviation of any mean thermal conductivity computed for formations or lithologies for any given borehole.

3. REGIONAL THERMAL PATTERNS

In this section we describe and present maps displaying the general patterns of geographic variability of the mean geothermal gradients, mean thermal conductivity and heat flow .

3.1 Geothermal gradients

The map in Figure 2.7 displays each geothermal gradient at its geographic location. Sites located along the central part of the basin appear to exhibit lower mean geothermal gradients, usually in the range of 19 to 23 K km^{-1}. Near the margin of the basalt cap and on the exposed sedimentary cover along the eastern basin margin, geothermal gradients show greater variability, and greater frequency of values in the range 26 to 28 K km^{-1}.

3.2 Mean thermal conductivity

The map in Figure 2.8 displays geometric mean thermal conductivity for each site. The values vary within the range 1.8 to 3.1 W $m^{-1}K^{-1}$. A decrease in thermal conductivity is observed from the eastern margin of the Paraná Basin towards its center. The basalts of the Serra Geral formation are the significant stratigraphic unit with the lowest conductivity in the basin (see Table 2.2). This unit has a thickness that ranges from 300 m to 1,700 m from the margin to the central part of the basin, situated approximately at 22 °S, 52 °W. This distribution means that the contribution of this unit in the mean thermal conductivity of the stratigraphic column increases also from the margin to the center, decreasing the mean thermal conductivity in that direction. The geographic variation in mean thermal conductivity shown on the map of Figure 2.8 can mostly be attributed to the presence and variation in thickness of the Serra Geral basalt cover, with theregion of lowest mean thermal conductivity coinciding with the location of maximum basalt thickness.

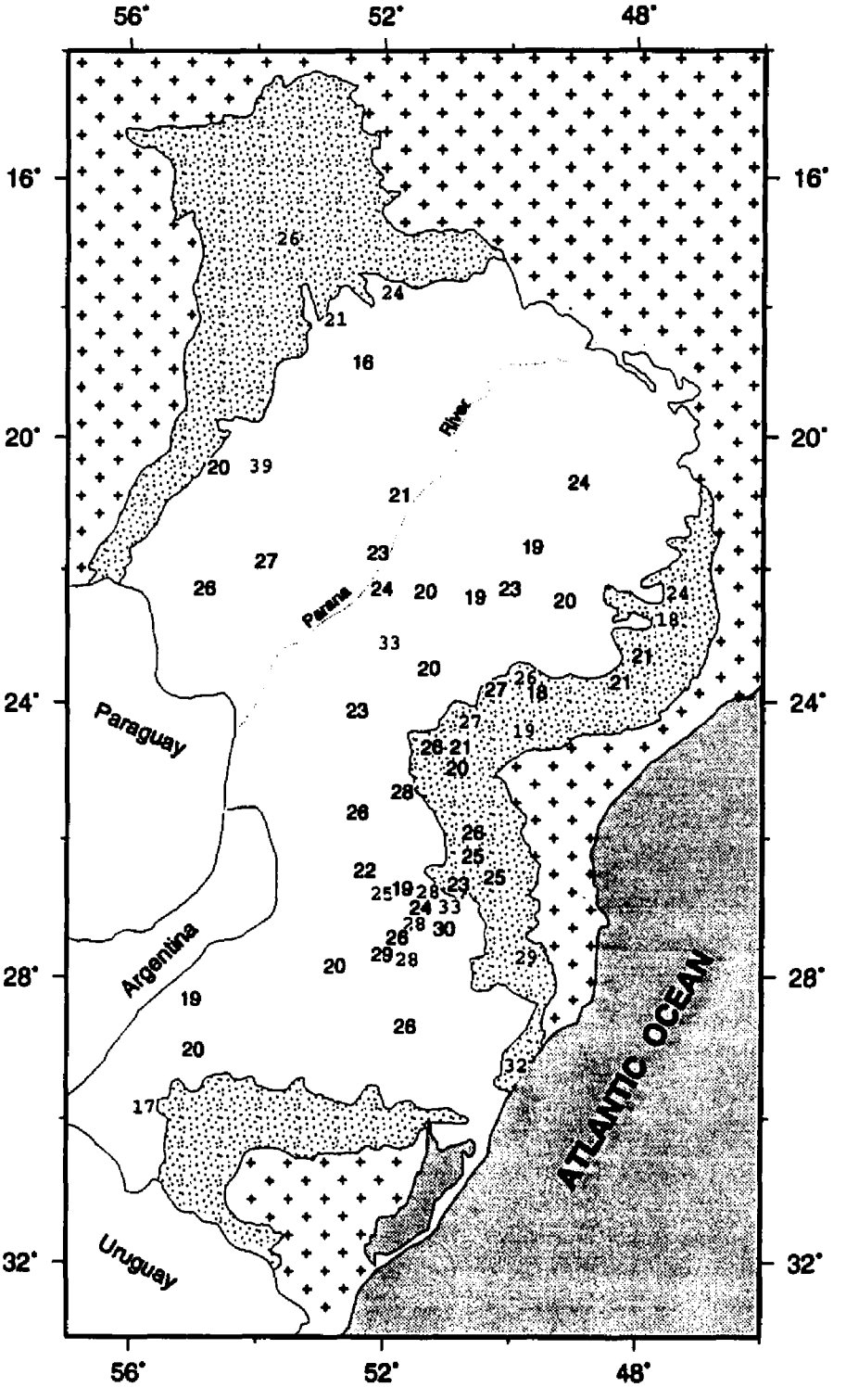

Figure 2.7 Map of the mean geothermal gradient at each site. Units are K km^{-1}. Numbers in light characters refer to geothermal gradients without a standard deviation estimate. Map patterns are as shown in Figure 2.1.

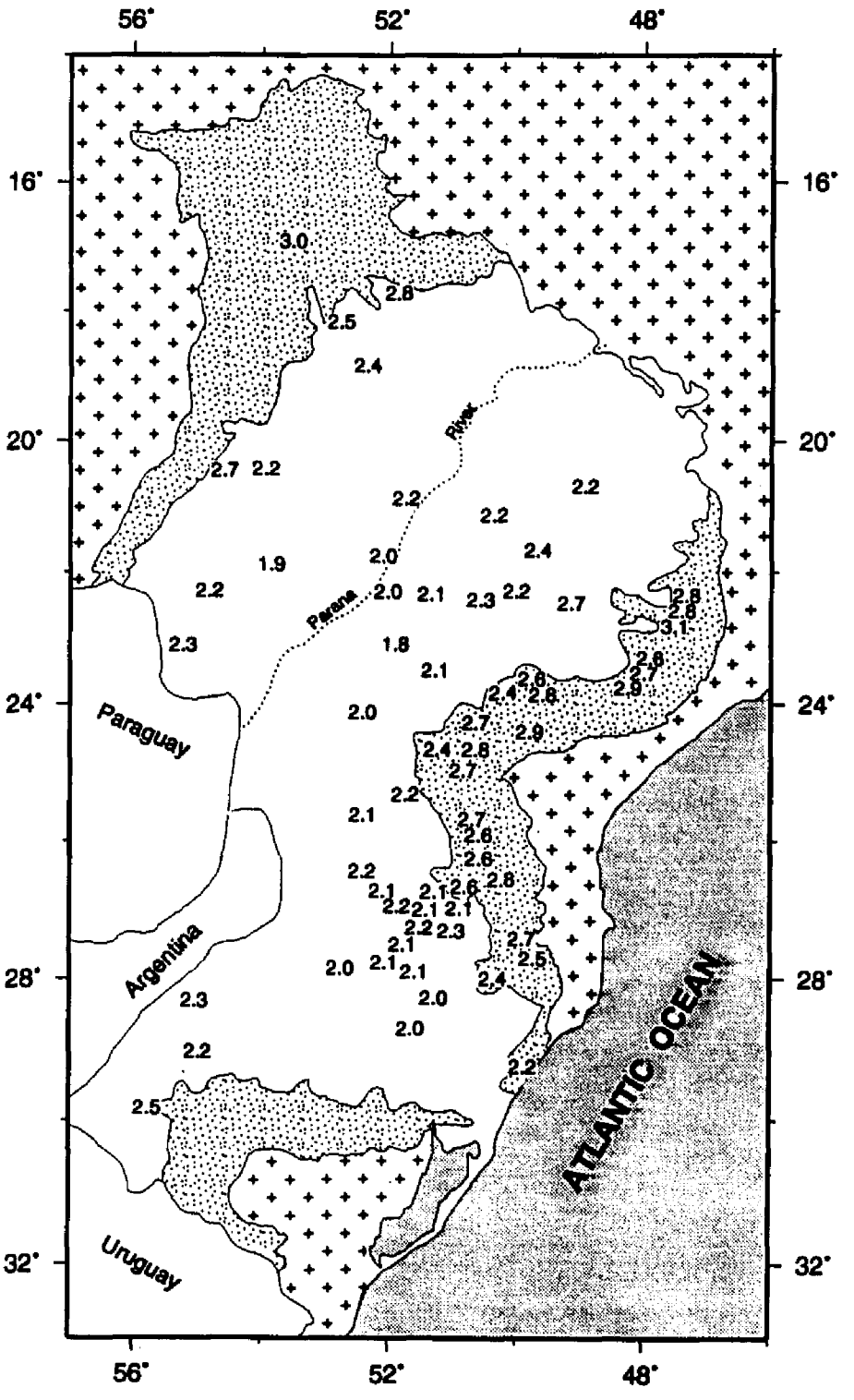

Figure 2.8 Map of the geometric mean thermal conductivity (temperature corrected) at each site. Units are W $m^{-1}K^{-1}$. Map patterns are as shown in Figure 2.1.

3.3 Heat Flow

Heat flow can be computed by several methods. We have selected the approach taken by Henry and Pollack (1988) in which terrestrial heat flow at each site is computed using Fourier's law of conduction, $q = \bar{k} \cdot \overline{gradT}$ where $\bar{k}$ is the geometric mean thermal conductivity of the site as determined by equation 2.1 and $\overline{gradT}$ is the mean geothermal gradient. Table 2.3 contains the geothermal gradients, mean thermal conductivity and resulting heat flow values for each site and Figure 2.9 presents the distribution of heat flow values. Most heat flow values are between 40 and 75 mW m-2. When plotted on the map in Figure 2.10 the larger heat flow values and greater variability generally occur along the eastern margin of the basin where basalt cover is absent. Lower heat flow of 40 to 50 mW m-2 is found in the central northern region and towards the south along the major NNE axis of the basin. Heat flow values displayed in Figure 2.10 with lighter characters refer to data with no uncertainty estimate for the geothermal gradient, and those in italic characters are from an earlier study by Vitorello (1978). In the next section we compare these heat flow values and their pattern to observations made in other intracratonic basins and continental flood basalt provinces.

4. DISCUSSION

The mean heat flow for the Paraná Basin is 56 ± 11 mW m^{-2}(standard deviation of the mean). The inspection of the geographic variation of these heat flow values among the 56 sites in the basin reveals a coherent pattern of lower heat flow (40 - 50 mW m^{-2}) in the central part of this basin, covered by up to 1.7 km of flood basalts, and a higher frequency of occurrence of heat flow values of 50-70 mW m^{-2} along the eastern margin of the basin, where no basalts cover the sediments. In the following discussion we examine heat flow from previous studies from the Paraná Basin and compare these with our new data. We then compare heat flow data from other intracratonic basins with the heat flow data in the Paraná Basin to gain insight into the factors and processes that affect heat flow in these settings.

The conventional method for determining heat flow (i.e. direct measurements of temperature as a function of depth combined with thermal conductivity measurements from cores or cuttings) was applied by Vitorello (1978) and Santos (1986) to sites in the Paraná Basin. The five sites reported by Vitorello (1978) in the Paraná Basin are included on Figure 2.10, with heat flow values presented in italics. All these sites are located along the eastern and southern basin margin, where flood basalt cover is absent. The northern most value of 36 mW m^{-2} is considered by Vitorello (1978) of poor quality possibly due to water circulation. The remaining four sites withvalues of 56, 75, 76 and 77 mW m^{-2} are on the higher end of but compatible with the range of new heat flow values in this region. Although Vitorello's data originated from shallow boreholes (up to 350 m deep), they fit in the overall heat flow pattern of the new data.

TABLE 2.3 Summary of heat flow data

Borehole Name	Latitude S	Longitude W	Elevation (m)	Borehole Depth (m)	T_0 (°C)	Number of BHTs	Mean Geothermal Gradient ($K\,km^{-1}$)	Standard Deviation ($K\,km^{-1}$)	Thermal Conductivity ($W\,m^{-1}\,K^{-1}$)	Heat Flow ($mW\,m^{-2}$)
AA1SP*	22.30	50.02	432	2992	21	4	23.1	1.0	2.17	50.1
AG1MT	16.92	53.53	750	1947	22	1	26.1	-	3.01	78.8
AL1RS*	28.82	55.77	80	2044	19	1	17.1	-	2.47	42.3
AL1SC*	26.45	52.18	1014	3876	16	5	22.2	1.5	2.15	47.8
AM1MT*	23.10	55.24	550	3371	21	2	29.0	6.7	2.34	-
AO1RS	28.70	51.66	686	2251	16	2	25.7	2.6	1.99	51.2
AP1PR	23.49	51.22	823	4300	20	4	20.3	1.0	2.06	41.8
AR1SP*	21.13	50.37	363	3605	22	2	22.0	5.6	2.23	-
AS1SP	22.52	47.58	539	1335	20	1	23.9	-	2.78	66.3
AT1SP	22.67	47.81	460	1262	20	1	18.2	-	3.05	55.5
AV1PR*	23.09	51.91	509	2787	21	1	32.6	-	1.77	57.8
BN#SC	27.51	49.76	723	1101	18	3	30.6	5.0	2.69	-
CA#PR	24.53	51.39	482	2792	19	12	25.7	4.4	2.37	61.0
CA1SC*	26.86	50.84	1098	1935	16	1	32.6	-	2.10	68.4
CB#SP*	22.30	52.04	397	4804	22	22	23.9	1.2	1.99	47.6
CG1MT*	20.45	54.62	510	2668	22	2	19.6	1.2	2.69	52.6
CM1PR*	24.11	52.43	632	4455	19	2	22.9	1.5	1.99	45.7
CN#SC	26.27	50.52	784	1775	16	2	25.4	0.9	2.78	70.4
CP1SP	23.38	48.51	683	1545	20	2	37.2	15.2	2.67	-
DO#MT*	22.28	54.83	450	4162	21	8	26.4	1.2	2.24	59.0
GP1PR*	25.31	51.66	985	3650	17	2	28.3	0.7	2.20	62.3
GU#SP	23.40	48.20	670	981	20	2	21.3	1.4	2.56	54.5
HV1SC*	27.22	51.46	825	2700	16	1	27.8	-	2.17	60.2
IT1RS*	29.02	54.99	356	2533	20	3	19.9	1.8	2.23	44.4
J1PR	23.22	49.87	505	2684	20	1	26.3	-	2.62	69.1
JA1GO	17.81	51.78	595	2107	22	1	24.2	-	2.81	68.1
JT1PR	23.47	49.96	574	2334	20	3	18.1	3.1	2.78	50.2
LA1SC	27.64	50.37	408	1343	16	3	34.5	7.0	2.38	-
LI1SP*	21.67	49.68	412	3460	22	3	18.8	3.4	2.35	44.2

continued on the following page

TABLE 2.3 Summary of heat flow data (continued)

Borehole Name	Latitude S	Longitude W	Elevation (m)	Borehole Depth (m)	T_o (°C)	Number of BHTs	Mean Geothermal Gradient (K km^{-1})	Standard Deviation (K km^{-1})	Thermal Conductivity (W m^{-1} K^{-1})	Heat Flow (mW m^{-2})
LS1PR*	25.41	52.42	837	3968	16	3	25.5	0.6	2.10	53.5
LV1PR*	28.17	51.50	684	2362	16	2	20.2	5.8	2.02	-
M1APR	25.88	50.79	844	1861	16	3	28.1	5.1	2.65	-
MA1RS*	27.59	51.66	728	2715	17	1	27.9	-	2.06	57.6
MC1PR*	26.59	51.12	908	1967	16	1	27.8	-	2.08	57.9
MO#PR	24.37	50.87	834	2017	18	2	20.8	0.5	2.81	58.3
MR1RS*	27.53	51.93	367	2589	17	3	28.6	0.8	2.12	60.7
O1PR	24.17	50.90	733	2025	19	1	27.4	-	2.65	72.6
OL1SP*	20.69	48.93	495	2568	22	3	24.2	1.3	2.21	53.4
PA1SC	27.60	49.74	930	1126	17	1	29.4	-	2.51	73.9
PA1SP	22.47	49.15	568	2105	21	3	20.1	3.4	2.68	54.0
PE1SP*	21.75	52.10	258	3954	22	4	23.5	2.0	1.98	46.5
PG1SP	22.55	47.64	634	1228	20	3	32.2	5.3	2.82	-
PI1SC*	27.42	51.78	437	2271	17	3	25.5	1.4	2.07	52.8
PN1SP	23.44	48.77	609	1683	20	4	21.4	2.3	2.93	62.5
PP1SP*	22.42	50.58	469	3663	21	2	18.5	0.8	2.25	41.6
PU1SC	26.27	51.02	754	2336	16	2	23.2	3.3	2.59	60.0
QT1PR	23.61	49.95	526	1386	20	1	19.3	-	2.85	55.0
R1PR	24.63	50.88	918	1909	18	4	20.1	3.9	2.65	53.3
RA1MS	18.84	52.36	572	3474	22	3	15.9	3.0	2.44	39.0
RC1PR	26.01	50.70	810	1999	16	2	26.4	0.2	2.64	69.9
RCH1SC*	26.66	52.04	1065	3273	16	1	25.1	-	2.14	53.7
RD1RS*	27.84	52.77	645	3422	18	2	19.7	1.8	2.01	39.4
RI1RS*	28.30	55.05	151	2403	20	2	19.4	0.8	2.31	44.7
RP1MT*	20.42	53.95	411	3366	22	1	39.1	-	2.21	86.7
SD1MT*	21.88	53.87	281	3003	20	3	26.5	1.5	1.93	51.2
SJ1PR	23.28	50.64	1047	2346	20	3	26.5	1.8	2.42	64.2
TB1SP*	22.33	51.35	496	4951	22	8	20.4	0.8	2.12	43.3
TG1SC*	27.08	51.25	639	2431	16	5	30.3	1.9	2.27	68.7
TL1MT*	20.88	51.75	310	4582	22	2	20.6	4.6	2.23	46.0

continued on the following

TABLE 2.3 Summary of heat flow data (continued)

Borehole Name	Latitude S	Longitude W	Elevation (m)	Borehole Depth (m)	T_0 (°C)	Number of BHTs	Mean Geothermal Gradient ($K\,km^{-1}$)	Standard Deviation ($K\,km^{-1}$)	Thermal Conductivity ($W\,m^{-1}\,K^{-1}$)	Heat Flow ($mW\,m^{-2}$)
TO1RS	29.33	49.80	28	990	19	1	31.7	-	2.23	70.7
TP1SC*	26.71	51.43	1290	3002	16	2	18.7	0.6	2.21	41.4
TQ1MT*	17.87	53.26	850	2021	22	1	21.4	-	2.54	54.3
TV#SC*	26.74	51.32	1070	2235	16	11	24.3	1.9	2.10	51.0
UV1PR	26.19	51.03	768	2162	16	2	25.0	0.8	2.59	64.5

* Boreholes that penetrate flood basalts

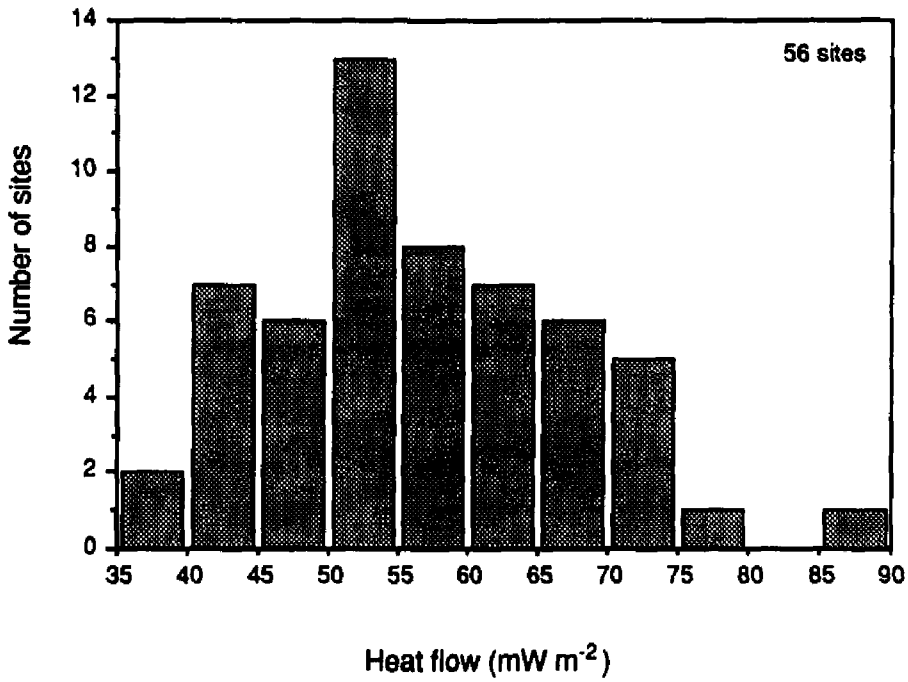

Figure 2.9 Histogram of heat flow values.

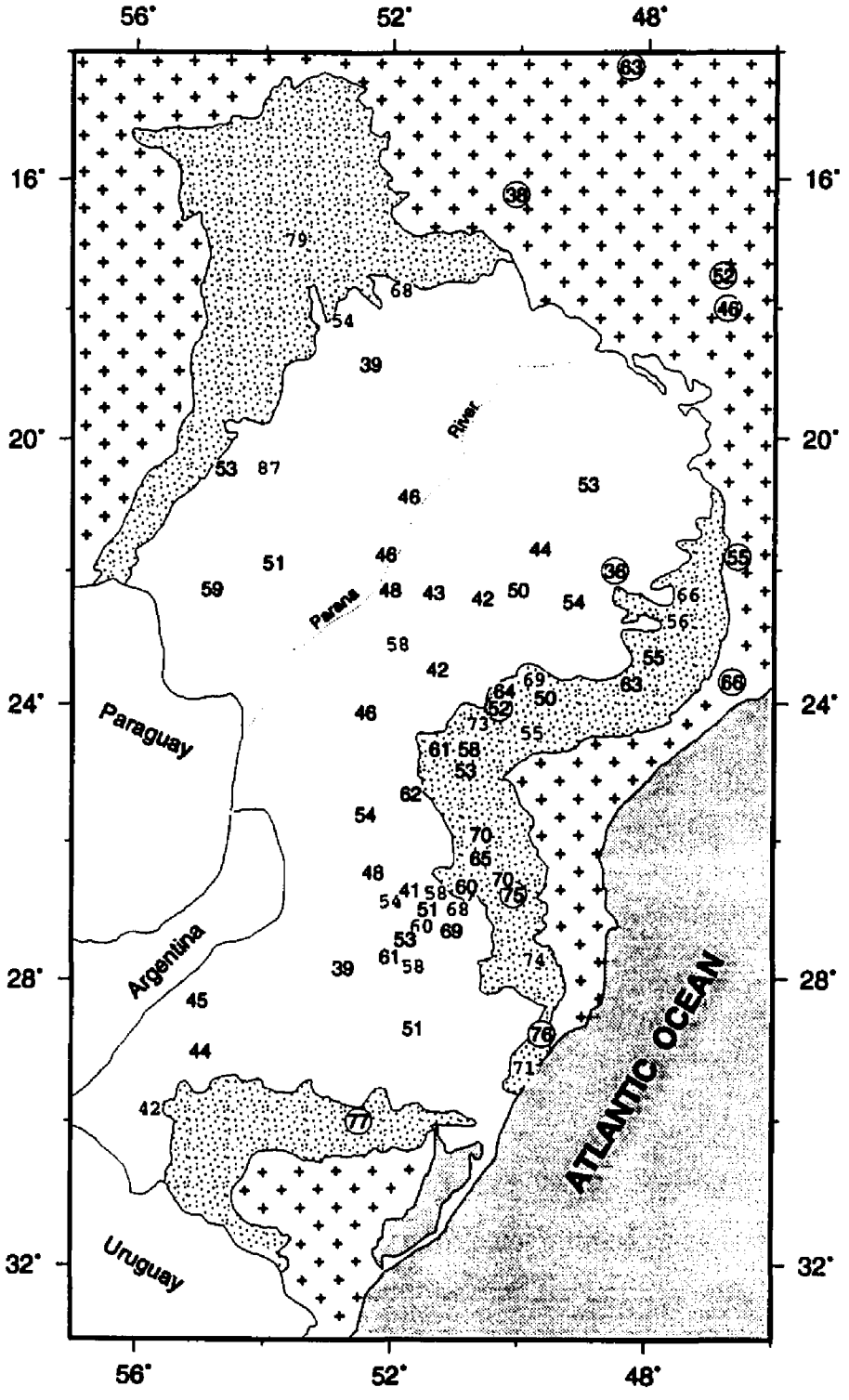

Figure 2.10 Map of heat flow values in the Paraná Basin. Units are mW m^{-2}. Bold and light symbols indicate heat flow computed in this study. Light symbols represent sites where a standard deviation to the geothermal gradient could not be computed. Circled heat flow values are from Vitorello (1978).

Santos (1986) reported heat flow values for 22 sites in the São Paulo State region of the Paraná Basin (20° - 23° S, 47° - 52° W); all sites are located on flood basalt covered areas. The reported mean heat flow is 58 ± 11 mW m^{-2}. Only in nine of the 22 sites was it possible to use the conventional method; in the other sites the 'aquifer method' was used to estimate a formation temperature from a pumping well. The mean heat flow of values derived from the conventional method is 51 ± 14 mW m^{-2} (standard deviation of the mean), within the range reported for our new heat flow data from areas with flood basalt cover. Santos also suggests that there may be a small increase of heat flow toward the center of the basin. As pointed out by him and evidenced graphically in his thermal profiles (Santos, 1986), temperature profiles are clearly perturbed, and a reliable estimation of geothermal gradients is exceedingly difficult, with large uncertainties. Most boreholes used in that study are water wells that penetrate the basalt cover into the underlying Botucatú formation, an extensive eolian sandstone aquifer. One possibility of explaining increasing heat flow towards the center of the basin is the effect of groundwater flow in the Botucatú aquifer. Much of its recharge may derive from the topographically elevated regions to the east, with the groundwater flowing in direction of the lower topographic region of the Paraná River to the west and southwest. The lower heat flow closer to the recharging area would then be the result of downward migration of surficial fluids. The work by Santos (1986) perhaps gives a perspective on the heat transfer in the uppermost part of the basin fill, but we feel that these heat flow values should be excluded from a regional analysis because of the very large uncertainties associated with them.

We now survey thermal characteristics of other basins of the world developed on continental crust. Within South America, the Recôncavo Basin, a half-graben on Precambrian basement along the northeast coast of Brazil has a mean heat flow and standard deviation of 46 ± 6 mW m^{-2} (Carvalho and Vacquier, 1977). This is a minimum estimate because it was computed using BHT data that were not corrected for drilling disturbances. The intracratonic Maranhão Basin (also referred to as the Paraíba Basin) of northeastern Brazil displays a similar tectonic setting as the Paraná Basin: mobile belts originated in the Brasiliano orogenic cycle surrounding an inferred cratonic nucleus. Meister (1973) reports an average geothermal gradient of 21 K km^{-1} for the Maranhão Basin. The estimated gradients in the central part of this bulleye shaped basin are higher than around the margins, with the highest values (>26 K km^{-1}) in the central northern region and locally in the southern central part of the basin. These are likely minimum estimates, as they were derived from probably uncorrected BHT data. The same investigation reports a mean geothermal gradient of 17 K km^{-1} for the Paraná Basin, similar to our linear regression slope of 18.5 K km^{-1} for uncorrected BHTs. Thus on the basis of the comparison of uncorrected temperatures the geothermal gradient in the Maranhão Basin appears to be somewhat higher than in the Paraná Basin. In the sedimentary platform of Peru to the east of the

main Andean Cordillera, in the upper reaches of the Amazon Basin, Henry and Pollack (1988) report heat flow in the range 50 to 55 mW m^{-2} .

Several West African basins show consistency in the mean heat flow values given with the standard deviation of the mean (Lucazeau et al.,1991): the Volta basin on the West African craton has low mean heat flow (38 ± 5 mW m^{-2}), although the Taoudenni basin also on this craton has a higher mean value of 57 ± 8 mW m^{-2}, but based on only three determinations. Basins located on younger mobile belts like the Niger basin and the Chad basin have mean heat flow of 60 ± 10 mW m^{-2} and 67 ± 26 mW m^{-2}, respectively. The high heat flow of 90 ± 20 mW m^{-2} recorded in the Tindouf basin of Algeria, is attributed by Lucazeau et al. to Cenozoic-Quaternary rejuvenation due to alkali volcanism in this area.

The cratonic Gondwana basins in Peninsular India are small elongate, elliptical depressions. Gupta et al. (1991) report systematically high heat flows (mean values with standard deviation): Damodar basin (74 ± 4 mW m^{-2}), Satpura basin (79 ± 28 mW m^{-2}), Son-Mahanadi basin (83 mW m^{-2}), Pranahita-Godavari basin (57 ± 11 mW m^{-2}) and the Chintalpudi subbasin (73 ± 20 mW m^{-2}). Overall the mean heat flow is 75 mW m^{-2}, and according to Rao et al. (1979) such values are consistent with a basement of high radiogenic heat production rate and not due to the effects of tectonic activity. However, localized igneous activity recorded by dykes and sills of Upper Jurassic to Early Cretaceous and Upper Cretaceous to Early Paleocene age in these basins and associated thinner lithosphere (Gupta,1982; Gupta et al., 1991) would suggest the possibility of high heat flow explained by a transient effect due to tectonic activity.

The Paris and Aquitaine cratonic basins show generally high and variable heat flow: mean heat flow and standard deviation are 111 ± 24 mW m^{-2} and 88 ± 21 mW m^{-2}, respectively (Gable, 1979). The Paris Basin overlies pre-Permian basement of crystalline and Paleozoic sedimentary rocks, and contains sediments of Permo-Triassic to Tertiary age. The basement of the Aquitaine Basin consists of Ordovician to Carboniferous sedimentary rocks, and its sediments are Jurassic to Quaternary. Its southern region has been extensively deformed during the formation of the Pyrenees (Pomerol et al., 1980). These basins are much younger than the Paraná Basin and show evidence of a more complex and recent tectonic history, which may explain their high mean heat flow .

The Uinta Basin is an intermontaine sedimentary basin within the northern Colorado Plateau. On the basis of corrected BHT temperature data Chapman et al. (1984) determined an average geothermal gradient and heat flow for this basin of 25 K km^{-1} and 57 mW m^{-2}, respectively. Heat flow appears to decrease systematically from 65 to 40 mW m^{-2} from the Duchesne River northward to the south flank of the Uinta mountains. Further studies by Willet and Chapman (1989) relate this heat flow pattern to subsurface hydrologic flow from the Uinta mountains southward to the Duchesne River.

Conventional heat flow determinations for the Michigan basin are available in nine sites (Judge and Beck, 1973; Combs and Simmons, 1973) and range between 33 and 58 mW m^{-2}, although most values lie within 42-54 mW m^{-2}. An inversion analysis of more than 400 BHTs from the Michigan Basin by Speece et al. (1985) led these authors to conclude that fluid flow and/or thermal conductivity contrasts within the sediments were not likely causes of the pattern of the temperature field in the basin. On the other hand, their thermal models show that thermal conductivity contrasts and heat production contrasts due to the existence of the Keweenawan mafics in the lower crust/upper mantle underneath the basin can produce a heat flow variation at the surface of the order of 15 mW m^{-2}, in good agreement with the observed heat flow variation of 12 mW m^{-2} and the known distribution of the Keweenawan rocks.

The Western Canada Sedimentary Basin lies on a Precambrian platform and covers a vast area between the Canadian Shield on the east and the Cordillera on the west. It actually comprises a number of sub-basins separated by a network of arches. Its basement consists of Archean crystalline rocks and supracrustal rocks modified by deformation, metamorphism and magmatism. This sedimentary basin has been the object of several geothermal studies based on BHT data. Majorowicz and Jessop (1981 a,b), Majorowicz et al. (1985) and Majorowicz et al. (1986) have shown that heat flow increases from 40-50 mW m^{-2} at the western Rocky Mountain Foothills to values in excess of 80 mW m^{-2} in the north and east. Additionally these authors note a variation of heat flow and geothermal gradient with depth: a decrease with depth in the Foothills area and an increase with depth to the northeast. The relation between low gradients, low heat flow and high elevations and high hydraulic gradients suggests that the heat flow pattern is controlled by subsurface fluid flow on a large scale. However, Bachu (1985,1988) and Bachu and Burwash (1991) studied the same region employing a different approach, and advocate a very different interpretation. On the basis of dimensional analysis of hydrologic data, they argue that heat transport by advection is insignificant on a regional scale, although it may attain local importance. Furthermore, they compare basement geology and measurements of the heat production rate of basement rocks with the thermal pattern, and show a relationship of high gradients and temperatures with regions of high basement heat production.

We now discuss three continental flood basalt provinces for which heat flow determinations exist. The Permo-Triassic extrusion of flood basalts accumulated up to three kilometers of basalt in places over the Tunguska basin in Siberia. The Siberian platform basement beneath the Tunguska Basin comprises Archean to Lower Proterozoic intensely folded rocks. Basic magmatism has a long history in this area, beginning in the Upper Proterozoic (Bazanov et al., 1976; Zolotukhin and Al'Mukhamedow, 1988). The Permo-Triassic activity is dated 200 to 240 Ma and each extrusive cycle was initiated by a pyroclastic phase. Bazanov et al. (1976) point out that the volume of Lower Triassic subsidence in this area is comparable to the volume of

erupted material. Estimated rates of subsidence of 100 m Ma^{-1} are high when compared to the 10 to 30 m Ma^{-1} rates for previous epoches. This contrasts with less than 100 m subsidence of the Paraná Basin following the Serra Geral flood basalt event. We also note that the Siberian flood basalt event was not related to successful continental rifting accompanied by continental breakup as was the case for the Serra Geral flood basalts. Heat flow data for the Siberian platform are presented and reviewed in Duchkov (1991). The old Precambrian Siberian platform is characterized by a mean heat flow of 38 mW m^{-2}, and the Tunguska basin area of the Siberian Traps shows heat flow in the range 40-50 mW m^{-2}. In this case comparison with the Paraná Basin is more difficult as the Siberian heat flow data is averaged over large areas on the published maps and more direct geographic relationships cannot be observed. Nevertheless the reported magnitude ranges are comparable to somewhat lower than in the Paraná Basin.

The Deccan Traps in peninsular India were extruded within the interval of 65-50 Ma (Basalt Volcanism Study Project, 1981; Mahoney, 1988). The basalt covers parts of the Archean Dharwar craton. An upwarping by about 2 km of the Moho correlated to gravity highs in this area is interpreted as evidence of continental rifting underlying the Deccan Traps. Seismic studies (Kaila et al., 1989) show that in places basalts lie directly over crystalline basement, and in other places the basalts overlie up to1.7 km of probably Mesozoic sediments. Two heat flow measurements at sites several hundred kilometers apart yield a mean of 44 mW m^{-2} (Gupta and Gaur, 1984), values comparable to heat flow in the thickest part of the basalt cover in the Paraná Basin, as well as to heat flow in Archean cratons.

The Karoo basalt province of southern Africa most resembles the Serra Geral province. The basalts erupted over an intracratonic basinal sequence of Late Cambrian to Triassic age. The estimated extent of basalts is about 2,000 km in the north-south direction and 2,800 km in the east-west direction; the reduced present-day extent is the result of erosion. This province is generally older than the Serra Geral, with eruptions occurring in concentrated periods spanning 209-132 Ma (Cox, 1988). The Karoo basalt event is thought to precede the continental breakup between the African and Antarctic portions of Gondwana. A Lower Cretaceous extrusion, the Etendeka plateau of Namibia along what was to become the western margin of southern Africa, is directly correlated to the Serra Geral basalts (Erlank, 1984), preceding the opening of the South Atlantic. The Karoo basin sedimentary rocks cover parts of the Archean Kaapvaal craton and the Proterozoic Namaqua-Natal mobile belt. A relationship between heat flow values and the locus of flood basalt cover in South Africa is made difficult because most of the flood basalt cover has been eroded. The area influenced by the Karoo flood basalt event is inferred from the regional pattern of dyke swarms and dolerite sill intrusion. For comparison with the Paraná Basin, Figure 2.11 shows southern Africa, the extent of the Karoo Basin and present-day remnants of flood basalts. Heat flow values were taken from Jones (1981, 1987), Ballard et al. (1987) and Nyblade et al.

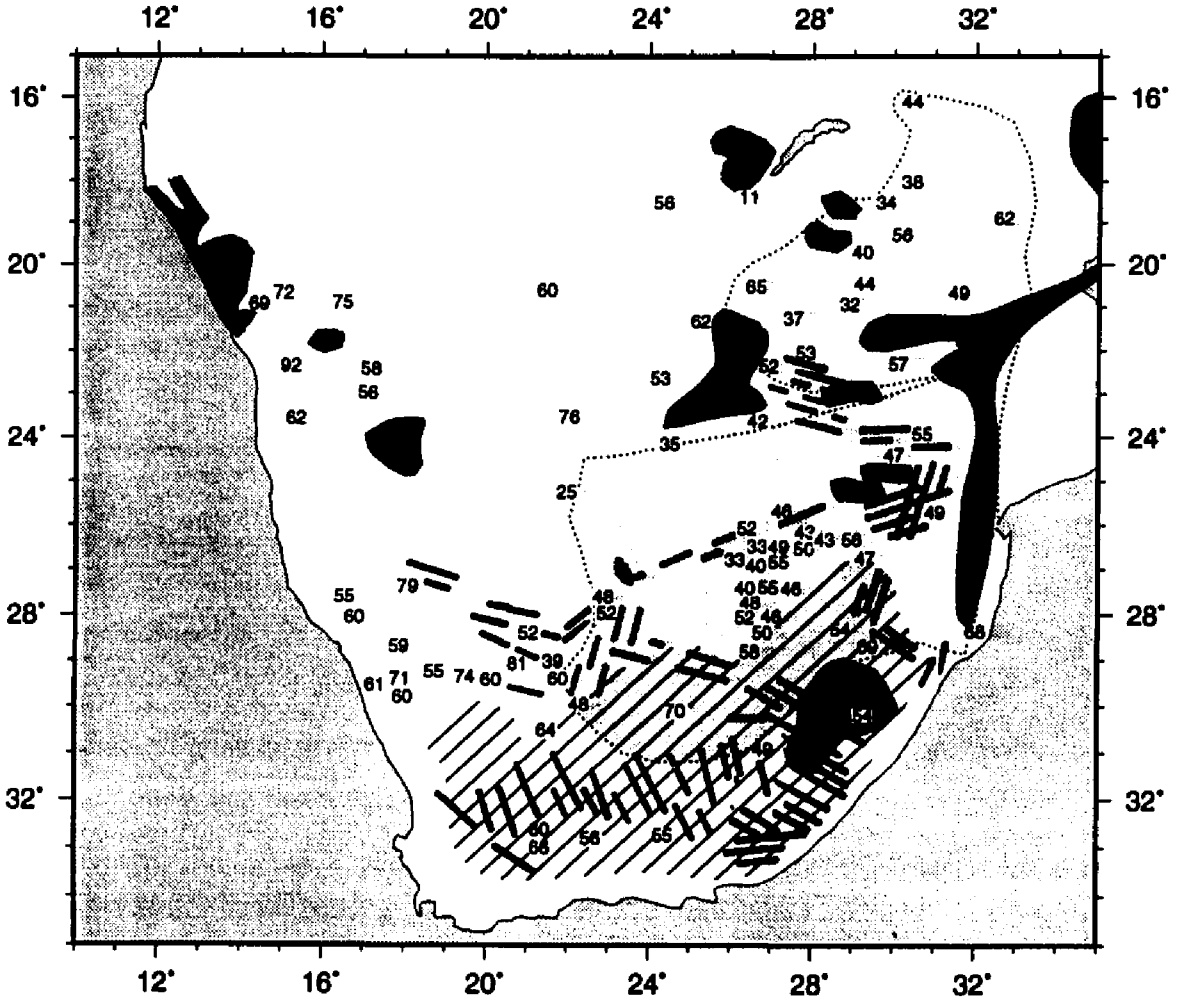

Figure 2.11 Map of heat flow values (mW m^{-2}) in southern Africa. Heat flows are taken from Jones (1981, 1987), Ballard et al. (1987) and Nyblade et al. (1990). The dark shaded areas represent the present day extent of Karoo basalts and the thick black lines are dike swarms. Light shading corresponds to the Archean Kaapvaal and Zimbabwe cratons and parallel lines to the Karoo Basin.

(1990). We observe no obvious relationship between lower heat flow and proximity to the present-day flood basalt patches. Gough (1963) reports a range of 55 - 66 mW m^{-2} in the region south of the 'dolerite limit' that marks the limits of the Karoo basalt influence. These values are comparable to heat flow in the Paraná Basin along the eastern margin of the basin, where no basalt cover exists. According to Jones (1981), heat flow values in the Kaapvaal craton average 44 ± 10 mW m^{-2} (standard deviation of the mean), comparable to values measured in the basalt covered central part of the Paraná Basin. A mean heat flow of 61 ± 11 mW m^{-2} is found in the Namaqua mobile belt surrounding the Kaapvaal craton (Jones, 1981). This mean value and range of variation is similar to heat flow values in the Paraná Basin that occur in the eastern margin with no basalt cover. That region overlies the Ribeira mobile belt that outcrops at the eastern basin margin (Cordani et al., 1984). The heat flow pattern in southern Africa has been discussed in detail by Ballard et al. (1987) and Nyblade et al. (1990). The favored interpretation for the low heat flow observed in the Archean cratonic area but increasing towards the surrounding mobile belts is that thick Archean cratonic roots cause deep heat flow to diverge into the surrounding mobile belts.

This survey of thermal studies on intracratonic basins shows that heat flow variation occurs at several scales and suggests that it is a function of the following factors: age, structure and composition of the basement upon which a basin has developed, subsurface fluid flow and possibly igneous activity. Small scale variations are likely related to shallow crustal features, such as the presence of heat production contrasts due to granitic plutons for example. Old cratonic basements display lower heat flow and basements comprised of younger mobile belts yield higher heat flow. These larger scale features likely reflect the lithospheric structure and thickness of these tectonic elements. Archean cratons are believed to have developed thick lithospheric roots that explain the low heat flow measured generally in such areas. Basins developed on younger basement such as the Paris and Aquitaine basins have higher mean heat flow than older basins such as the Michigan and Paraná basins. Generally heat flow in the Paraná Basin is consistent with a tectonically stable setting, such as that which characterizes the Michigan Basin.

The effect of subsurface fluid flow is to redistribute heat within the basin following the regional hydrologic flow pattern: fluids move from topographically high recharge areas to lower discharge areas. Surface heat flow is decreased in the recharge areas where cool fluids migrating downward absorb heat from the surrounding rocks, and is increased in the discharge areas, where warm rising fluids deliver heat to higher levels.The Uinta Basin shows mean geothermal gradient and heat flow comparable to the Paraná Basin, although the regional pattern is opposite: heat flow increases toward the higher elevation areas to the east in the Paraná Basin, while it decreases toward the Uinta Mountain foothills in the Uinta Basin. The same observation is valid in comparing the West Canada Basin and the Paraná Basin. Heat flow values and variation is comparable, but

the regional pattern is again opposite. In West Canada heat flow diminishes toward the higher elevations at the Rocky Mountains Foothills.

Heat flow from the three continental flood basalt provinces discussed earlier appears to be comparable to the range and magnitude determined for the Paraná Basin. The Karoo province in South Africa (with many more heat flow data than the Deccan and Siberian flood basalt provinces), has many characteristics in common with the Serra Geral province: both overlie intracratonic sedimentary Gondwana type sequences, were related to continental breakup and show the same range in heat flow, with the Karoo province having the lower heat flow in the domain of the Archean Kaapvaal craton. Heat flow in the mobile belts of both provinces is very similar.

In the following Chapter III we will address quantitatively the possible causes of variable heat flow in the Paraná Basin as suggested by factors and processes that have influenced the heat flow in other intracratonic basins.

5. SUMMARY AND CONCLUSION

BHT data from 79 boreholes in the Paraná Basin yielded 187 temperature values that after correction for drilling disturbances and combined with surface temperatures were used to compute mean geothermal gradients at 56 sites. These range mostly between 20 and 30 K km^{-1}. Thermal conductivities measured from numerous core samples form the basis for computing the thermal conductivity structure of the basin. Geometric mean thermal conductivities vary generally from 3.0 to 2.0 W $m^{-1}K^{-1}$ from the eastern basin margin to the center as a function of the thickening of the Serra Geral flood basalt cap. Geothermal gradients and thermal conductivities combine to yield heat flow values in the range 40 to 75 mW m^{-2}. This variation has a coherent geographic expression: higher heat flow occurs more frequently along the eastern basin margin, while lower and more uniform heat flow values found in the central axial region of the basin, the region of greatest basalt cover.

The range and mean of the heat flow in the Paraná Basin is comparable to that in the Michigan Basin, and similar to heat flow in the Uinta Basin and the West Canada Basin, although the regional pattern of the Paraná Basin with respect to broad topographical gradients is opposite to that observed in the Uinta and West Canada basins. Other continental flood basalt provinces show similarities with the Serra Geral province in the Paraná Basin. The data in the Deccan and Siberian Traps are sparse, but are compatible with the magnitude and ranges observed in the Paraná Basin. The Karoo flood basalt province has better data coverage and resembles the Serra Geral province in several aspects of its history and geology, although the exposure of flood basalts in this older province has been severely reduced through erosion. Heat flow in the cratonic portions of the Karoo is comparable to heat flow in the basalt covered area in the Paraná

Basin and heat flow from the basalt free mobile belts within the Karoo and similar belts along the eastern margin of the Paraná Basin are also similar in range.

CHAPTER III

INTERPRETATION OF HEAT FLOW IN THE PARANÁ BASIN, SOUTHERN BRAZIL

ABSTRACT

Heat flow in the Paraná Basin varies between 45 and 70 mW m^{-2}, generally increasing from the central part to the margin of the basin. The lower more uniform heat flow values (40-50 mW m^{-2}) are located in the central part of the basin, most of which is covered by the Serra Geral flood basalts which erupted just prior to the opening of the South Atlantic. Higher and more variable heat flow values (50-70 mW m^{-2}) have been determined along the eastern margin of the basin, where this basalt cover is absent. Causes that may explain variable heat flow in the Paraná Basin include steady state effects attributed to variation in thermal properties (conductivity and radiogenic heat production) of the crust, variable thickness of the sub-basinal lithosphere, and subsurface fluid flow, and transient thermal effects due to the cooling of igneous bodies and the processes of deposition, uplift and erosion. We investigate these possible causes with a series of simple geophysical model calculations. Transient effects due to the uplift of the eastern margin and the rapid deposition of flood basalts in the center of the basin are shown to be able to account for only a small part of the heat flow variation across the basin. Among the steady state effects, subsurface fluid flow, if significant at all is likely to produce a heat flow pattern opposite to that observed. If such a regional flow pattern exists and is of sufficient magnitude, it would imply that the observed heat flow contrast from basin center to margin is a muted expression of what would exist in the absence of a hydrologic perturbation. Topographical effects related to the mountain ranges at the eastern margin of the basin are shown to be insignificant. The diversity of rock types and tectonic units covered by the Paraná Basin suggest a variability in radiogenic heat production contrasts of practically one order of magnitude in the sub-basinal basement. However, the very limited number of basement samples show no evidence of a spatially coherent distribution of radiogenic heat production in the basement that could explain the heat flow pattern. The largest thermal conductivity contrast within the basin itself is defined by areas with and without flood basalt cover. The low conductivity flood basalt cap is not capable of diverting enough heat to the basin margin to account for the observed variability in heat flow. If the Serra Geral flood basalts are interpreted as only a surface manifestation of a larger volume of mafic melt, most of which has

intruded and underplated the lower crust, then this intruded/underplated material provides a large scale thermal conductivity contrast extending to depths on the order of crustal thickness, much greater than the depth of the basin itself. Calculations show that such intrusion and underplating could promote divergence of heat flow into the surrounding terrains and account for about half of the observed heat flow contrast. Differences in lithospheric thickness can easily explain the balance of observed heat flow variation. The Serra Geral igneous event through the process of basalt depletion may have thickened the lithosphere underlying the basin, producing a thick zone of conduction capable of diverting deep mantle heat into the surrounding thinner lithosphere, producing a heat flow contrast of the proper order of magnitude.

1. INTRODUCTION

Investigations of geothermal aspects of the Paraná Basin began in the early 1970s, with studies by Vitorello (1978), Vitorello et al. (1980) and Santos (1986) producing the first heat flow data for this basin. Vitorello (1978) observed an increase in heat flow from north to south along the eastern basin margin and reported a mean heat flow of 68 mW m^{-2}, larger than is characteristic for Paleozoic intracratonic basins. He suggested that this enhanced heat flow could be due to some residual heat within the lithosphere, deriving from the thermal disturbance created by the magmatic activity that lead to the extrusion of the Serra Geral flood basalts at about 130 Ma. Santos (1986) observed a slight increase in heat flow in the part of the Paraná Basin contained within the State of São Paulo, which he tentatively associated with increasing depth to basement.

In Chapter II we presented a more comprehensive body of thermal data comprising 56 new heat flow sites, significantly increasing the number and geographic coverage of heat flow data. Since the earlier studies many more data from other fields of study have also been produced: gravity (Molina et al., 1989), aeromagnetic (Ferreira, 1982), magnetotelluric surveys (Padilha et al., 1989, 1992; Stanley et al., 1985), paleomagnetic (Ernesto and Pacca, 1988) and geochemical studies (Piccirillo and Melfi, 1989). New hypotheses for the structure and evolution of this area have been proposed (Molina et al., 1989; Peate et al., 1990). These observations along with the new heat flow data of the previous chapter makes this an opportune occasion to integrate this information and interpret surface heat flow and the regional thermal structure of the Paraná Basin and underlying lithosphere.The interpretation of the pattern of surface heat flow is the subject of the present chapter.

We begin by briefly reviewing the heat flow pattern of the Paraná Basin as revealed by the new measurements reported in Chapter II and the few heat flow data from previous studies. We then turn to presenting simple geophysical calculations to assess the possible interaction of several factors and processes that may affect and explain the observed heat flow pattern and other geophysical observations.

2. REGIONAL HEAT FLOW PATTERN IN THE PARANÁ BASIN

In Chapter II we reported new heat flow values for 56 sites in the Paraná Basin. These values are displayed on the map depicted in Figure 2.10. The mean heat flow for all sites is 56 ± 11 mW m^{-2} (standard deviation of the mean); individual values range mostly between 40 mW m^{-2} and 75 mW m^{-2}. The geographic distribution of heat flow values reveals a coherent pattern. Generally lower heat flow values of 40-50 mW m^{-2} occur in the northern and south central region of the Paraná Basin, roughly parallel to the Paraná River, that flows along the basin's major axis and overlies the locus of greatest flood basalt thickness. Along the eastern basin margin, where flood basalt is absent, higher heat flow values in the range of 50-75 mW m^{-2} are encountered, although with greater variability than in the flood basalt covered areas. In Figure 3.1 the heat flow data is plotted as a function of distance from the axis of the basin taken along the Paraná River, illustrating this increase in heat flow away from the region of thickest basalt cover. Heat flow is about 45 mW m^{-2} in the central region, increasing to 60 mW m^{-2} towards the edge of the flood basalt cover and increasing further to 70 mW m^{-2} at the margin of the basin. Although there is considerable scatter, a variation of the order of 20 - 25 mW m^{-2} occurs between the center and the margin of the basin.

3. FACTORS AND PROCESSES THAT INFLUENCE HEAT FLOW

In this section we discuss factors that influence heat flow and several possibilities to generate the observed heat flow pattern. We separate the factors and processes into steady state and transient. Steady state thermal influences include long term features such as topography, crustal and lithospheric structure and subsurface fluid flow, whereas transient refers to shorter lived processes like the cooling of intrusions or time dependent processes such as surface temperature history, sedimentation, uplift and erosion. We attempt to assess the magnitude of the effects of each variable separately, and also of the superposition of effects when such processes are simultaneously at work.

3.1 Transient Thermal Effects

3.1.1 Igneous activity

The major igneous activity in the Paraná Basin area is related to the extrusion of the Serra Geral flood basalts and associated intrusives that preceded the opening of the South Atlantic Ocean. In extensional regimes, the extruded igneous rocks may represent only a fraction of the total amount of melt generated during such an event with a large volume thereof intruding and

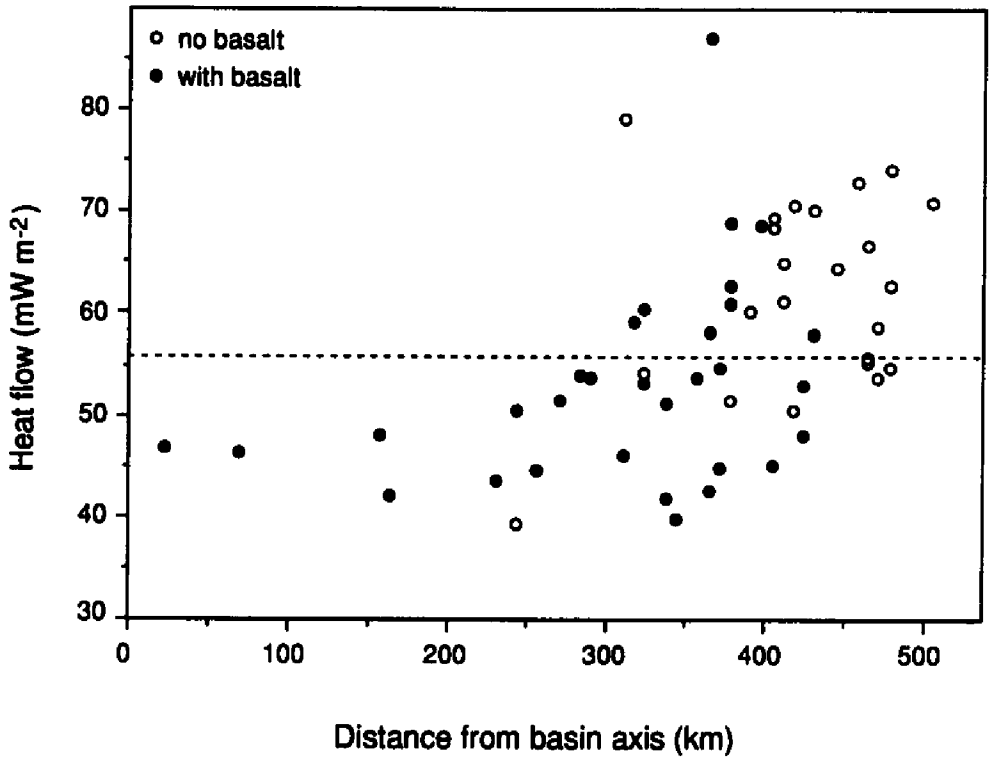

Figure 3.1 Heat flow as a function of distance from the axis of the Paraná Basin, roughly overlying the Paraná River. Filled circles refer to sites on flood basalt cover and empty circles to sites on outcropping pre-volcanic sediments. The dashed line indicates the mean heat flow of 56 mW m^{-2}.

underplating the lower crust (McKenzie and Bickle, 1988; White and McKenzie, 1989a,b). We will further discuss underplating beneath the Paraná Basin in the next section. Here we only mention that supporting evidence for an underplate beneath the Paraná Basin is found from gravity studies in the area (Molina et al., 1989). Here we evaluate the transient thermal signature of the cooling igneous bodies. We specifically address and evaluate the Serra Geral igneous event and its effects on the sediments in the basin in Chapter V with a numerical model based on an analytical solution to the heat conduction equation; details on the derivation and implementation of this model can be found in Chapter V. This model allows temperatures to be calculated at a given location at any time after intrusion of multiple sills, arbitrarily distributed throughout the sedimentary column. Here we shall use it to estimate the lifetime of the perturbation to temperature and heat flow due to the extrusion of the flood basalts and emplacement of a hot underplate.

Assuming that the total thickness of flood basalt extrudes instantaneously at a temperature T_i at the surface of a semi-infinite medium of diffusivity α, bounded by the surface at z=0, the temperature perturbation as a function of time since extrusion of a basalt flow of thickness (b-a) is expressed as:

$$T(a,b,z,t) = \frac{1}{2}(T_i - T_o)\left\{\operatorname{erf}\left(\frac{z-a}{\beta}\right) - \operatorname{erf}\left(\frac{z-b}{\beta}\right) + \operatorname{erf}\left(\frac{z+a}{\beta}\right) - \operatorname{erf}\left(\frac{z+b}{\beta}\right)\right\}$$
$$-\frac{1}{2}gz\left\{\operatorname{erf}\left(\frac{z-a}{\beta}\right) - \operatorname{erf}\left(\frac{z-b}{\beta}\right) - \operatorname{erf}\left(\frac{z+a}{\beta}\right) + \operatorname{erf}\left(\frac{z+b}{\beta}\right)\right\} \qquad (3.1)$$
$$+\frac{\beta g}{2\sqrt{\pi}}\left\{\exp\left(-\frac{(b-z)^2}{\beta^2}\right) - \exp\left(-\frac{(b+z)^2}{\beta^2}\right) - \exp\left(-\frac{(a-z)^2}{\beta^2}\right) + \exp\left(-\frac{(a+z)^2}{\beta^2}\right)\right\}$$

where $\beta = 2\sqrt{\alpha t}$ and T(a,b,z,t) is the resulting temperature perturbation due to one flow with top at depth 'a' and bottom at depth 'b'. In the case of a basalt flow, a=0.

We evaluated equation 3.1 for an extrusion temperature of T_i =1,200 °C, a surface temperature T_o = 20 °C and an unperturbed geothermal gradient of g = 25 K km^{-1}. The temperature perturbation due to the extrusion of a layer of basalt 2 km thick decays to less than 1 % of the unperturbed temperatures within 8 Myrs after the extrusion event at all depths between the surface and 5 km in the basin. Thus the cooling of the surface extrusion or near surface intrusive bodies is completed within a few million years after the event and therefore does not contribute to the present-day heat flow.

The duration of a thermal perturbation due to an underplate in the lower crust between 30 km and 40 km depth can also be evaluated with equation 3.1. For an underplate 10 km thick, the perturbed temperatures will decay to less than 1 % of the unperturbed temperatures in the basin

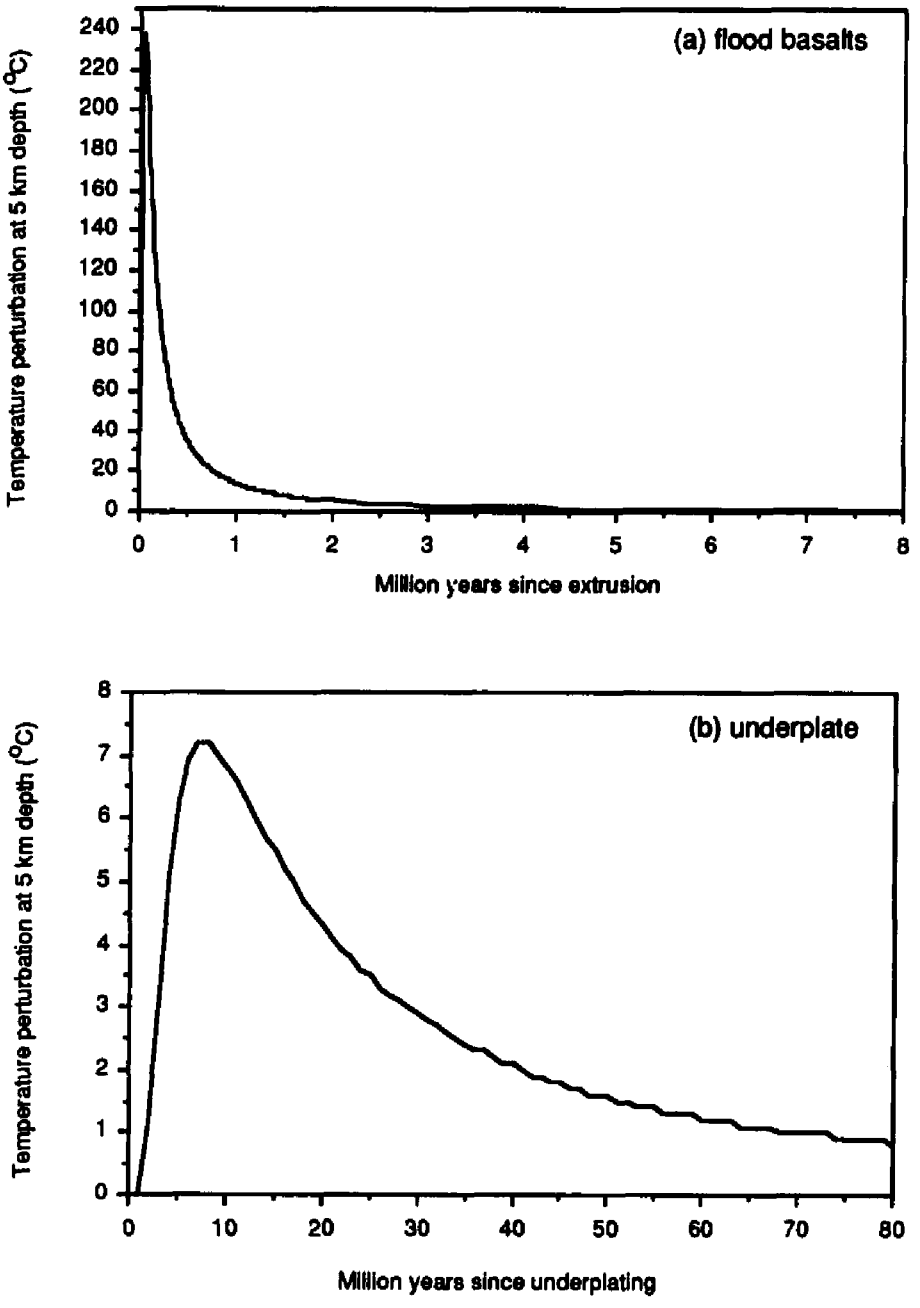

Figure 3.2 Temperature perturbation at 5 km depth due to (a) cooling of 2 km thick flood basalts and (b) cooling on an 10 km thick underplate with upper surface at a depth of 30 km in the lower crust. The thermal perturbation amounts to less then 1 % of the undisturbed temperatures after 8 Ma of flood basalt extrusion and after 100 Ma of the underplating event. Note the different time scales of (a) and (b): the perturbation shown in (a) decays completely before (b) reaches peak temperatures.

within less than 100 Myrs after the intrusive event. The effects of both the extrusion and underplate are summarized in Figure 3.2. We conclude that the transient effects of igneous activity at 130 Ma do not affect the present-day heat flow in the Paraná Basin.

3.1.2 Uplift, erosion and sedimentation

Following the Serra Geral igneous event and preceding the opening of the South Atlantic, the future coastal region was uplifted to form the Serra do Mar mountain ranges that at present form the topographically high region along the eastern margin of the Paraná Basin. Also following the extrusion event the Ponta Grossa Arch was uplifted. These uplifted regions have since been subject to erosion. The effect of uplift and erosion is to decrease the surface temperature and expose warmer rocks, both of which contribute to an increase in the thermal gradient. Integration of the heat conduction equation yields the temperature perturbation as a function of time and depth, $\Delta T(z,t)$ due to an instantaneous change in surface temperature ΔT_0:

$$\Delta T(z,t) = \Delta T_o \mathrm{erf}\left\{\frac{z}{\sqrt{4\alpha t}}\right\} \tag{3.2}$$

Differentiation of equation 3.2 yields the perturbation to the geothermal gradient, $\Delta g(z,t)$:

$$\Delta g(z,t) = \frac{\Delta T}{\sqrt{\pi \alpha t}} \exp\left\{\frac{z^2}{4\alpha t}\right\} \tag{3.3}$$

At the surface (z=0) this perturbation to the temperature gradient is given by:

$$\Delta g = \frac{\Delta T}{\sqrt{\pi \alpha t}} \tag{3.4}$$

where ΔT is the temperature change at the surface due to uplift and erosion, and α the thermal diffusivity ($\alpha = 10^{-6}$ $m^2 s^{-1}$). Uplift by an amount z_u will change the surface temperature by $\Delta T_0 = z_u g_e$, where g_e is the decrease in surface temperature with elevation (approximately 7 K km^{-1}). According to equation 3.4, rapid uplift of 3,000 m at 120 Ma affects the present-day geothermal gradient by less than 0.2 K km^{-1}, i.e. less than 1 % of an unperturbed gradient of 25 K km^{-1}. We also use expression 3.4 to assess the effects of rapid erosion. If the thickness of the eroded material is z_e and g_u is the unperturbed geothermal gradient, the surface will have experienced a temperature change of $\Delta T_0 = z_e g_u$. The present-day effect of 2,000 m of rapid erosion at 100 Ma computed with the same equation is 0.5 K km^{-1}, about 2 % of the unperturbed

gradient. The above results show that rapid uplift and erosion 120 Ma ago contributed insignificantly to the present-day heat flow.

A slower and more continuous uplift and erosion, continuing to the present-day, may have a small effect on the present-day heat flow. Carslaw and Jaeger (1959) present an analysis that leads to the following equation to evaluate the effects of continuous uplift and erosion at a constant rate upon the geothermal gradient at the surface:

$$g(t) = g_u + \frac{1}{2}\left(g_u + \frac{g_e u}{v}\right)\left[-\operatorname{erf}\left\{\frac{-vt}{2\sqrt{(\alpha t)}}\right\} - \frac{vt}{\sqrt{(\pi\alpha t)}}\exp\left\{-\left(\frac{vt}{2\sqrt{(\alpha t)}}\right)^2\right\}\right.$$
$$\left. - \frac{vt}{\sqrt{(\pi\alpha t)}}\exp\left\{-\left(\frac{-vt}{2\sqrt{(\alpha t)}}\right)^2\right\} + \left\{1 + \frac{v^2 t}{\alpha}\operatorname{erf}\left(\frac{vt}{2\sqrt{(\alpha t)}}\right)\right\}\right] \quad (3.5)$$

where g(t) is the affected gradient as a function of time t, g_u is the unperturbed gradient, g_e is the decrease of surface temperature with elevation, v is the velocity of the medium (negative for erosion) with respect to the moving surface boundary, u is the rate of movement of the surface boundary with respect to a fixed reference (i.e. the velocity of uplift) and α is the thermal diffusivity of the medium. We choose extreme values for the variables to assess the maximum expected effect: the area of the Ponta Grossa Arch and eastern margin of the basin (presently at 1,000 m) is assumed to have been uplifting continuously since 120 Ma by 3,000 m and that 2,000 m have been removed by erosion. This translates to an uplift rate of 25 m Myr^{-1} and an erosion rate of 17 m Myr^{-1}. The present day perturbation to the gradient, and thus to the heat flow, would be an increase of up to 5 % with respect to an undisturbed gradient of 25 K km^{-1}.

Most thick sedimentary sequences in the Paraná Basin represent deposition of hundreds of meters of sediments over time periods of a few millions of years, whereas the 'deposition' of the flood basalts was much quicker. Paleomagnetic studies by Ernesto and Pacca (1988) suggest that up to 1,000 m of lava were piled up in 1 Myr or less during the Serra Geral igneous event. Of the order of 1.7 km of basalt has been deposited in the basin center in a short period of time. Rapid deposition results in the subsidence of the cold rock beneath the basalt into the subsurface, thus decreasing temporarily the geothermal gradient. Calculations show that the perturbation to the temperature gradient within the basin decays to insignificance within 6 Ma of the sudden subsidence caused by the flood basalt extrusion, thus the depositional aspect of the basalt has no effect on the present-day heat flow. This is a maximum estimate of the effect, as it will be attenuated because the basalt is deposited 'hot' so that the underlying cold rock is warmed both from above and from below.

To summarize, the processes of uplift and erosion have been active principally at the eastern margin of the Paraná Basin, and the thermal effects tend to increase the geothermal gradient in this region. The central part of the basin was last affected by deposition of the Serra Geral flood basalts. The calculations carried out above suggest a maximum increase of about 5 % to the present-day geothermal gradient at the basin margin due to uplift and erosion and no effect in the basin center due to the rapid deposition of the flood basalts. Taken together, transient effects could amount to a variation of 5 % in the geothermal gradient and heat flow across the basin. We note that these effects produce the same pattern in heat flow as the observed one, but the magnitude is too small, less than 3 mW m^{-2}, i.e. a factor of 7 smaller than the full regional variation of 20-25 mW m^{-2} that is observed.

3.1.3 Surface Temperature History

Surface temperature changes occur at many different time scales: diurnal, seasonal and longer periods related to climatic variations. Changes in vegetation (agriculture, deforestation), construction (urbanization) and in the distribution of bodies of water (lakes, dams) influence the surface heat dynamics, and accompanying surface temperature changes are propagated in the subsurface. Short period changes affect only shallow depths while changes over longer time spans penetrate deeper, but are damped in amplitude. It is easily shown that for whatever reason the surface temperature in the Paraná Basin may have changed anthropogenically or climatically over time, the effects on the deep temperatures we have used to determine the heat flow can be neglected. Long period temperature changes related to periods of glaciation, for example, or to the change in latitude due to continental drift penetrate deeper, affecting the subsurface temperature field at depths of the order of kilometers. Nevertheless these changes affect large areas uniformly, so that no heat flow variation across the region is created.

3.2 Steady State Thermal Effects

3.2.1 Topography

Isotherms in the subsurface tend to follow the topography, with a crowding of isotherms under valleys, and a separation of isotherms beneath topographic highs, with the result that thermal gradients under hills are lower than under valleys (Kappelmeyer and Haenel, 1974; Powell et al., 1988). The affected depth scale is roughly equivalent to the wavelength of the topography (Turcotte and Schubert, 1982). Although thermal effects of locally rugged topography are more likely to be significant, these would affect temperatures measured at shallow depths of the order of hundreds of meters. In most of the Paraná Basin the shorter wavelength topography comprises smooth rounded low hills with some valleys deeply incised in the Serra Geral flood basalts.

However, the temperatures on which this study is based were taken mostly at depths greater than 1,000 m, so small wavelength topography can be neglected, as the perturbation will have decayed to insignificance at the measurement depths. The effects of large wavelength topography can also be easily assessed. At present the highest elevations of the order of 1,000 m are found on the eastern border of the Paraná Basin in the Serra do Mar mountain range that follows the Atlantic margin of most of southern Brazil. The elevation drops towards the west and southwest to altitudes of less than 200 m at the Paraná River some 500 km away. We represent the Serra do Mar mountain range as a longitudinally extended range with a peak elevation of 1,000 m and a width at half-height of 250 km. The maximum perturbation to the surface geothermal gradient at the peak of the mountain is given by Lees (1910) as:

$$\Delta g = \frac{-b_o}{b_1^2} \quad \text{, where} \tag{3.6}$$

$$b_0 = (g_u - g_t) h \sqrt{\frac{h^2}{4} + b^2}$$

$$b_0 = (g_u - g_t) h \sqrt{\frac{h^2}{4} + b^2}$$

where Δg is the difference between the measured (perturbed) gradient and the unperturbed thermal gradient g_u (assumed for calculation purposes to be 25 K km^{-1}), g_t is the gradient of mean annual air temperature with elevation (approximately 7 K km^{-1}), h the height of the mountain ridge crest (1 km), and b the half-width of the mountain at half height (125 km). The substitution yields $\Delta g \approx -0.12$ K km^{-1}, or less than 0.5 % of the unperturbed gradient. Therefore, long wavelength topographic effects related to the Serra do Mar range are also insignificant.

3.2.2 Large scale thermal conductivity contrasts

The geometric mean thermal conductivity of the basin fill decreases from 3.0 W m^{-1}K^{-1} at the eastern margin to less than 2.0 W m^{-1}K^{-1} in the central region of the Paraná Basin (Figure 2.8). The flood basalt cover increases in thickness from a few hundred meters to 1.7 km in this same direction. The basalt is the unit with lowest thermal conductivity in the stratigraphic column of this basin and contributes increasingly to the total thermal resistance towards the center. One can conceive that such a large body (10^6 km^2 surficial extent) of low conductivity may induce a divergence of heat around it into the surrounding areas without basalt cover. In order to estimate the effect of this low conductivity unit upon heat flow we have computed the heat flow contrast expected between a location at the center of the basalt cover and one distant from it. We describe

the basalt cover as a hemiellipsoidal trough of low conductivity (k_b =1.8 W $m^{-1}K^{-1}$) basalt within the higher conductivity sediments (k_s = 3.0 W $m^{-1}K^{-1}$). The hemiellipsoid is described by its three axis m, n and l (Figure 3.3). We assume that m=n (circular surface) = 300 km and l = 2 km (maximum basalt thickness). The ratio of heat flow in the two locations is given by :

$$R = \frac{\frac{k_b}{k_s}}{1+\left[\frac{k_b}{k_s}-1\right]F} \text{ ,where } F = \frac{lm^2}{(m^2-l^2)^{\frac{3}{2}}}\left\{-\frac{\pi}{2}+\arctan\left(\frac{l}{(m^2-l^2)^{\frac{1}{2}}}\right)+\frac{(m^2-l^2)^{\frac{1}{2}}}{l}\right\} \qquad (3.7)$$

where R is the ratio of heat flow at the center of the hemiellipsoid to that of the unperturbed background heat flow (Von Herzen and Uyeda, 1963). On substitution, R = 0.995, i.e the resulting heat flow contrast amounts to less than 0.5 % the mean heat flow for the Paraná Basin (less than 1 mW m^{-2}), too little to account for the observed contrast between basin center and margin. The basalt cover has great lateral extent compared to its thickness, and heat from below is mostly transported through the sheet instead of diverted around it. Thus the flood basalts themselves are not the direct cause of the heat flow contrast.

Molina et al. (1989) in interpreting and modeling gravity anomalies from surveys in the northern Paraná Basin, suggest that the extrusion of flood basalt may be accompanied by underplating and intrusion of mafic material in the lower 10-20 km of the crust. White and McKenzie (1989a,b) argue that large volumes of melt can be generated under lithosphere in extension, by adiabatic decompression of rising mantle material, a situation that may precede continental rifting. McKenzie and Bickle (1988) show that decompression of upwelling asthenospheric material will produce basaltic liquids and form tholeiitic basalts typical of continental flood basalt provinces when extruded. Only a fraction of the melt produced by decompression is extruded at the surface. White (1989) estimates that at least the same amount of melt is trapped as an underplate beneath the crust and that perhaps the total volume of igneous rocks emplaced could be a factor of two to three greater than the extruded portion. Furlong and Fountain (1986) argue on the basis of model calculations that a layer of 10-15 km of underplated material can be generated and emplaced within 5 Ma. The Serra Geral flood basalts thus may represent only a fraction of the total volume of melt generated in the mantle during the igneous event that preceded the opening of the South Atlantic. Molina et al. (1989) suggest that the residue that did not ascend to the surface may have solidified in the subsurface, intruding the lower crust and underplating it with high density mafic material as illustrated schematically in Figure 3.4. Such intruded and underplated mafic low thermal conductivity material beneath the central part of the Paraná Basin could contribute to a heat flow contrast at the surface.

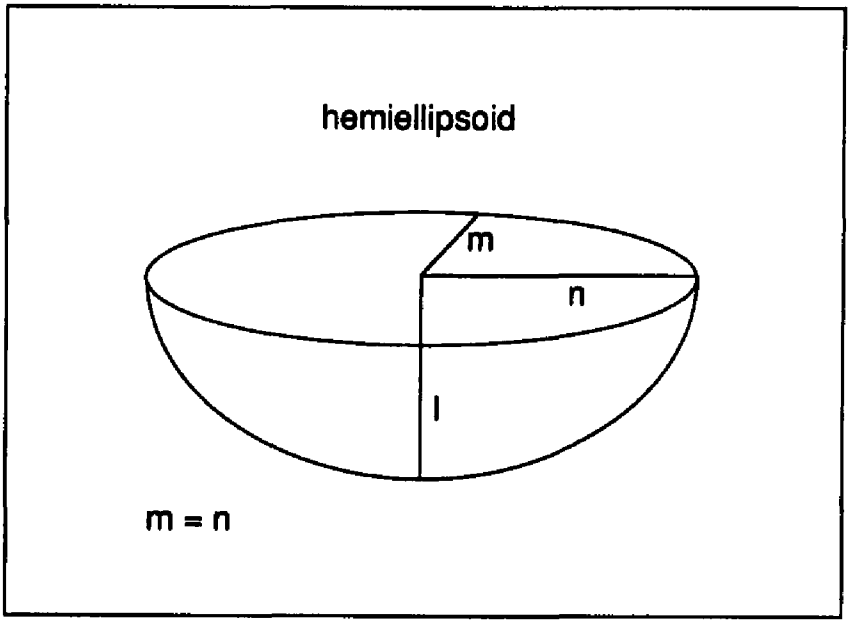

Figure 3.3 Hemiellipsoid model adapted from Von Herzen and Uyeda (1963).

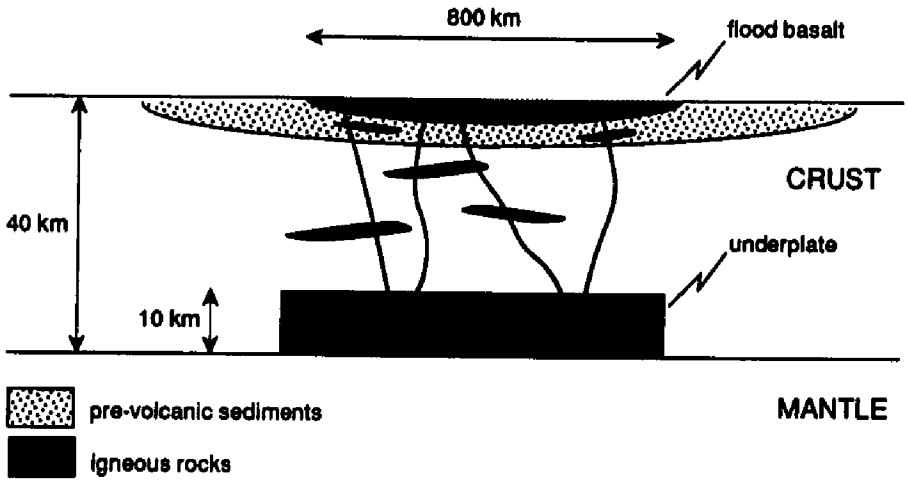

Figure 3.4 Cross-section of Paraná Basin (modified from Molina et al., 1989) showing flood basalts, sills, dykes and underplate.

Underplating can affect surface heat flow in at least three ways: (1) by introducing a low thermal conductivity region within the crust that diverts heat around it, (2) by introducing material with a low heat production rate relative to the host crustal rocks, and (3) by thickening and stabilizing the magma source region in the lithosphere through basalt depletion (Jordan, 1978, 1981, 1988), thus causing lower temperatures and gradients in the depleted lithosphere. The latter two effects will be assessed subsequently, but the conductivity effect is considered here.

The effect of crustal conductivity contrast can be assessed making use of a numerical finite difference model that solves the heat conduction equation allowing vertical and lateral variation in thermal conductivity and radiogenic heat production rates (Speece et al., 1985; Henry and Pollack,1988). We assume a 'normal' crust and lithosphere with mean thermal conductivity of 3 W $m^{-1}K^{-1}$, intruded by an underplate with a conductivity of 1.8 W $m^{-1}K^{-1}$ and the geometry shown in Figure 3.4. The underplate is set between 30 km and 40 km depth in the lower crust and has the same lateral dimensions as the surface basalt flows. The 10 km corresponds to a volume more than five times the extruded basalt volume. The extent of flood basalt at the surface suggests a constraint on the maximum lateral extent of underplating, as heat flow increases with distance from the basalt rim. The heat flow contrast at the surface predicted from this model is 3 % with respect to the unperturbed heat flow of the region, amounting to 2 mW m^{-2}, less than the 20-25 mW m^{-2} observed difference across the Paraná Basin.

3.2.3 Large scale heat production contrasts

Variable heat flow from the sub-basin basement can arise also from differences in radiogenic heat production in the basement rocks. The present day extent of the Paraná Basin is of the order of 10^6 km^2. On the basis of crustal variability observed in exposed areas of basement both in South America and elsewhere in the world, the Paraná Basin can be expected to cover a variety of crustal rocks of different origins and compositions that invariably contain lateral differences in the rate of radiogenic heat production. The actual configuration of the sub-basin basement is largely unknown, although some attempts have been made to relate basement core samples to the outcroping basement surrounding the basin. Cordani et al. (1984) carried out a systematic petrologic and geochronologic investigation of drill cores from the basement of the Paraná Basin. The identification of lithologic types and ages permitted correlation of many samples with the surrounding outcropping basement of cratonic blocks and mobile belts. Most ages correspond to the Brasiliano orogeny, although a few older ages of 900-2200 Ma were recorded. Generally there seems to be agreement that the Paraná Basin covers a complex mosaic of crustal segments from different mobile belts, and perhaps including even an Archean cratonic nucleus.

Samples from the drill cores included andesite, rhyolite, gabbro, diorite, granodiorite, granite, quartzite, gneiss, amphibolite and granulite. A survey of radiogenic heat production rates for these rock types in Rybach (1988) shows values ranging from 0.31 $\mu W\ m^{-3}$ (gabbro) to 2.45 $\mu W\ m^{-3}$ (granite), practically an order of magnitude in variation. Vitorello (1978) reports a mean heat production rate for the Brazilian Coastal shield of 1.41 $\mu W\ m^{-3}$. In order to estimate the effect upon surface heat flow of heat production contrasts it is necessary to know, in addition to the lithologies and respective radiogenic heat production rates, also their thickness and extent. A detailed discussion of the different approaches of estimating mean heat production values for the crust is found in Ballard (1987) and Nyblade (1992), but none are without considerable uncertainty. Although we know that the basement underlying the Paraná Basin comprises several crustal units of differing ages and composition, an assessment of the heat production variation is precluded on the one hand from the scarcity of samples and heat production determinations, and on the other hand, from the lack of constraints on geographic and depth extent of these crustal units. However, unless the scale of crustal heterogeneity beneath the Paraná Basin differs markedly from the heterogeneity exhibited in exposed Precambrian terrains, we believe that heat production contrasts due to the heterogeneity of the crust underlying the Paraná Basin would not produce a coherent regional pattern as is shown by the heat flow .

A possible source of anomalously high heat production are alkaline intrusions. Herz (1977) discusses various alkaline intrusions within the basement surrounding the Paraná Basin and relates them to the history of the opening of the South Atlantic. We mention as an example the alkaline intrusion of Poços de Caldas located on the boundary between the states of São Paulo and Minas Gerais within the Ribeira mobile belt, with a radiogenic heat production rate of 29 $\mu W\ m^{-3}$, an order of magnitude or more greater that most igneous rocks. Of more specific interest here are intrusions within the Paraná Basin proper. Zalán at al. (1991) report that several geophysical anomalies are interpreted as probable alkaline intrusions without surface expression. However, the effects of these bodies are localized, and are unlikely to be the source of the widespread higher heat flow in the eastern part of the Paraná Basin.

The extruded flood basalts mentioned earlier in the context of a large scale thermal conductivity contrast, may provide a large scale heat production contrast as well: mafic rocks have low heat production rate compared to most other continental crustal rocks. We again use the finite difference numerical model applied earlier to compute the effects of thermal conductivity contrasts, to determine the difference in surface heat flow caused by heat production contrasts that arise from the extruded basalt and underplating in addition to the thermal conductivity contrast. A value of 0.4 was assigned for the heat production ratio between mafic and average crustal material; zero radiogenic heat production was assigned for the ultramafic lithospheric and asthenospheric mantle. The heat flow contrast produced by the model at the surface is 10 %,

such that with respect to the mean heat flow of 56.3 mW m^{-2}W, this would account for a variation of about 6 mW m^{-2} in the surface heat flow. Although this is not sufficient to produce the full variation in heat flow observed in the Paraná Basin, we believe that heat production and thermal conductivity contrasts in the crust as a result of underplating must be considered as part of the explanation of the heat flow pattern in the Paraná Basin. Considerable uncertainty exists in estimating crustal thickness, the thickness of the underplated region, and the heat production contrast between underplated and host rocks; the lack of data precludes a well constrained estimate of the heat production contrast and its variation with depth. To summarize, if we consider the combined effects of thermal conductivity and heat production contrasts of both flood basalt at the surface and the subsurface underplated material, the finite difference model predicts heat flow variations of the order of 6 mW m^{-2}, thus accounting for about 25 % of the observed variation.

3.2.4 Lithospheric thickness

Lower heat flow in Archean cratonic terrains increasing from the craton center towards surrounding mobile belts appears to be a first order heat flow pattern in East and Southern Africa (Ballard and Pollack, 1987) and is also recognized in other Archean cratonic areas of the world (Nyblade, 1992).The mechanism proposed to explain this pattern is the existence of deep cratonic roots capable of diverting deep mantle heat away from the craton into the thinner surrounding mobile belts (Ballard and Pollack, 1987). We have noted the similarity between heat flow patterns in the Paraná Basin and southern Africa in the preceding Chapter II. The pattern of heat flow variation as a function of distance from the basin's axis displayed in Figure 3.1 shows a striking similarity with figures depicting heat flow variation as a function of distance from cratonic centers presented for the African, European and North American cratons by Nyblade (1992). The existence of a thick Archean cratonic nucleus underlying the central part of the Paraná Basin has not been demonstrated, but if one existed, the heat divergence mechanism could be invoked to explain the heat flow.

An alternative hypothesis is a thickening of the lithosphere as a result of the Serra Geral igneous activity. Basalt melts are believed to be generated by partial melting of small fractions (of the order of 5 - 10 %) of mantle material (Yoder, 1976). Therefore, the voluminous flood basalts, ubiquitous associated intrusives, and likely underplate of the Serra Geral igneous event indicate that a substantial portion of the lithospheric mantle must have been involved in this large scale melting event. The extraction of melts from the upper mantle leaves an altered residuum in the upper mantle, depleted in basaltic components and volatiles. This depletion has been suggested as the mechanism for cratonization and thickening of the continental lithosphere (Jordan, 1978, 1981, 1988; Pollack, 1986), making it more refractory to further thermal and mechanical

perturbation. This residual mantle acts as a zone of increased thermal resistance allowing the heat diversion mechanism mentioned earlier in the context of Archean cratonic root to operate, but in this case the thickened zone underlying the Paraná Basin would be of Mesozoic age.

The extent of a zone of basalt depletion depends upon the total volume of melt, i.e. the extruded flood basalts plus the underplate, extracted from the parental material, and upon the degree of partial melting needed to produce the basaltic liquid of the appropriate composition. As discussed earlier, the igneous rocks extruded, intruded and underplated in the Serra Geral event may yield contrasts of 6 mW m^{-2} in surface heat flow. To make up the balance of the observed contrast of 20-25 mW m^{-2}, a thickened lithospheric region should redistribute enough heat to produce a contrast of 32 % of the mean heat flow of the basin. The finite difference numerical model introduced earlier is applied to assess the effects of a lithospheric thickening of 20 km and 100 km beneath the Paraná Basin. A schematic of this situation is given on Figure 3.5. Here two different thermal regimes are active: within the lithosphere and the thickened zone heat transfer is by conduction, whereas in the underlying asthenospheric mantle it is by convection. We simulate the effects of convective heat transfer by using a parameterized convection approach embodying an enhanced thermal conductivity in the asthenospheric region of the model (see Nyblade (1992) for a discussion of parameterized versus full thermal convection algorithms). We have included in Figure 3.5 an example of the results for this model and for comparison purposes also the results of previous calculations involving the effects of the surface flood basalt and underplated region. The measured heat flow data to the east of the Paraná River is also displayed for comparison. The heat flow in this figure is normalized to a background heat flow, i.e. heat flow that would result in the absence of flood basalts, underplate and thickening of the lithosphere. We use here as a reference 60 mW m^{-2}. The application of the finite difference numerical model shows that a heat flow variation of 7 - 25 % (4 - 18 mW m^{-2}) can be obtained with thickened zones extending 20 - 100 km beneath the original lithosphere. The model results also suggest that variations between 4 and 14 mW m^{-2} can be obtained due to the thickened zone alone and that the combined effects of flood basalts, underplate and lithospheric thickening will account for variations of 10 to 20 mW m^{-2}. The curves on Figure 3.5 indicate the magnitude of these effects. The models do not attempt to resolve the geographic pattern of variation in detail, but virtually any transition can be achieved by varying the shape of the subsurface structures.

We now estimate the range in degrees of partial melt capable of producing a thickened region of this magnitude. Very low degrees of partial melt must deplete larger regions of the mantle and vice-versa. We have computed the degrees of partial melt required to produce a thickening of 20 - 100 km to an initial lithosphere for a range of total resulting igneous rock volume, corresponding to 2 km of flood basalt plus 2 - 10 km of underplated material. Depending on the amount of underplated material, partial melting in the range 4 - 13 % is required in order to

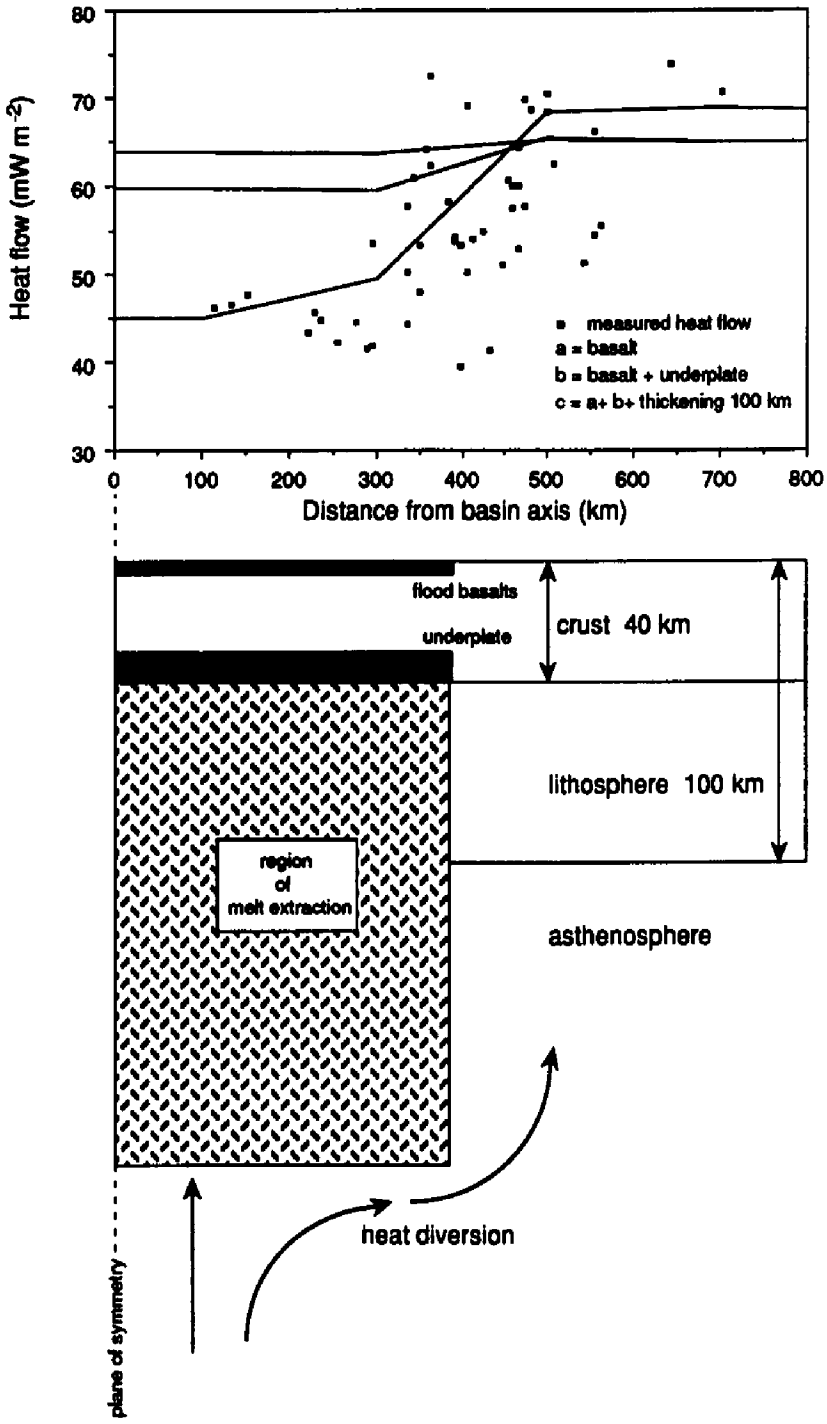

Figure 3.5 Lithospheric model for the Paraná Basin. Graph shows variation of heat flow arising from thermal conductivity and heat production contrasts and variations in lithosphere thickness. Curves correspond to the effects of: (a) flood basalt only, (b) flood basalt plus underplate, (c) cumulative effects of flood basalt, underplate and lithospheric thickening by 100 km.

produce the desired thickening. These fractions of partial melting are in agreement with estimates (5-10 %) for the generation of basaltic fluids from a parental garnet peridotite (Yoder, 1976; McKenzie and Bickle, 1988). Therefore a thickened lithosphere with the characteristics described above is one mechanism capable of providing sufficient heat flow contrast to account for the observed difference in heat flow across the Paraná Basin.

Another mechanism to explain the enhanced heat flow at the eastern margin of the Paraná Basin with respect to its center, also involving a lithosphere of variable thickness, is lithospheric thinning from the center to the margin of the basin in association with the extension that led to rifting and the opening of the South Atlantic (Harry and Sawyer, 1992). As with the basalt thickening model, calculations show that a thinning of 20 - 100 km will produce about 0.25 to 1.0 of the required heat flow contrast, with more severe thinning yielding even more. Together with the effects of the igneous rocks, thinning of this order can also reproduce the observed heat flow pattern.

Numerical modelling of variation in lithospheric thickness has shown this to be a viable mechanism for producing the large scale heat flow contrasts observed in the Paraná Basin. Thickening the lithosphere beneath the basalt by 20 - 100 km, by means of basalt depletion, can provide heat flow contrasts of 4 - 20 mW m^{-2} at the surface, if partial melting degrees in the range of 4 to 13 % has occurred. Alternatively, the same effect is accomplished by thinning the lithosphere by 20 - 100 km from the center to the eastern margin of the basin by extension.

3.2.5 Subsurface fluid flow

Heat flow patterns elsewhere have also been explained as arising from subsurface fluid flow, for example in the Uinta Basin (Willett and Chapman, 1987) and the Alberta Basin (Majorowicz et al., 1986), among others. Generally the observations show lower heat flow in the topographically high recharging areas, compared to heat flow measured in the topographically lower discharge regions of these basins. The Serra do Mar uplift has created a possible system for subsurface flow, in which meteoric water flows from the elevated recharge area (eastern basin margin at 1,000 m) through the subsurface towards the Paraná River discharge area along the axis of the basin at 200 m elevation. A schematic representation of this scenario is given in Figure 3.6. Temperature profiles in Hamza et al. (1978) and Santos (1986) show evidence of pervasive hydrologic disturbance in shallow wells (300 m deep) penetrating sedimentary rocks and basalt flows. Fractured regions within the Serra Geral basalts and probably in the contacts between individual basalt flows provide vertical and horizontal pathways for fluids. The hydrologic role of the ubiquitous diabase sills in subsurface fluid flow is not clear. Sill intrusion appears to preferentially intrude shaly formations such as the Irati formation (Zalán et al. 1991) and may provide fracture permeability within formations otherwise considered of very low permeability. These

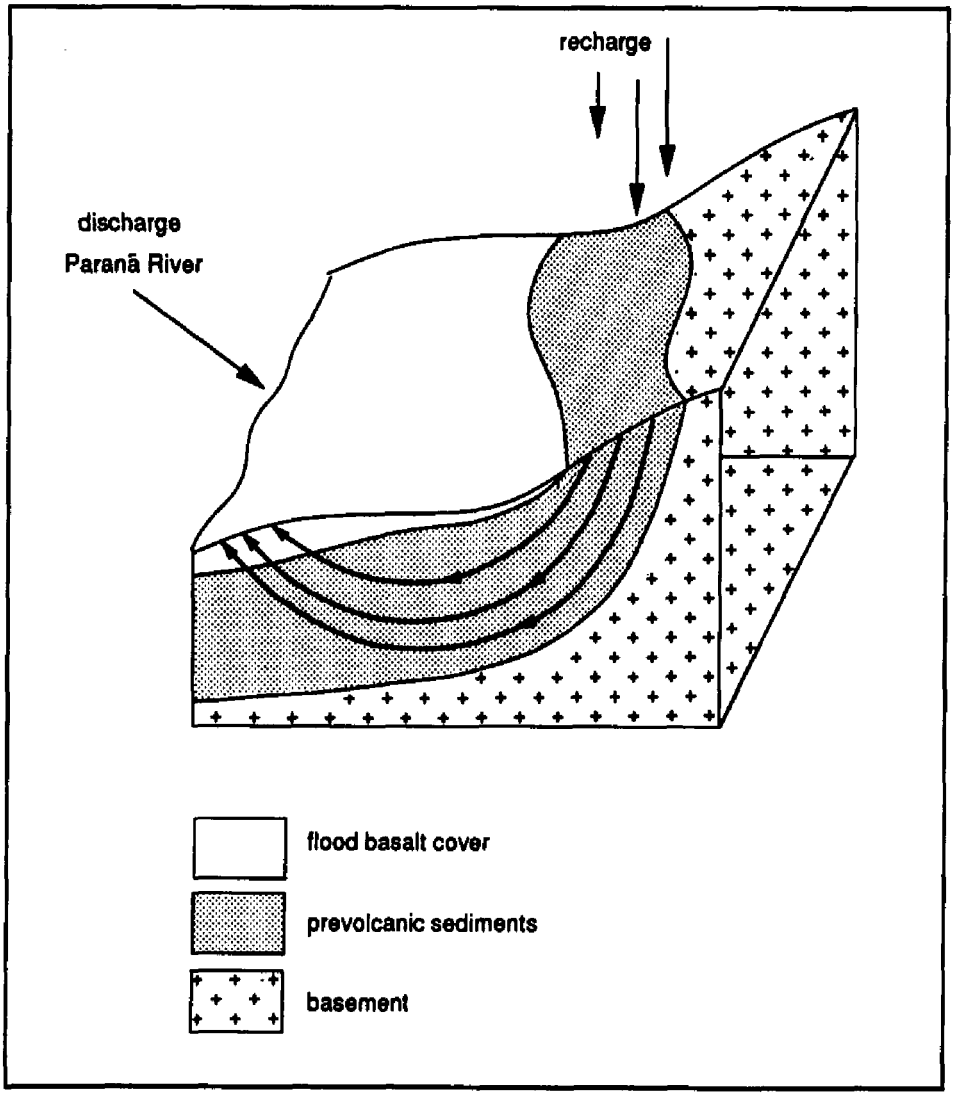

Figure 3.6 Schematic diagram of subsurface fluid circulation for the Paraná Basin.

considerations suggest that the details of subsurface fluid flow may be quite complex. The general effect from downward migrating cool fluids in the subsurface would be to decrease heat flow close to the recharge area (eastern margin) and increase it in the discharge areas (along the Paraná river), where the fluids migrate upwards. This pattern is opposite to that of the observed heat flow pattern, but we cannot preclude its possible existence. If such a regional flow pattern does exist and is of sufficient magnitude, it would imply that the observed heat flow contrast from basin center to margin is a muted expression of what would exist in the absence of a hydrologic perturbation.

Rebouças (1976) proposed a hydrostratigraphy of the Paraná Basin, in which the Botucatu and Rio do Rasto formations (see stratigraphic column in Figure 2.2) are the most permeable aquifers with permeabilities ranging from 10^{-12} m^2 to 10^{-11} m^2, followed by the Palermo and Rio Bonito formations and possibly the Furnas formation with permeabilities one to two orders of magnitude lower than the first. The Teresina, Serra Alta and Irati formations and the Itararé and Ponta Grossa formations are considered aquicludes with permeabilities of less than 10^{-15} m^2. This permeability data suggests that fluid flow may be concentrated in the upper 1,500 m (average maximum depth of the Botucatu + Rio do Rasto aquifer) of the basin and therefore temperatures at greater depths may suffer very little perturbation. Only 17 BHTs among the 187 upon which the heat flow data is based originated in the Botucatu + Rio do Rasto aquifer, hence most temperature measurements in boreholes used in this study reach beyond the more permeable shallow formations. The investigation of a fluid flow component to the thermal field within the Paraná Basin depends on a more detailed regional analysis of the temperature structure, and is adressed in Chapter IV.

4. DISCUSSION AND SUMMARY

We have examined factors and processes that may affect heat flow in the Paraná Basin and explain its variability. Now we summarize and discuss the results of these effects. There is no evidence of residual effects related to the cooling of the Serra Geral igneous rocks (flood basalt, intrusives and underplate) in the present-day heat flow. Changes in surface temperature history upon the temperature measurements used to determine heat flow are negligible. The effects of uplift and erosion reinforce each other to increase present-day gradients at the eastern margin of the basin, while the deposition of the flood basalt in the basin center at 120 Ma has no present-day effect on heat flow in that area. The combined effects of uplift, erosion and sedimentation can account for a maximum difference in heat flow between the central region and the basin margin of 7 %, but more likely less. The observed variation in heat flow (see Figure 3.1) is about a factor of five larger and cannot be explained by these processes alone.

Subsurface fluid flow would tend to produce effects opposed to the heat flow pattern that is observed. If a significant effect could be attributed to subsurface fluid flow, this would imply that the observed heat flow pattern has been attenuated and that in the absence of heat advection by fluids the observed differences in heat flow would be amplified. A more detailed study of the thermal consequences of fluid flow is addressed in Chapter IV, but the preliminary inspection of available hydrologic data suggests that subsurface flow may be significant only in the upper more permeable formations of the basin. The heat flow being discussed here derives mostly from temperature measurements made within the deeper less permeable formations.

A two-part hypothesis to explain the pattern of heat flow variation in the Paraná Basin relates to the crustal/lithospheric structure and history of the basement underlying the basin: (1) underplating associated with the extrusion of the Serra Geral flood basalts could provide a region of low thermal conductivity and low radiogenic heat production in the lower crust beneath the central region of the Paraná Basin and (2) the existence of thickened lithosphere generated as a consequence of basalt depletion underlying the central part of the basin may divert deep mantle heat away from the central region into the thinner lithosphere underlying the basin margin and surrounding folded belts. These two mechanisms of producing lower heat flow in the basin center and higher heat flow towards the eastern margin are not mutually exclusive. The thermal effects of flood basalts at the surface and underplating in the lower crust due to the combination of thermal conductivity contrast and radiogenic heat production contrast yield differences of the order of 10 % of the mean heat flow. An underplate alone can account for only part of the observed heat flow variation. The modelling of heat diversion by a zone of thickened lithosphere generated through basalt depletion suggests that this mechanism can provide a heat flow contrast at the surface of the appropriate amount or larger. The same effect can be achieved by thinning the lithosphere at the eastern margin of the basin. It appears that crustal and shallow processes and structures cannot alone explain the large scale heat flow pattern across the Paraná Basin. Deeper causes must be invoked; variation in lithosphere thickness (thickening beneath the basin center or thinning beneath the basin margin) can easily provide the observed contrasts in heat flow.

In order to choose or dismiss any of these possibilities more geophysical data is needed. Deep seismic studies could provide the evidence supporting underplating, if high velocities were recorded in the lower crust as predicted to occur in underplated regions by Furlong and Fountain (1986). High Bouguer anomalies over the northern central region of the Paraná Basin (Molina et. al., 1991) support the existence of underplating, but a thinned lithosphere also is capable of explaining this anomaly. The same comments can be made for interpreting the region of the Ponta Grossa Arch, also a locus of a high Bouguer anomaly. Evidence for the existence of thickened lithosphere typically comes from seismic tomography (see, for example, Grand, 1984)

or from petrological studies of mantle xenoliths (Boyd and Gurney, 1986). Such studies are still lacking, however, for the lithosphere of southern Brazil.

CHAPTER IV

THE PRESENT-DAY THERMAL STRUCTURE OF THE PARANÁ BASIN, SOUTHERN BRAZIL

ABSTRACT

We present an analysis of the present-day thermal structure of the intracratonic Paraná Basin in southeastern South America. Bottom hole temperature (BHT) and stratigraphic data were subjected to a least squares inversion to obtain estimates of formation gradients for 14 representative formations. A perturbation analysis, involving the introduction of random temperature perturbations of varying magnitude into the data set shows that the inversion is quite stable: the range in geothermal gradients obtained from perturbed data sets does not extend beyond that given by the standard deviation computed from the original data set. The inverted gradients and formation thicknesses yield a best fitting temperature field for the Paraná Basin. Temperature residuals, i.e. the difference between best fit temperature and measured BHT, represent mostly noise in the data due to measurement error and local geology. The best fit temperature field shows a coherent pattern in which above average temperatures occur persistently with depth in the northern basalt covered part of the basin, whereas below average temperatures are found at the eastern margin of the basin without basalt cover. We examine several possible contributions to the temperature field: measurement and geological noise, conductive and non-conductive heat transport. Deviations from mean best fitting temperatures and deviations from mean temperatures obtained from modeling conductive and advective heat transport are compared. Mean model temperatures and their deviations obtained from conductive heat transport show agreement with best fit mean temperatures and deviations. Modeling advective heat transport showed that perturbation to subsurface temperatures are restricted to narrow zones of recharge and discharge, not affecting heat flow over most of the basin. Subsurface temperature variations in the Paraná Basin appear to arise mostly from the lateral variation in stratigraphic units, and the heat flow at the surface reflects the heat input from the basement with only minor , if any, redistribution by fluid flow.

1. INTRODUCTION

Analysis of BHT data sets in sedimentary basins have been applied successfully to reveal details of the subsurface thermal structure and to evaluate the effect of subsurface fluid flow, lateral facies changes in the sediments and varying basement heat flow (Bachu 1985, 1988; Bachu and Burwash, 1988; Chapman et al., 1984; Majorowicz, 1985, 1986; Majorowicz and Jessop, 1981a, 1981b, 1985; Majorowicz et al., 1985, 1986; Speece et al., 1985; Willett and Chapman, 1989). Here we use a discrete least squares inversion procedure to analyze in more detail the regional variation in subsurface temperature field of the Paraná Basin and factors that may affect it. In particular this inversion methodology provides estimates of the geothermal gradient in each stratigraphic unit encountered in the basin. This approach is similar to that used by Speece et al. (1985) in the Michigan Basin and by Chapman et al. (1984) and Deming and Chapman (1988) in the Uinta Basin. The resulting best fit temperature field for the Paraná Basin is examined and various possible factors that influence the thermal field are discussed: lateral heterogeneity in the basin , non-uniform heat flow from the basement and subsurface fluid flow. We employ a numerical model of conductive and advective fluid and heat transport to assess the magnitude of these effects and compare the best fit thermal field with the field resulting from the model.

2. INVERSION THEORY

In this inversion analysis we interrogate the data set for the mean temperature gradients *in each formation*, in contrast to the average temperature gradient calculated in Chapter II for the entire sedimentary section penetrated by each borehole. We structure the problem initially by assuming that heat transfer is by thermal conduction and is one-dimensional (vertical). Under these assumptions, at the j-th borehole the temperature difference ΔT_j between the bottom of the hole and the surface can be written in terms of the sum of temperature increments across each of n formations:

$$\Delta T = (T_{BH} - T_o)_j = \sum_{i=1}^{n} \left\{ \frac{\partial T}{\partial z} \right\}_i h_{ij} = \sum_{i=1}^{n} g_i h_{ij} \qquad (4.1)$$

where h_{ij} is the thickness of the i-th formation in the j-th borehole and $g_i = (\partial T/\partial z)_i$ is the geothermal gradient within this i-th formation. A system of equations representing all boreholes can be written in matrix notation

$$\Delta T = g\, H \qquad (4.2)$$

Here ΔT and $\mathbf{g}$ are vectors of dimension n, where n is the number of formations, and $\mathbf{H}$ is an n x m matrix, where m is the number of boreholes. This is a linear system of equations, where ΔT and $\mathbf{H}$ are the data from which the model parameter vector $\mathbf{g}$, the estimates of the formation temperature gradients, is to be determined. This overdetermined least-squares type problem has the solution (see Menke, 1989):

$$\mathbf{g} = [\mathbf{H}^T \mathbf{H}]^{-1} \mathbf{H}^T \Delta T \tag{4.3}$$

where the superscript T indicates matrix transpose. The least squares inversion also returns an estimate of the variance of the solution vector $\mathbf{g}$ as detailed in Menke (1989). The expected temperature (T_{exp}) can then be computed by substituting the solution vector $\mathbf{g}$, i. e. the estimated formation gradients into equation 4.2, as shown below:

$$T_{exp} = T_o + h_1 g_1 + h_2 g_2 + ... + h_n g_n \tag{4.4}$$

These temperatures constitute the best estimate of the temperature field according to the model assumptions. They can be compared to the original temperature data, using the temperature residual defined as

$$T_{res} = T_{BH} - T_{exp} \tag{4.5}$$

Temperature residuals arise from both noise in the data and departures of the model assumptions. We later examine the temperature residuals as to magnitude and distribution, and assess their probable causes.

We apply this inversion technique to the stratigraphic and temperature data of the Paraná Basin. Chapter II contains a detailed description of these data, and their characteristics are summarized in Table 2.1. For the purpose of the inversion analysis, we have attributed each BHT to an individual borehole. This means for example that a borehole with three BHTs at different depths is represented as three individual boreholes, each with a stratigraphic column extending from the surface to the depth of BHT measurement. The thicknesses of formations (including the cumulative sill thickness) is properly referred to the section above the individual BHT. Therefore the system of equations contains 167 equations written as a function of gradients and formation thicknesses of 14 formations.

3. RESULTS OF INVERSION

3.1 Estimated formation gradients

Best fitting (in the least-squares sense) geothermal gradients and respective standard deviations obtained for each of the 14 stratigraphic units from the inversion appear in Table 4.1.

Table 4.1 Inversion gradient estimates

Number	Formation	Gradient ($W\,m^{-1}\,K^{-1}$)	Standard Deviation
1	Baurú	7.3	8.6
2	Serra Geral	24.6	1.8
3	sills	20.0	4.7
4	Botucatú	16.7	3.3
5	Rio do Rasto	27.9	2.6
6	Teresina	35.4	4.0
7	Serra Alta	31.5	8.4
8	Irati	11.3	6.6
9	Palermo	15.3	6.7
10	Rio Bonito	27.8	5.0
11	Itararé	21.0	1.6
12	Ponta Grossa	25.1	6.7
13	Furnas	14.4	5.4
14	basement	3.7	4.0

The resulting geothermal gradient estimates range between 3.7 K km^{-1} and 35.4 K km^{-1}. The inversion does not preclude negative gradients, which could occur (mathematically) in formations that are thin and/or poorly represented, but none resulted. The basement and the Baurú formation gradient estimates, 3.7 ± 4 K km^{-1} and 7.3 ± 8.6 K km^{-1}, respectively, are the lowest formation gradients and have the largest standard deviations. These formations are least well represented in the data set: they have the smallest mean thickness, therefore contributing least to the total stratigraphic section. In contrast the Itararé and Serra Geral formations have gradient estimates and standard deviations of 21.0 ± 1.6 K km^{-1} and 24.6 ± 1.8 K km^{-1}, respectively. These gradients are much more typical of gradients in continental platform settings than those estimated for the basement or the Baurú. The Itararé and Serra Geral are the thickest units in the basin. The Itararé is well represented in the data set: it makes up over 24 % of the cumulative mean formation thickness (computed by summing the mean thickness of all 14 stratigraphic units), most boreholes penetrate it fully, 21 boreholes bottom in it, and 59 BHTs have been determined in it (see Table 2.1). The Serra Geral formation is similarly thick and penetrated by 46 boreholes, but has no BHTs. Its standard deviation is slightly smaller with respect to the magnitude of its estimated geothermal gradient than is that for the Itararé formation.

The correlation between high standard deviations and poor representation in the data ensemble as recorded by the cumulative drilled thickness of a unit is displayed in Figure 4.1 for all 14 formations. Less well represented formations (small percentage cumulative thickness) have large estimated standard deviations. This also has been observed by Speece et al. (1985) in the Michigan Basin and by Deming and Chapman (1988) in the Uinta Basin.

3.2 Stability analysis

The estimated geothermal gradient for each formation is the result of the inversion of a typically noisy data set. Sources of measurement noise (see Speece et al., 1975 for a fuller discussion) include the lack of calibration of thermometers, the temperature measurement not being made at the actual bottom of the hole, random rounding up or down of temperatures by the logger, errors in converting temperatures to Fahrenheit units when measured in Celsius units, recording guesses of temperature instead of actual measurements, and mis-identification of stratigraphic boundaries resulting in erroneous formation thicknesses.

In addition to measurement noise, the possibility also exists of 'geological noise'. Lateral facies changes occur most certainly within the formations of the Paraná Basin, particularly in the non-marine units, and probably at several different scales. Thermal conductivity is a function to first order of the mineral composition of the rock and to second order of its porosity (Brigaud et al., 1990). Therefore facies changes from sandier to shalier facies or from greater to lesser porosity within a formation will translate into conductivity variations. A local increase in the shaly component or increase in porosity means a local decrease in thermal conductivity. Even given no regional variations in heat flow into the sediments, regions of locally lower thermal conductivity compared to the mean will have higher thermal gradients and temperatures. Thermal conductivity measurements made on 247 core samples from 28 boreholes in the Paraná Basin were reported in Chapter II. The mean thermal conductivity and standard errors of the mean for the individual formations are listed in Table 2.2. The standard errors of the mean thermal conductivity include not only measurement uncertainties, but also the lithologic variability in the individual formation to the degree represented by the sampling. Table 2.2 shows that the standard errors of the mean are generally higher than 4 % (the estimated measurement uncertainty), evidence of the heterogeneity of individual formations. Chapman et al. (1984) analyzed lateral facies changes in formations in the intermontane Uinta Basin and report typical variations of 30 % regionally, although locally these could be much larger. In the tectonically more stable intracratonic Paraná Basin regional variations are likely to be less.

Other sources of geological noise are associated with the presence of igneous intrusions and structural features such as faults. The Paraná Basin contains a great number of sill intrusions. Within the inversion these have been taken into account in terms of their expression in thickness

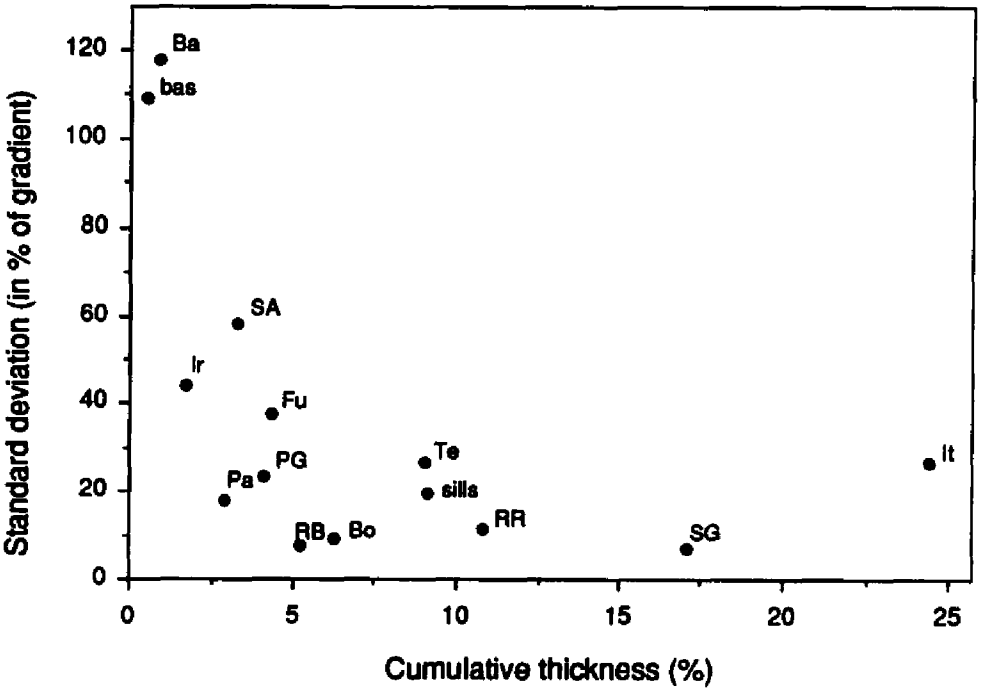

Figure 4.1. Plot of % cumulative drilled thickness of each formation versus the respective standard deviation of the least-squares estimated geothermal gradient.

under the assumption of great lateral extent (one dimensional heat flow). However, it is known that many intrusive bodies loosely termed sills and dykes have very much more complex shapes, constituting bodies of low conductivity embedded in a more conductive sedimentary matrix and altering therefore the thermal field around them. The magnitude of this effect upon the temperature field is proportional to the lateral and vertical dimensions of such bodies. Jones and Oxburgh (1979) have modeled the effect of lenticular bodies of contrasting thermal conductivity and found that variations of 5 - 10 % in the vertical component of heat flow occur in proximity to these bodies, but these effects become insignificant at distances of a few times the lateral dimension of the body. As these kinds of bodies appear rarely to exceed horizontal dimensions of a few tens of kilometers, their thermal effect will be of a local nature. Lateral heterogeneities may arise also from structural features in the basin fill. The structural characteristic of the Paraná Basin is dominantly one of normal blockfaulting. The juxtaposition of different formations due to faulting, provides a temperature perturbation arising from the heat refraction at the boundary between the dissimilar units. The effect is local, contained within proximity of the structure and does not affect the regional temperature field. We conclude that igneous intrusions and faults contribute to the local thermal field, but from the perspective of a regional interpretation of the temperature field their effects can be included in the noise.

In order to assess the sensitivity of the inversion results with respect to uncertainties in the data set, we have computed a series of inversions on a data set in which a random temperature perturbation within the range ± 5.0 °C was added to the original BHT data set. Speece et al. (1985) estimated the noise in the Michigan Basin to be of this order and Deming and Chapman (1988) make an a priori estimate of this order for the error in any individual corrected BHT. Thirty successive data realizations were inverted, each with a temperature perturbation drawn at random in the range ± 5.0 °C. The range of geothermal gradients obtained in these 30 realizations is a measure of the relative stability of each resulting formation gradient. In Figure 4.2 the mean geothermal gradient and its standard deviation, determined from the actual unperturbed data is displayed along with the range in perturbed geothermal gradients. The range in perturbed geothermal gradients is with but one exception (basement) always within the spread given by the standard deviation of the mean geothermal gradients resulting from the inversion of the original unperturbed BHT data set. We can therefore conclude that in the presence of noise of this magnitude the inversion technique has produced stable results for this data set.

4. SUBSURFACE TEMPERATURE FIELD

4.1 Expected temperatures and residuals

The 'expected' temperatures (T_{exp} as defined in equation 4.4) constitute the best estimate of the actual temperature field at a location in the Paraná Basin according to the model

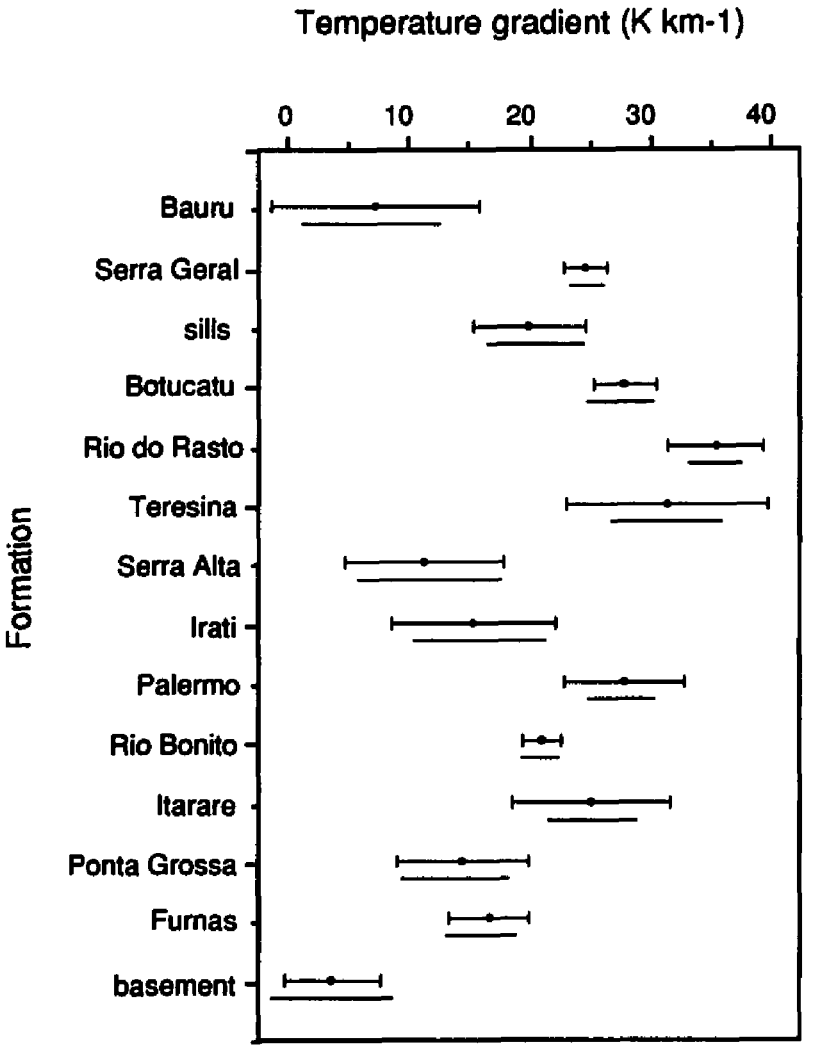

Figure 4.2. Inverted geothermal gradient with standard deviation for each formation, below which the range of inverted geothermal gradients obtained using BHTs perturbed with ± 5 °C random noise. The range of perturbed gradients is less than the standard deviations of inverted gradients with the exception of the basement.

assumptions. As the expected BHTs are obtained based on formation geothermal gradient estimates that result from a best fit from data distributed over the whole basin, an individual T_{exp} will probably deviate from the BHT (T_{BH}) observed at that same point. The difference between the measured and expected BHT is the temperature residual (T_{res}) at that point. The existence of temperature residuals reflects noise in the data, or that a model assumption is not satisfied. Figure 4.3 shows a histogram of these residuals. The mean and standard deviation of the temperature residuals is 1.0 ± 7.7 °C. As expected from a least-squares type procedure, residuals appear to be randomly distributed around $T_{res} = 0$. The distribution of T_{res} with depth in Figure 4.4 shows no obvious depth dependence. We have also examined the geographic distribution of these temperature residuals and find no coherent geographic pattern. We conclude that most temperature residuals represent either measurement error or local geologic noise.

4.2 The best fit temperature field

In this section we explore in more detail the geographic and depth structure of the Paraná Basin temperatures as revealed by the best fit temperature field. We calculated the temperatures at the depths of 1, 2 and 3 km by adding the temperature differences across each individual formation computed from its thickness and the gradient obtained from the inversion to that depth (equation 4.4). Boreholes that bottom before reaching the depth of interest had their temperatures extrapolated to that depth. Formation gradients obtained from the inversion were used and formation thicknesses were estimated using the stratigraphy from the nearest borehole. Because the thermal gradient for the basement resulting from the inversion is unreliable, a temperature gradient for the basement was obtained by dividing the heat flow at the site (see Table 2.3) by a thermal conductivity of 3.0 W $m^{-1}K^{-1}$. Because of this extrapolation procedure expected subsurface temperatures at depths beneath shallow boreholes and at sites where basement is encountered at shallow depths have larger uncertainties than at other sites. This situation generally occurs at sites close to the eastern margin of the basin.

The calculated mean temperature and standard deviation for depths of 1, 2 and 3 km are, respectively: 24 ± 2 °C, 47 ± 3 °C and 69 ± 6 °C. These mean temperatures refer to temperature increments above the local surface temperature, such that the influence of the varying surface temperature over the basin is excluded. The mean temperature was then subtracted from the best fit temperature at each site to yield deviations from the mean at that depth. The resulting deviations from the mean allow us to examine the spatial structure of the thermal field in the basin. Figure 4.5 shows the distribution of these deviations at each depth. A larger number of sites, located mostly in the eastern margin of the basin required extrapolation of the temperature to great depths in the basement. Twelve of the 56 sites required some extrapolation to 2 km, and 25

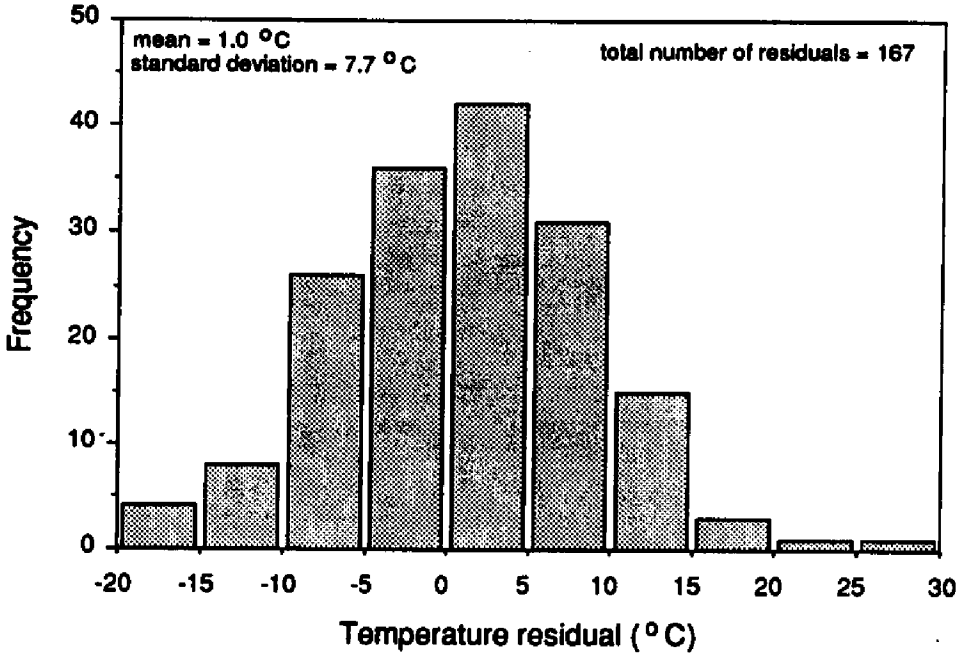

Figure 4.3. Histogram of temperature residuals.

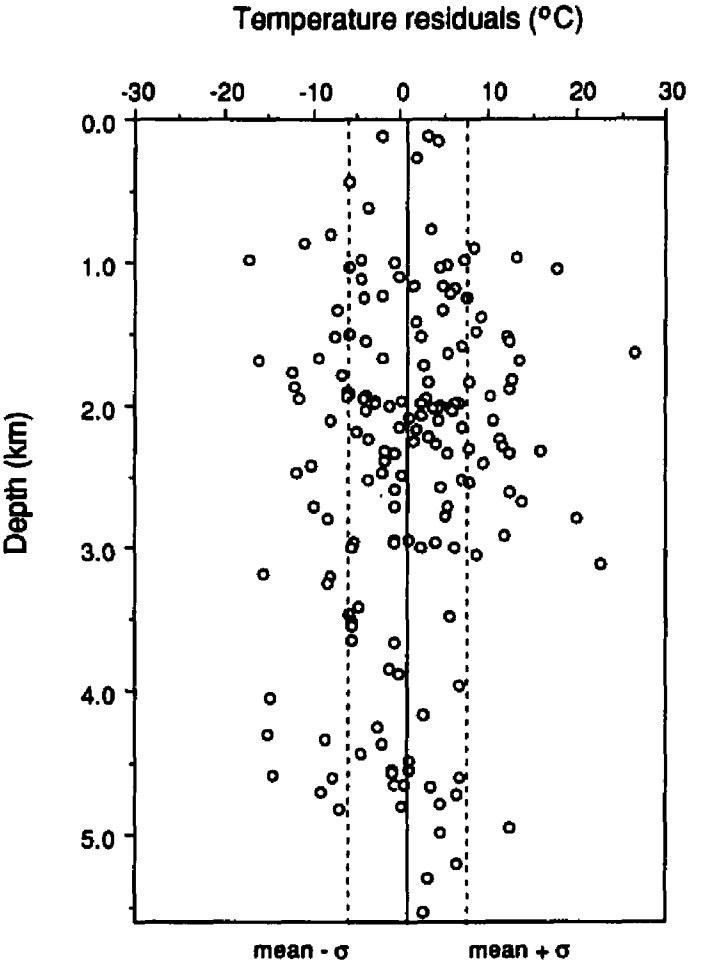

Figure 4.4 Temperature residuals versus depth of BHT measurement. The solid line shows the mean value for temperature residuals and dashed lines bracket one standard deviation to each side of the mean.

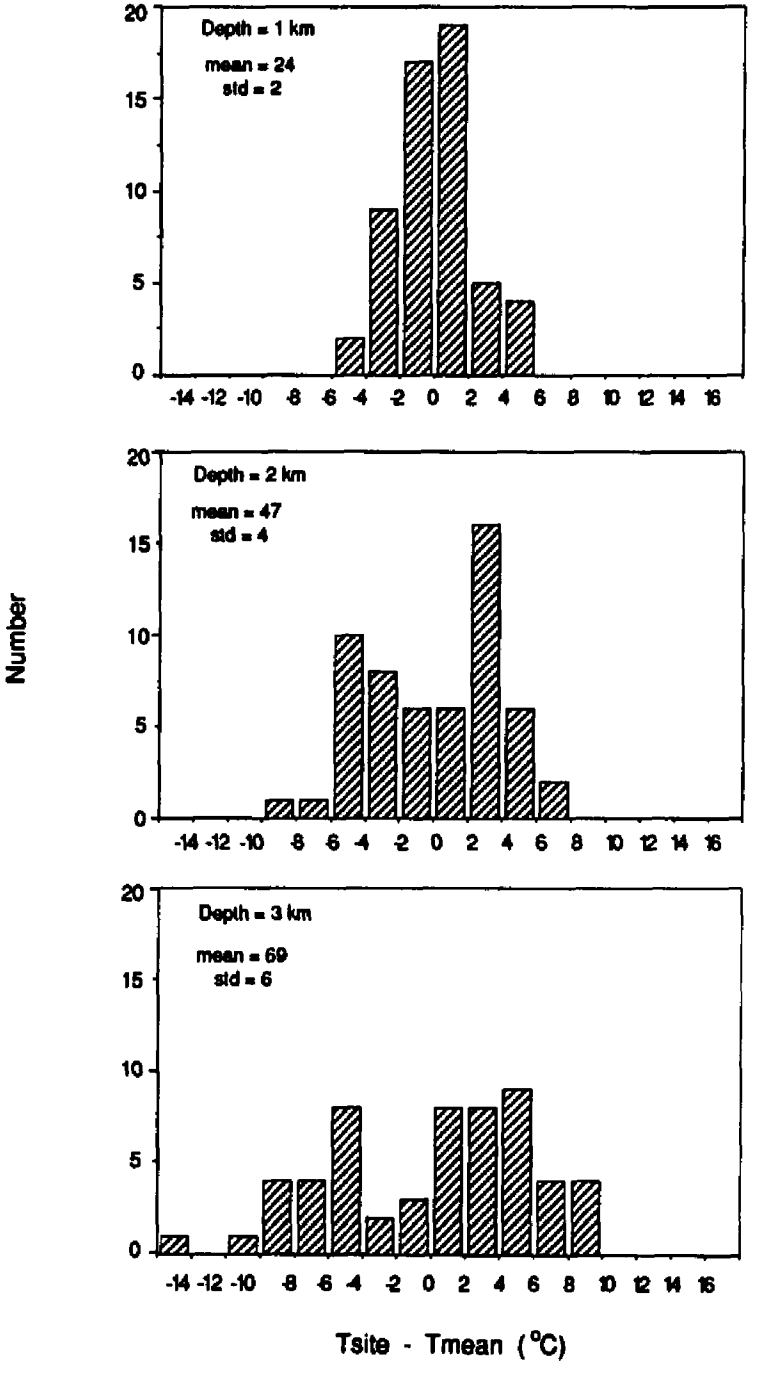

Figure 4.5 Histograms of deviations from mean temperature at depths of 1, 2 and 3 km, respectively. Positive deviations correspond to temperatures above the mean and negative deviations to temperatures below the mean.

to 3 km. The 3 km deviations show a distribution over a greater range of deviation magnitude than the deviations at 1 or 2 km.

Maps in Figure 4.6 display the geographic pattern of deviations above and below the mean temperature at each depth of interest. The pattern of deviations at 1 km depth (Figure 4.6a) is spatially coherent: large areas have deviations of same sign. Negative deviations (i.e. lower than average temperatures) are observed north of 23 °S; following the edge of the flood basalt between 22 °S and 25 °S on the eastern margin, and also in the southwest (south of 28 °S). Sites with temperatures higher than average (i.e. positive deviations) are located along a zone between 23 °S and 29 °S, mostly but not exclusively on flood basalt covered areas, that follows roughly the contour of the edge of flood basalt. The general coherent pattern observed at 1 km depth is maintained at 2 km depth, although there occurs an increase in the number of sites north of 23 °S with lower than average temperatures. The resulting pattern is one of lower than average temperatures along the northwestern, eastern (22 °S to 25 °S), southwestern basin margin, and a central zone at 22°S/52°W. This central zone is flanked by sites with higher than average temperatures. Finally at 3 km depth the general pattern can be described as a large zone of higher than average temperatures surrounded in the northwest, partly in the east and in the southwest by lower than average temperatures. In a few cases the behavior of the sign of the deviation changes at each depth of interest and we attribute this to local effects. Summarizing, the deviations from the mean temperature show a coherent spatial pattern at all depths investigated. We now turn to a discussion of this temperature pattern and its possible causes.

5. INTERPRETATION OF THE SUBSURFACE TEMPERATURE PATTERN

5.1 Conductive heat transport

The analysis of the regional heat flow pattern described in Chapter II and Chapter III has indicated that the heat flow is not uniform in the Paraná Basin. Heat flow increases from 45 mW m^{-2} in the center of the basin, the area of thickest basalt cover, to values of 75 mW m^{-2} towards the eastern margin. An interpretation involving the structure of the crust and lithosphere underlying the Paraná Basin (developed in Chapter III) explains the observed heat flow pattern and suggests that heat flow from the basement is not uniform, increasing from the center to the margin of the basin. This regional variation in heat flow must arise either from an increase in thermal conductivity or in the geothermal gradients, or both, from the center to the margin of the basin. The mean thermal conductivity in the basin increases from the center to the margin and is directly related to the thickness of the low conductivity flood basalt which is greatest in the center, thinning towards the eastern margin. Therefore the temperature gradients at the margin may actually be lower than in the center even though the heat flow at the margin is higher. This implies that, depending on lithologies and formation thicknesses, sites of high heat flow may be characterized by lower

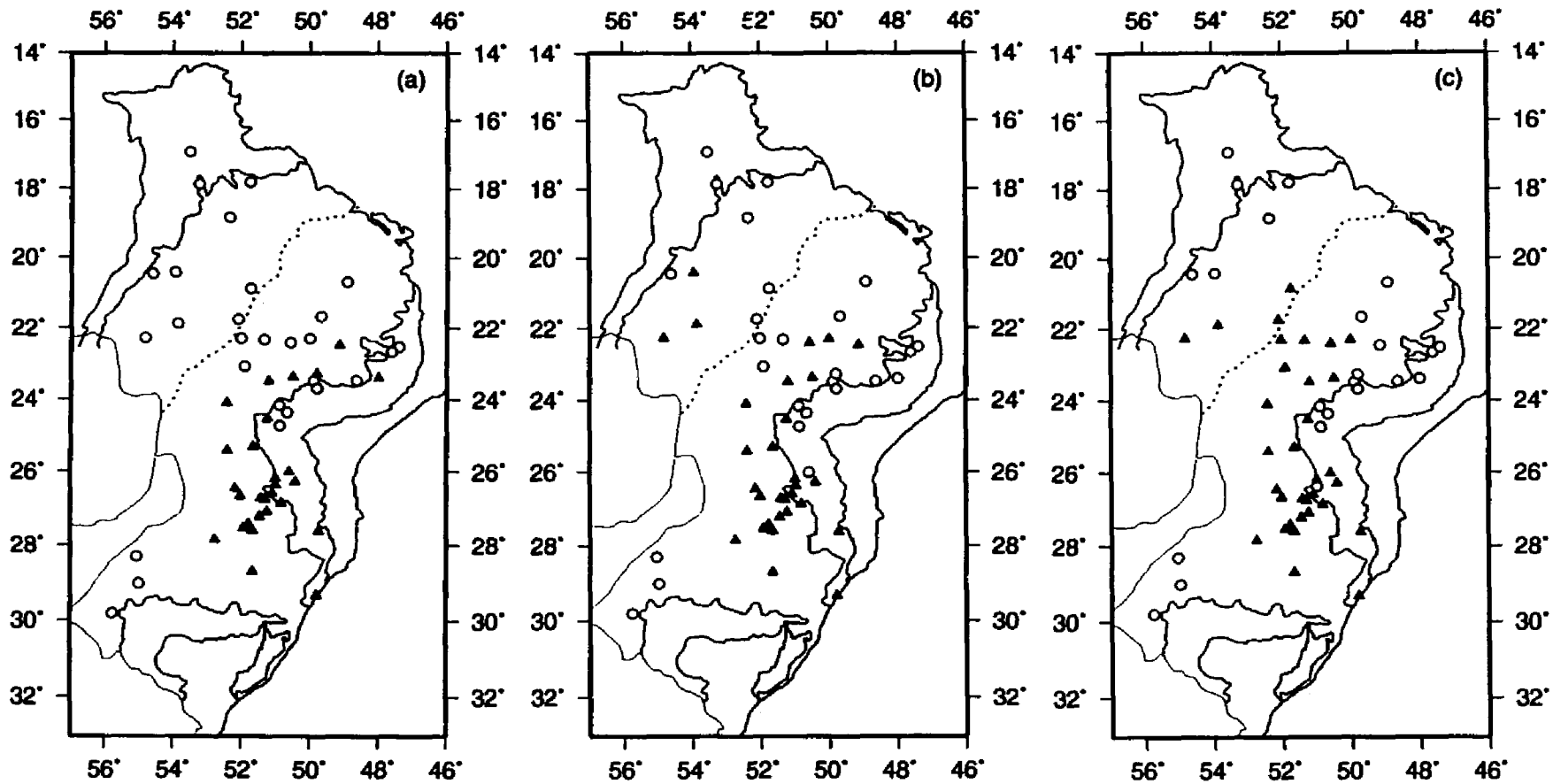

Figure 4.6 Maps of deviations from mean temperature at (a)1 km, (b) 2 km and (c) 3 km depth. Circles represent higher than average temperatures and triangles lower than average temperatures. Solid lines show boundaries of the basin and the flood basalt cap (see also Figure 2.1). Dotted line is the Paraná River, displayed for reference.

temperatures than sites with lower heat flow, and that regions of high and low subsurface temperatures at a given depth may not be related to high and low heat flow respectively.

We have used the same finite difference code (described in Chapter III) to calculate the temperature distribution within the basin arising from non-uniform heat flow from the basement and from thermal conductivity contrasts within the basin, assuming a purely conductive heat transport regime. Figure 4.7 depicts the model for the basin structure. The two-dimensional model was divided into three zones of contrasting thermal conductivity: the basement, sedimentary rocks and flood basalts with thermal conductivities of 3.0 W $m^{-1}K^{-1}$, 2.5 W $m^{-1}K^{-1}$and 1.8 W $m^{-1}K^{-1}$, respectively. The geometry is based on an approximate EW cross-section through the basin. Heat flow varying linearly from 46 to 65 mW m^{-2} from west to east, simulating the general increase of heat flow observed across the basin, was specified as input to the base of the model. As can be observed in Figure 4.7 the heat flow at the surface mimics the heat flow from the basement (with a deviation of less than 0.05 %). This result is consistent with the conclusion in Chapter III, that the pattern of heat flow at the surface was insignificantly affected by the conductivity structure within the basin itself. Also depicted are the resulting deviations of the mean temperatures at the depths of 1 km, 2 km and 3 km. The mean temperatures at these depths and their standard deviations are 25 ± 2, 48 ± 3 and 69 ± 2 °C. When compared to the mean temperatures at these same depths obtained from the best fit temperatures discussed in the previous section, we note that the means are very similar, and standard deviations are less (see Table 4.2 below), as expected from a simplified model calculation in which the sediments are considered to have uniform thermal conductivity .

Table 4.2 Best fit and model mean temperatures

Depth (km)	Mean temperature ± standard deviation (°C)	
	best fit	model
1	24 ±2	25 ±2
2	47 ±3	48 ±3
3	69 ±6	69 ±2

The model temperature deviations are of the same order as the best fit deviations at 1 km and 2 km. These deviations of the model temperatures arise from the lateral change in thermal conductivity at a given depth due to the dip and varying thickness of the various formations in the basin. Another observation is that the regions of high heat flow, at the eastern edge of the model, have lower subsurface temperatures than in the western lower heat flow area. The western half of

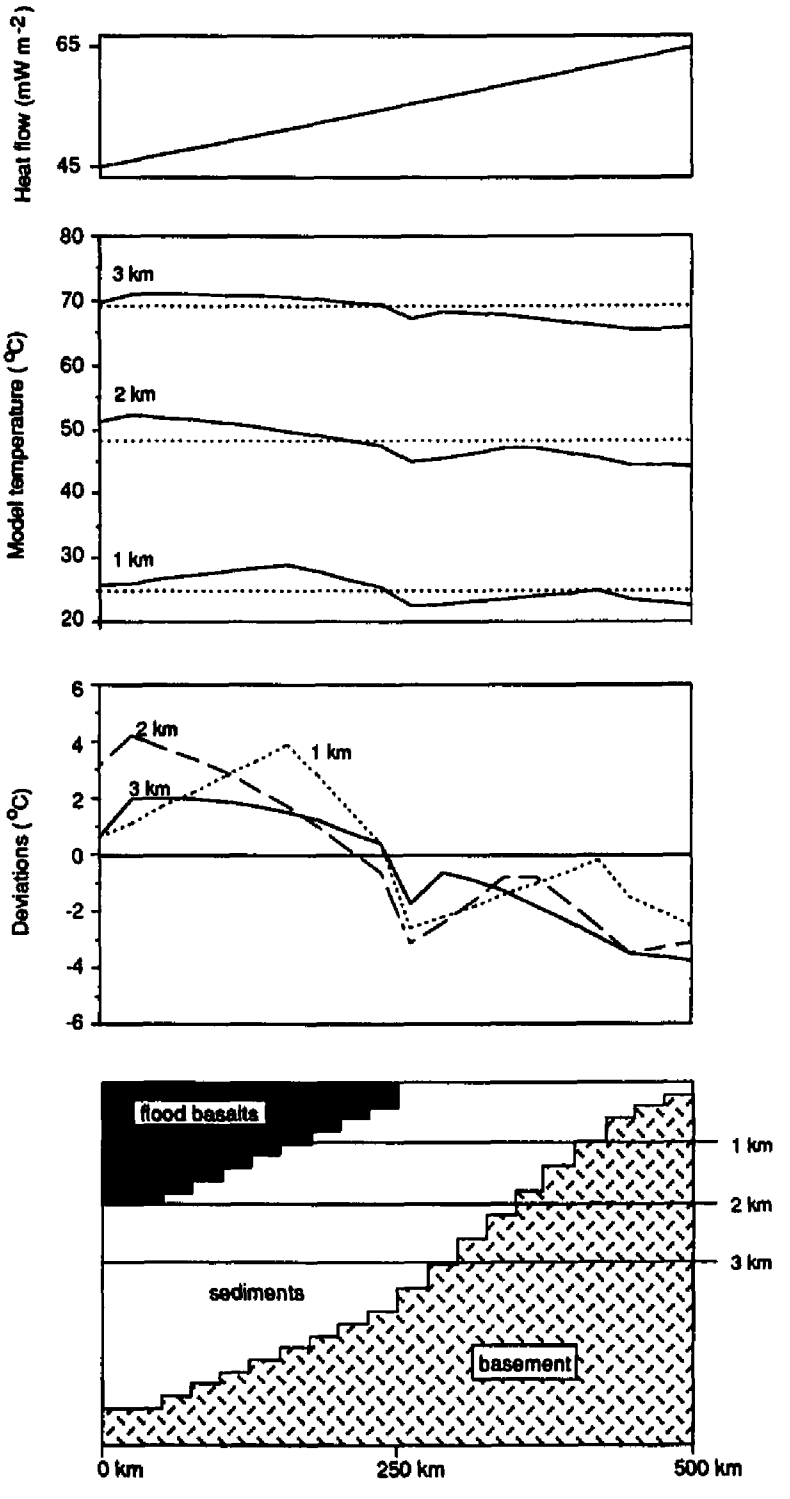

Figure 4.7 Conductive regime model and results. From top to bottom, heat flow at the surface (practically indistinguishable from the heat flow input from the basement), mean model temperatures at depths of 1, 2 and 3 km, temperature deviations at these depths, and a schematic of the model. Thermal conductivities of 1.8, 2.5 and 3.0 were used for the flood basalts, sediments and basement, respectively.

the model is dominated by the low conductivity basalt region which yields higher temperatures than the eastern part, which is dominated by higher conductivity sediments and high conductivity basement at shallower depths. In summary, the conductive heat transport model shows that the pattern of heat flow at the surface reflects that which enters the basin from the basement. The resulting model temperature structure within the basin has the same characteristics as the best fit temperature field obtained from the inversion of BHT data for the Paraná Basin.

5.2 Non-conductive heat transport

Subsurface fluid flow as a means of redistributing heat has frequently and at times successfully been invoked to explain the thermal structure of sedimentary basins (Willettt and Chapman, 1989; Deming et al., 1992; McCord et al., 1992). Smith and Chapman (1983) provide a review of work on the influence of fluid flow on subsurface temperatures. In the Paraná Basin, one possible scenario for a subsurface fluid circulation system was described in Chapter II and illustrated schematically in Figure 3.4. Surficial meteoric waters may penetrate the sediments at the eastern basin margin, a region of higher topography which could provide hydraulic head to drive the flow. These cool fluids absorb heat, increasing their temperature and diminishing the rock temperature. If these fluids later find appropriate pathways to rise to shallow depths, they will give rise to shallow temperatures and surface heat flow higher than expected from an exclusively conductive regime. The overall effect of the fluid flow on the heat flow is to diminish it in the recharge area and increase it in the discharge area.

Most hydrologic studies in the Paraná Basin have focused on the Baurú and Botucatú formations in the State of São Paulo because they are the major aquifers for this region. Little is known about hydrological characteristics of the other formations in the basin (Rebouças, 1976). Based mostly on geologic characteristics Rebouças (1976) suggests that sandstones in the Rio Bonito, Palermo and Furnas formations could sustain fluid flow. Based on data reported by Rebouças (1976) and a few values measured during formation tests we collected from the archives of PETROBRÁS, the ranges in permeabilities range from 10^{-18} m^2 to 10^{-13} m^2, the latter for the most permeable and shallow formations. The Serra Geral flood basalts may provide fracture permeability locally and in the region of its margin where fractures are more intense. Most of the area covered by flood basalts exhibits artesian conditions, suggesting that for the most part the basalt cap acts as an impermeable unit.

We have used two methods to assess the effects of fluid flow in the Paraná Basin. The first uses an analytical solution to the flow equation presented by Tóth (1962) and the second applies the finite element numerical code used by Smith and Chapman (1983) to calculate both heat and fluid transfer simultaneously. We consider the elevation difference between the recharge and discharge area, respectively at 1,000 m and 200 m elevation as the source of the

head gradient that drives the flow. Uniform and isotropic hydrologic and thermal properties are used in the geometry shown in Figure 4.8.

The solution to the flow equation for the setting depicted in Figure 4.8 was derived by Tóth (1962):

$$h(x,z) = z_o + \frac{cs}{2} - \frac{4cs}{\pi^2}\sum_{m=0}^{\infty}\frac{\cos\left[(2m+1)\pi\frac{x}{s}\right]\cosh\left[(2m+1)\pi\frac{z}{s}\right]}{(2m+1)^2\cosh\left[(2m+1)\pi\frac{z_o}{s}\right]} \qquad (4.1)$$

where h(x,z) is the hydraulic head, c is the tangent of the topographic slope and s is the lateral dimension of the flow region. The vertical component of the hydraulic gradient is obtained by differentiating equation 4.1 with respect to the coordinate z. The maximum vertical hydraulic gradients and Darcian velocities occur at the vertical boundaries of the model. For a model representing the dimensions of the Paraná Basin the peak hydraulic gradients are 3×10^{-3} m/m. The resulting velocities are obtained by multiplying this gradient by the hydraulic conductivity of the medium. Hydraulic conductivities in the range of 10^{-8} to 10^{-9} m s^{-1}, characteristic of a typical blend of basin sediments, yield velocities of 3×10^{-11} m s^{-1} to 3×10^{-12} m s^{-1}. These maximum velocities decrease by two orders of magnitude within a few tens of kilometers from the maximum hydraulic gradient, with the implication that the thermal effects will also be confined to these narrow zones.

The effect this fluid flow has on the heat flow at the surface can be estimated using the expression for advective heat flux,

$$\Delta q = \rho c \Delta T v \qquad (4.2)$$

where $\rho c = 4.2 \times 10^6$ J m^{-3} K^{-1} for the fluid (water), v is the Darcian fluid velocity and ΔT the temperature difference. Assuming that the fluid penetrates to a depth of 3 km and acquires a temperature of 70 °C above surface temperature, and that in the subsequent ascent to the surface no heat is lost in transit (clearly the maximum possible effect), equation 4.2 predicts a change in heat flow of only 1 to 10 mW m^{-2} for the range of hydraulic conductivities considered. We therefore conclude that this model predicts at most a small perturbation in heat flow (compared to the observed regional variation) that is confined to narrow zones of a few kilometers in the principal recharge and discharge areas.

The finite element code by Smith and Chapman (1983) solves the coupled fluid and heat transport problem simultaneously. We used a grid of 2400 triangular elements and investigated the same flow problem addressed with the analytical solution and depicted in Figure 4.8. Heat flow

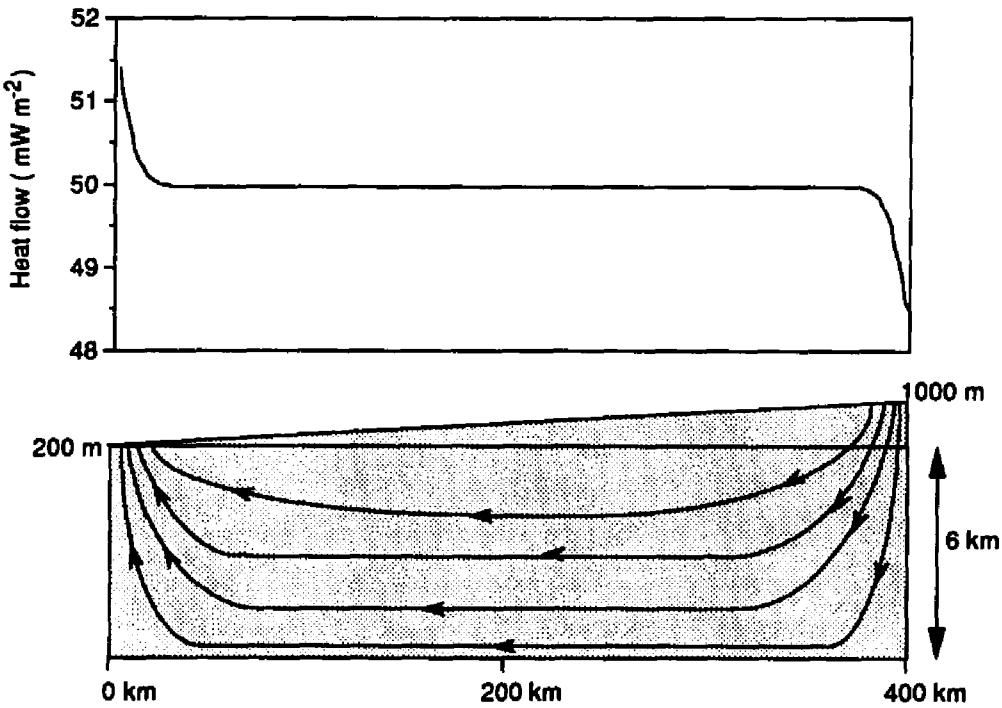

Figure 4.8 Advective regime model (below);. modeling results on the influence of hydrology on heat flow in the Paraná Basin (above). Flow lines show the direction of fluid flow.

into the flow domain was uniformly 50 mW m^{-2} at the base of the model, and a range in hydraulic conductivities was considered. Very low hydraulic conductivities inhibit the flow and do not alter the purely conductive temperature profile. At a hydraulic conductivity of 10^{-10} m s^{-1} the first noticeable albeit marginal effect on the surface heat flow occurred. Increasing the hydraulic conductivity to 10^{-9} m s^{-1} caused a maximum perturbation to the heat flow of less than 2 mW m^{-2}. An example of the resulting variation in surface heat flow is shown in Figure 4.8. Heat flow is decreased in the recharge area and increased in the discharge area, but most of the basin exhibits unperturbed heat flow. This is because only in those narrow zones is there a significant vertical component to the velocity field. The results from the finite element calculation are in agreement with the conclusions from the analytical solution. Both model approaches predict fluid velocities of the order of 10^{-11} m s^{-1} to 10^{-10} m s^{-1} and the same magnitude in heat flow perturbation. These model calculations suggest that fluid flow affects only narrow zones at the principal recharge and discharge areas and that the magnitude of heat flow perturbation is small compared to the regional variability observed in the Paraná Basin.

Smith and Chapman (1983) show in their study that anisotropic permeability up to1:100 (produced by the layering in sedimentary rocks) can increase the threshold for advection by a factor of 15, and reduce the advective perturbations compared to the effects in an isotropic medium. Our simplified models therefore represent upper limit cases, where model perturbations likely exceed the 'natural' ones. We conclude that fluid flow in the Paraná Basin is unlikely to have a significant effect on the regional pattern of heat flow at the surface. Small but non-trivial perturbations will be restricted to narrow zones within principal recharge and discharge areas of the basin. These results suggest the thermal regime in the Paraná Basin is principally a conductive one, a conclusion supported by the results from the modeling of conductive heat transport discussed earlier in section 5.1.

6. SUMMARY

Based on 187 BHTs and stratigraphic data a discrete least-squares inversion was applied to extract best fitting geothermal gradients for 14 representative formations and from these compute a best fit thermal field for the Paraná Basin. The thermal field across the basin at several depths was analyzed by mapping the deviations of the expected temperatures with respect to the mean expected temperature at a given depth. At all depths the deviations showed a spatially coherent pattern with above average temperatures for a given depth found beneath the thick basalt flows, and below average temperatures beneath the eastern margin of the basin. Finite difference modeling of a purely conductive regime produced similar temperatures and deviations as observed from the best fit temperature field. Advective heat transport models suggest that subsurface fluid flow does not alter the regional heat flow pattern significantly. The conductive

and advective heat transport model results suggest that the temperature and heat flow pattern in the Paraná Basin is dominantly a conductive regime. The effects of advective heat transport through fluid flow are likely to be small and restricted to areas of limited extent within the principal recharge and discharge areas.

CHAPTER V

THERMAL EVOLUTION OF THE PARANÁ BASIN SEDIMENTS

ABSTRACT

We investigate the thermal evolution of the contents of the Paraná Basin at two time scales. The effects of subsidence, uplift and the variation of the heat flow introduced into the basin through time operate on a time scale of hundreds of millions of years, with maximum temperatures seldom exceeding 200 °C for the deepest lying sediments. The second time scale is associated with short-lived igneous activity, with the sedimentary rocks being heated to a few hundred degrees over an interval of less than one million years. An analysis of illite crystallinity data shows a record of burial history characterized by increasing degree of crystallinity and diminishing crystallinity range with depth. The Paraná Basin was the locus of intense igneous activity 130 Ma ago, when flood basalts extruded and covered 75 % of the basin surface, and ubiquitous sills and dykes intruded the sediments and surrounding basement rocks. An analytical model of the cooling of multiple intrusions and a flood basalt extrusion indicates the complexity and variability of thermal history caused by intrusion/extrusion. The duration of maximum temperature conditions is a function of the time interval between extrusion/intrusion of individual flows/sills. An X-ray diffraction investigation on mixed-layer illite/smectite clay minerals from a typical borehole explores the effects of these igneous rocks on the sediments. The clay minerals are from sediments situated beneath 860 m of flood basalt and intruded by ten sills of thickness ranging from 1 to 12 m. The S/I ratio of 38 ± 2 % smectite is quite uniform over the depth interval investigated showing that the conversion of smectite to illite is incomplete. These data are compatible with the present-day temperatures established by the geothermal gradient, thus suggesting that the igneous event may have been too short lived to influence the I/S ratio. Other hypotheses involving fluid flow and retrograde reactions to explain the partial conversion cannot be excluded. We compare the sedimentary record of two sites within the Paraná Basin: one in the center of the basin, locus of the thickest accumulation of igneous rocks, and a second site on the eastern basin margin upon the uplifted Ponta Grossa Arch. Numerical modeling of the thermal history of these sites indicates that the differences in the present-day temperatures and surface heat flow arise from changes in lithospheric structure associated with the Serra Geral igneous event and the opening of the South Atlantic Ocean. Burial depth beneath the thick flood basalts

is shown to be the most important factor in terms of promoting the maturation of the sediments and hydrocarbon generation on a regional scale.

1. INTRODUCTION AND OVERVIEW

The thermal evolution of basin sediments is of special interest in hydrocarbon maturation studies. The present-day heat flow and thermal structure of the Paraná Basin were discussed in Chapters II, III and IV, and provide end constraints on calculations of the temperature history of this basin. In this chapter we investigate the time-temperature history of the contents (sediments) of the Paraná Basin. We investigate the thermal effects of processes occurring on two different time scales: (1) the effect of the geothermal gradient on sediments undergoing subsidence or uplift, a process characterized by temperatures ranging upward to 200 °C acting over time periods of hundreds of millions of years and (2) the effects of igneous activity, characterized by temperatures up to 1200 °C, and acting over hundreds of thousands of years.

During subsidence the sediments are buried to increasing depths and increasing temperatures. The rate of increase of temperature with depth is controlled to first order by the geothermal gradient which is in turn controlled by the local heat flow and thermal conductivity structure of the underlying lithologies. Uplift events followed by erosion act with reverse effects, with sediments after uplift and erosion residing at shallower and consequently cooler depths. In addition to the effects of subsidence and uplift mentioned above, the temperature history of the basin fill depends on the thermal properties that change during burial as a response to increasing temperatures, compaction and dewatering.

The temperature history of the sediments is also affected by the change of the regional heat flow through time. A basin-initiating thermal event implies an initially high heat flux into the basin; alternatively 'mechanical' basin initiation (e.g. flexure due to distant loading) may occur under 'normal' heat flow conditions. Episodes of volcanism and intrusion such as the Mesozoic Serra Geral igneous event also temporarily increase the heat flow.

Paleothermal indicators such as vitrinite reflectance, 'illite crystallinity" and the I/S ratio of illite/smectite mixed layer clays and the generation of hydrocarbons are used to infer thermal conditions in the past. Generally it is believed that these record maximum temperature conditions or conditions at which some maximum time-temperature threshold is exceeded. These indicators, however, are based on chemical reactions that may be influenced in complex ways by factors other than temperature and time, factors such as fluid flow, pressure, and initial composition, among others. Therefore the interpretation of observations derived from the sediments in terms of paleothermal conditions bears considerable uncertainties. As will be discussed later, the Paraná Basin thermal history has been dominated by burial/uplift for most of its 400 Ma history, but punctuated with a Mesozoic igneous event of only a few million years duration. If maximum

temperature conditions determine to first order the state of a paleothermal indicator, then the brief but intense Mesozoic igneous event will imprint the indicator. On the other hand, if the long integrated time-temperature effect is the principal factor controlling the state of the indicator, the long term thermal history of subsidence will be the process recorded. In this study we relate illite crystallinity and mixed layer illite/smectite data to the thermal evolution of the Paraná Basin sediments.

2.SUBSIDENCE AND UPLIFT HISTORY OF THE PARANÁ BASIN

2.1 Subsidence and uplift: sediment accumulation and erosion

The following summary of the history of sedimentation in the Paraná Basin has been drawn from Zalán et al. (1991). The mechanism of origin of the Paraná Basin is still a matter of speculation. No evidence of an initiating rift has been discovered, but very little geophysical data relevant to the question has been assembled. The Braziliano orogeny, with principal deformation occurring about 700 to 650 Ma and granitogenesis taking place at about 610 to 580 Ma, is thought to be associated with the assembly of the supercontinent of Gondwana. Lithospheric cooling followed during 500 to 450 Ma, which Zalán et al. (1991) consider a possible mechanism for inducing regional subsidence; however they do not rule out an extensional event. The oldest sediments in the basin are Late Ordovician in age. The analysis of the isopach map of the Late Ordovician/Early Silurian Rio Ivaí formation suggests a linear depocenter with subordinate branches, a pattern suggestive of a rift triple junction and a single seismic section the southern most branch in this area is suggestive of rift geometry. This is also the locus of a positive gravity anomaly that is suggestive of crustal thinning .

The subsequent history of this basin throughout the Paleozoic involves subsidence punctuated by uplift/erosion events generally associated with distant orogenies, probably related to the fact that the western margin of Gondwana was a convergent plate boundary during this time. Following basin initiation, three major subsidence episodes (Silurian-Devonian, Permian-Carboniferous and Late Jurassic-Early Cretaceous, respectively) are recorded in the stratigraphy of this basin, separated by major unconformities. At the end of the Silurian-Devonian deposition there followed a period of 60 Ma of uplift and erosion associated with what has been called the Eohercynian orogeny. In the second subsidence interval, tectonics was dominated by strong normal faulting, and a glacial environment prevailed. Subsidence may have been related to extension and flexure due to loading by continental glaciers. During the Pennsylvanian the basin was covered by a large epicontinental sea which receded in the Permian, with broad regional uplift associated with the Finihercynian orogeny ending this phase of deposition. Sedimentation became wholly continental from the Middle Triassic on. The last major 'depositional' event was the

outpouring of the Serra Geral flood basalt, followed by a thin Late Cretaceous unit, perhaps related to the cooling and slight subsidence of the crust following the igneous event.

The Ponta Grossa Arch (see Figure 2.1) was first subjected to uplift preceding the opening of the South Atlantic in the Late Triassic to Early Jurassic, and to renewed uplift in the Late Cretaceous to Tertiary along with the Serra do Mar uplift. White and McKenzie (1989) and Herz (1977) relate this to updoming of the future eastern coastline of South America preceding continental breakup.

2.2 Evolution of the thermal conductivity structure

2.2.1 Lithologies

The thermal conductivity of a rock is controlled to first order by its mineral composition (Brigaud et al., 1990). The common minerals and materials that make up sedimentary rocks in order of increasing thermal conductivity are coal, clay minerals, feldspar, calcite, dolomite, halite and anhydrite, and quartz, with approximate values (in $W\ m^{-1}\ K^{-1}$) ranging from 0.3, 2.0, 2.3, 3.6, 5.5, 6.0 to 7.0, respectively. Carbonates are limited to the Irati formation in the northern part of the Paraná Basin, and the coal bearing areas in the Rio Bonito formation are restricted to the southern states of Santa Catarina and Rio Grande do Sul. Hence the proportions of quartz and clay minerals in the sedimentary rocks determine the overall thermal conductivity of the sediments in the Paraná Basin. From the Late Ordovician up to the Late Jurassic, mostly siliciclastic sediments were deposited in the basin, thus imparting a relatively uniform thermal conductivity to the basin fill and over time the changes in thermal conductivity were associated with the increase in temperature accompanying deeper burial and the evolution of porosity in these sediments, as will be described below.

In the Mesozoic, the thermal conductivity structure of the Paraná Basin was changed by the addition of a new component to the thermal conductivity structure: the flood basalts of the Serra Geral formation. This thick unit has a low conductivity of 1.86 $W\ m^{-1}\ K^{-1}$. Generally the thermal conductivity of the sediments ranges from more than 2.0 to about 3.0 $W\ m^{-1}\ K^{-1}$. The large contrast between sediments and basalts in the thermal conductivity structure of the basin has existed only since the extrusion of the flood basalts at 130 Ma. Prior to this event the basin's thermal conductivity structure was more uniform, with a higher mean conductivity.

As noted in Chapter II, thermal conductivity of sedimentary materials is temperature dependent, generally decreasing with increasing temperature. During subsidence and burial the sediments are exposed to increasing temperatures, but the corresponding change in thermal conductivity is negligible for burial depths of less than 1 km. For rocks sampled from greater depths, thermal conductivities measured in the laboratory should be corrected for this effect.

Increasing pressure causes thermal conductivity to increase slightly, although much less than the decrease with temperature, such that under most conditions within sedimentary basins the pressure effect can be neglected. Pressure can of course alter porosity, a non-negligible effect which we discuss next.

2.2.2 Porosity and Compaction

Sedimentary rocks are porous. Porosity and the fluid that fills the pores determine to second order the thermal conductivity in the rocks. Pore space in sedimentary rocks can be filled with air, water, brine, and/or oil and gas, which have thermal conductivities much lower than the common minerals constituting the rocks (k_{water} = 0.6 W $m^{-1}K^{-1}$, k_{air} = 0.03 W $m^{-1}K^{-1}$). The bulk thermal conductivity of a rock decreases with increasing porosity, because an increasing fraction of its volume is filled with lower conductivity fluid. Sandstone with 20 % porosity has a thermal conductivity of 5 W $m^{-1}K^{-1}$, whereas with a porosity of 30 % the conductivity is only 3.5 W $m^{-1}K^{-1}$(Brigaud et al., 1990).

Subsidence and burial produce compaction of the sediments and a decrease in their porosity, therefore causing an increase in thermal conductivity with depth for a given lithology. This change in conductivity produces an adjustment of the geothermal gradient and temperatures. For an uniform heat flow through a sedimentary section, an increase of thermal conductivity would cause the gradient and the temperature difference across the section to decrease, while decreasing thermal conductivity will produce an increase in geothermal gradient, and therefore also increased temperatures. It is possible to obtain relatively high temperatures in sediments in spite of low heat flow. The extreme example relates to the presence of coal, with a conductivity nearly an order of magnitude less than most other sedimentary materials. Extremely high thermal gradients can develop in coal seams and high temperatures in the underlying sediments, a characteristic called the 'blanketing' effect of coal and carbonaceous rocks. This effect is greater for larger thicknesses of the low conductivity components in the sedimentary section.

In summary, the thermal conductivity structure of the Paraná Basin prior to the extrusion of the Serra Geral flood basalts at 130 Ma was determined largely by the proportion of quartz and clay minerals and the porosity of the sediments, and had no strong regional variation. The thermal conductivity of these materials has decreased slightly with time due to burial to greater depths and temperatures, but increased significantly due to the diminishing porosity by compaction. As the effects of diminished porosity outweigh those of increased temperature, the net effect of burial is an increase in conductivity. Since the Serra Geral igneous event, the thick flood basalts provide a thermal conductivity contrast with low conductivity in the basalt and higher conductivity in the sedimentary portion of the basin fill.

2.3 Evolution of heat flow

The mean surface heat flow measured in the Paraná Basin is a function of the amount of heat introduced into the basin through the basement, and the amount of radiogenic heat generated by the sedimentary and igneous rocks within the basin. The heat flow entering the basin from below reflects lithospheric history and heterogeneity.

Several mechanisms have been proposed to explain the origin, the stratigraphic evolution and present-day thermal state of sedimentary basins. In some cases subsidence is related to the cooling of the lithosphere after some initial thermal event. McKenzie (1978) proposed stretching and thinning of the lithosphere with a resulting upwelling of hot mantle material and then cooling and subsidence. Other mechanisms involve heating, uplift and erosion followed by cooling and subsidence of the thinned lithosphere (Sleep and Snell, 1976) or heating capable of inducing a phase change (gabbro-eclogite transition) within the lithosphere creating a high density load to drive subsidence (Haxby et al., 1976).

The thermal history of the Paraná Basin may have been punctuated by two events: a first thermal event marking the origin of the basin some 400 Ma ago and a second and final thermal event, the Serra Geral igneous activity preceding the opening of the South Atlantic at about 130 Ma. One initiating mechanism that has been suggested for the origin of the basin (Zalán et al., 1991) is subsidence as a response to cooling of the lithosphere following the Brasiliano orogeny that ended at about 450 Ma. Alternatively an extensional basin-initiating event can be envisioned, with stretching, thinning and cooling followed by subsidence (see section 2.1). For an extensional event of basin initiation, McKenzie (1978) showed that heat flow is strongly affected by the amount of extension only in the first 30-50 Ma after extension. As the Paraná Basin is older than 400 Ma, any initiating thermal event would have contributed to the heat flow only very early in the basin history and would be of no consequence to most of the basin history nor to the present-day thermal structure. Therefore, whatever the mechanism of basin initiation that operated for the Paraná Basin, an initial period of high heat flow would have very little effect on any but the earliest sediments.

Subsequently subsidence and uplift periods related to orogenic activity occurred as described in section 2.1. Several other intracratonic basins (Michigan, Illinois and Williston Basins) have experienced renewed subsidence during times of orogeny in adjacent orogenic belts (Ingersoll, 1988). This may occur due to changes in the flexural rigidity of the lithosphere resulting from the applied stresses or fluid fluxes associated with the orogeny, as envisioned by Howell and van der Pluijm (1990) for the Michigan Basin. Such events do not impart changes to the regional basal heat flow into the basin.

The scenario changed dramatically towards the end of the Jurassic. The Serra Geral igneous event, characterized by voluminous flood basalts and associated intrusive bodies, heralded the opening of the South Atlantic. This event is believed to have been initiated by a large plume impinging on the Gondwana continental lithosphere and leading to the rifting marking the opening of the South Atlantic Ocean (White and McKenzie, 1989). The large amount of melt extruded and probably underplated is evidence for enhanced mantle temperatures and a limited period of higher heat flow into the Paraná Basin. With the subsequent opening of the South Atlantic, i.e. production of an oceanic ridge system that exhausts heat more efficiently, excess heat from the mantle was delivered to the ridge, and heat flow on the continent decreased. The generation and extraction of large volumes of melt from the sublithospheric mantle could have thickened the lithosphere through basalt depletion (Chapter III). Deep heat flow would be diverted from the thickened region underlying the basin to the thinner lithosphere at the eastern margin, producing the present-day surface heat flow pattern of increasing heat flow from the center to the eastern margin of the basin.

In summary, the Paraná Basin's history may have initiated with a period of higher heat flow that decayed within a few tens of millions of years to a regionally uniform and temporally steady heat flow. This situation changed with the Serra Geral igneous activity. Heat flow increased due to the cooling of flood basalt extrusion and sill and dyke intrusion and lower crustal underplating. This transient variation in heat flow decayed, but as a consequence of the change in lithospheric thickness, the new steady state surface heat flow was lower in the central part of the basin than at the eastern margin, because deep mantle heat was diverted from the center to the margin.

2.4 Evidence of the effects of subsidence and uplift history in illite crystallinity

2.4.1 'Illite crystallinity'

In this section we address the thermal history of the Paraná Basin with published data on 'illite crystallinity' measurements of core samples. In the following we shall briefly describe 'illite crystallinity' and its relationship to the degree of diagenesis and/or very low grade metamorphism in pelitic rocks.

Crystallinity as defined by Kübler (1967, in Frey,1987) expresses the degree of ordering in a crystal lattice of a mineral. In the case of the clay mineral illite it is an increase in temperature that, among other factors, can be related to an increase in 'illite crystallinity' (Frey, 1987). The measure of illite crystallinity, termed 'illite crystallinity index' (IC index), is given by the shape and intensity of the 10 Å peak of illite obtained in XRD analysis. The sharper or narrower this peak, the higher is the degree of illite crystallinity. The width of the 10 Å peak at half height is the Kübler index. As this is an easily measured property, 'illite crystallinity' has often been used to define the

degree of diagenesis/low-grade metamorphism in pelitic rocks, because it is considered to record irreversibly the peak temperature conditions, although other factors may play a role in its characterization. For detailed reviews we refer the reader to Kisch (1983) and Frey (1987).

The distinction between the diagenetic zone and the first very low grade metamorphic zone (anchizone) is established at a Kübler index of 0.42° 2θ (7.5 mm) and extends to 0.25° 2θ (4.0 mm) at which the boundary between the anchizone and the next metamorphic zone, the epizone has been reached (Frey, 1986). Based on fluid inclusion studies (Mullis, 1970), Kisch (1987) sets the transition of diagenetic zone to anchizone at temperatures of about 180-200 °C. The transition of the anchizone to the epizone is set at 300 °C (Frey, 1986).

With increasing metamorphic grade the crystallinity of illite improves due to increasing crystallite size and ordering of the crystal layers, and therefore the Kübler index decreases. The high grade end-member is muscovite (Bons, 1989). A sample of pelitic rock may contain a mixture of detrital micas and authigenic micas (illite). In such cases measurement of the IC index yields a smaller index than that of the authigenic illite alone that would indicate the in situ degree of diagenesis/low grade metamorphism. To minimize the contribution of detrital micas to the IC index, the < 2 μm clay fraction is generally used for determining the 'illite crystallinity'. However, a detrital contamination must always be considered possible.

2.4.2 Illite crystallinity data in the Paraná Basin

Ramos and Formoso (1975) present clay mineral compositions and 'illite crystallinity' determinations (Kübler index) on over 1,000 core samples from 43 boreholes in the Paraná Basin. X-ray diffraction was applied to the < 2 μm clay fraction according to standard procedures described in Lucas et al. (1959). All formations are represented in the data set, which includes sandstones, siltstones, shales and glacial mudstones.

Figure 5.1 displays these data as a function of present-day depth. The data embrace a wide range in Kübler indices (1.5 to 20.0 mm). Although the amount of data decreases with depth, two observations can be made: (1) the range of Kübler index decreases with depth and (2) the index magnitude also decreases, indicating that 'illite crystallinity' increases with depth. We have examined the distribution and variation in magnitude of Kübler indices for individual lithologies and encountered the same pattern as depicted on Figure 5.1

The increase in 'illite crystallinity' with depth suggests that the increase in temperature with depth, controlled by the geothermal gradient, promotes an increase in 'crystallinity', i.e. both authigenic and detrital illite crystallites increase in size and ordering. The high 'crystallinities' encountered at shallow depths can be explained by three factors: (1) the presence of detrital illite of high crystallinity, (2) local effect of sill intrusions upon samples originally situated close to these intrusive bodies and (3) the effect of uplift, which is to move deep rocks to shallower depths. The

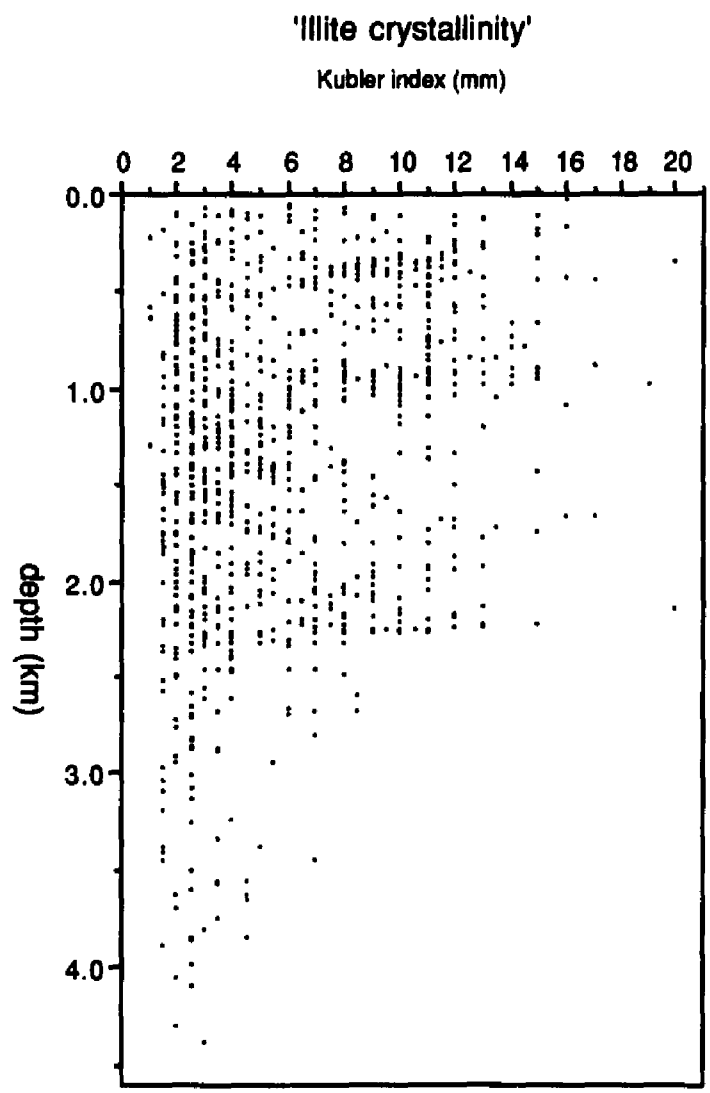

Figure 5.1 Illite crystallinity versus depth. 'Illite crystallinity' given in Kübler index (mm).

present-day range of subsurface temperatures can be observed on Figure 2.3. The highest temperatures are of the order of 160 °C. We note here that the thermal history calculations described later in Section 4, suggest that temperatures at depth generally have not reached much greater magnitudes than in the present-day although exceptions of course occur near sills and dykes. The boundary between the diagenetic and the anchizone is reached at 180-200 °C corresponding to a Kübler index of 7.5 mm (Frey, 1986). On this basis, the Paraná Basin sediments would be classified as in the diagenetic zone, with respect to 'illite crystallinity'. However, Figure 5.1 suggests that the anchizone may have been reached at depths greater than 2,500 m. This could indicate that the increase in 'illite crystallinity' may not be governed to first order by temperature alone, but rather by the combined effects of temperature and time (the time-temperature-integral: TTI). In this case, temperatures lower than 180 °C, but enduring over more than a hundred million years may bring the deeper sediments to the boundary of the anchizone. This observation also suggests that short-term effects such as the cooling of igneous intrusions, even when imparting high temperatures to the surrounding sedimentary rocks, may not be sufficient to promote an increase in 'illite crystallinity'.

Summarizing, a large data set consisting of 'illite crystallinity' determinations on core samples distributed over the whole Paraná Basin suggests that the sediments deeper than 2,500 m may have reached the anchizone boundary. This can be explained only if the combined effects of both time and temperature are considered, as the temperatures at these depths are lower than those required for the transition of the diagenetic zone to the anchizone. The large scatter in the data set, especially the presence at shallow depths of high crystallinities, can be explained by detrital high crystallinity material, the moving of higher crystallinity material to shallow depths through uplift, or perhaps locally to the effects of sill intrusions in the sediments, although the thermal effect of such intrusions may be too short-lived to contribute significantly to the time-temperature-integral and arfect 'illite crystallinity'.

3. MESOZOIC IGNEOUS ACTIVITY: INTRUSIVE AND EXTRUSIVE

3.1 Distribution, ages and intrusion of igneous rocks in the Paraná Basin

In Section 2 we have investigated the thermal history related to the temperature changes sediments experience due to subsidence/burial and uplift within the environment created by the geothermal gradient. Now we examine the effect of shorter lived thermal events in the history of the sediments, i.e. the effect of the high temperatures (ca. 1200 °C) of the intrusive sills and extrusive flows. The igneous event at the end of the Jurassic resulted in the extrusion of voluminous flood basalts and pervasive dyke and sill intrusion into the sediments of the Paraná

Basin. The present day extent of these basalt flows in the Brazilian territory is shown in Figure 2.1 and the total extent for the entire basin is of the order of 10^6 km^2.

Individual dyke intrusions and swarms are exposed mainly on the eastern border of the Paraná Basin, cutting through the Precambrian basement, while sill intrusions occur in the entire basin, with thicknesses of a few meters to hundreds of meters; in some boreholes the cumulative sill thickness comprises 30 % of the total stratigraphic column (Zalán et al., 1986). Lateral extension of these sills have been observed for only a few cases: areal extents of 100 km^2 and 900 km^2 were reported by Cordani and Vandoros (1967). Sills are found to be concentrated in the central and northern parts of the basin, with the locus of thickest sills (up to 1 km of accumulated thickness) roughly coinciding with the region of thickest basalt flow accumulation (1.7 km). Melfi (1967) measured ages for intrusions that do not differ significantly from the eruptive ages of the basalt, and Piccirillo et al. (1988) show that intrusives and extrusives in the northern portion of the basin have very similar chemistries.

Several arguments suggest that this igneous event had a duration of less than forty million years and perhaps as short as a few million years. Paleomagnetic studies show that the Etendeka volcanics of Namibia and those from the Paraná basin have coincident paleomagnetic poles when the relative motion of the Atlantic spreading is removed, suggesting that volcanism preceded the opening of the South Atlantic (Giedskehang et al., 1975). Moreover chemical studies suggest that the basalts derive from the same igneous province (Piccirillo et al., 1988). Rabinowitz and LaBreque (1979) set the onset of separation of South America from Africa at 130 - 135 Ma. Rocha Campos et al. (1988) review in detail some 200 available radiometric dates for the Serra Geral flood basalts and associated intrusives. The ages span an interval of 160 to 120 Ma, with the main eruptive phase occurring at 130-135 Ma with a stacking of about 20 flows (Ernesto and Pacca, 1988). Single flows range from a few meters to 100 m thick (Melfi et al., 1988) and average 10 - 20 m thick. Vertical profiles of basalt flows have yielded essentially contemporaneous K-Ar dates. Detailed chemical and paleomagnetic investigations of an apparent single flow 44 m thick (Montes-Lauar et al., 1987) show that this unit is in fact composed of three distinct flows that cooled almost simultaneously. Ernesto and Pacca (1988) argue from paleomagnetic studies of lava flows, dykes and sills, that up to 1,000 m of lava could have been piled up in 1 Myr or less.

Summarizing, the Serra Geral igneous event at 130-135 Ma extruded rapidly a great volume of flood basalts. The associated intrusive bodies (dykes and sills) are clearly related to the flood basalts, and their intrusion is practically simultaneous to the extrusion event. Estimates based on isopach maps indicate that the total volume of extruded basalt is of the order of 5×10^5 km^3 and that the sediments contain about 1×10^5 km^3 of intruded material. Igneous rocks make up 30 % in volume of the Paraná Basin's contents.

3.2 Theory of multiple intrusions/extrusions

Here we develop the theoretical analysis that yields the temperature history of the sediments due to the extrusion of basalt flows at the surface and the intrusion of sills in the subsurface. In the next section we present experimental data that describe the diagenetic stage of clay minerals in the sediments in proximity to intrusions and compare these to the theoretical temperature histories. As a first step in the assessment of the temperature evolution within the sediments due to sill intrusions, we have derived an analytical heat conduction model that allows temperatures as a function of depth and time to be calculated at any time after intrusion of multiple sills, arbitrarily distributed throughout the sedimentary column. Generally extrusion and intrusion of the individual sills occur sequentially, although over a short time. The maximum effect of the igneous rocks on the sediments would occur in the situation of simultaneous intrusion of sills in the subsurface and the extrusion of the total basalt thickness at the surface. As sills are by definition extensive laterally compared to their thickness, and the heat lost due to cooling is principally in the vertical direction, it is reasonable to use a one-dimensional model in which sills are represented by horizontally infinite slabs, bounded on top and bottom by parallel planes. The temperature as a function of depth and time since intrusion of a single sill can be obtained through the analytical solution to the one-dimensional time-dependent heat conduction equation with no sources or sinks, given below:

$$\frac{\partial^2 T}{\partial z^2} - \left[\frac{1}{\alpha}\right]\frac{\partial T}{\partial t} = 0 \qquad (5.1)$$

For a sill with top at depth z=a and bottom at z=b, intruding at a temperature T_i within a semi-infinite medium of diffusivity α, geothermal gradient g, bounded by the surface at z=0 with surface temperature T_o, the appropriate initial and boundary conditions are:

$T = T_i$	$a < z < b$	$t = 0$	(5.2a)
$T = T_o + g z$	$0 < z < a$ and $z > b$	$t = 0$	(5.2b)
$T = T_o$	$z = 0$	$t > 0$	(5.2c)

This equation under these conditions was solved using the method of images and direct integration of the expression found in Carslaw and Jaeger (1959). The solution is expressed by:

$$T(a,b,z,t)=\frac{1}{2}(T_i-T_o)\left\{\operatorname{erf}\left(\frac{z-a}{\beta}\right)-\operatorname{erf}\left(\frac{z-b}{\beta}\right)+\operatorname{erf}\left(\frac{z+a}{\beta}\right)-\operatorname{erf}\left(\frac{z+b}{\beta}\right)\right\}$$
$$-\frac{1}{2}gz\left\{\operatorname{erf}\left(\frac{z-a}{\beta}\right)-\operatorname{erf}\left(\frac{z-b}{\beta}\right)-\operatorname{erf}\left(\frac{z+a}{\beta}\right)+\operatorname{erf}\left(\frac{z+b}{\beta}\right)\right\} \qquad (5.3)$$
$$+\frac{\beta g}{2\sqrt{\pi}}\left\{\exp\left(-\frac{(b-z)^2}{\beta^2}\right)-\exp\left(-\frac{(b+z)^2}{\beta^2}\right)-\exp\left(-\frac{(a-z)^2}{\beta^2}\right)+\exp\left(-\frac{(a+z)^2}{\beta^2}\right)\right\}$$

where $\beta = 2\sqrt{\alpha t}$ and T(a,b,z,t) is the resulting temperature perturbation due to a single sill. The solution for the simultaneous intrusion of n sills of different thicknesses (bi-ai) is obtained by superposing the solutions of each individual sill, such that:

$$T(z,t)=T_o+gz+\sum_{i=1}^{n}T(a_i,b_i,z,t) \qquad (5.4)$$

In this solution rock thermal diffusivity is assumed uniform throughout. The thermal diffusivity of common rocks varies in the range 8 x 10^{-7} m^2s^{-1} (shale) to 2 x 10^{-6} m^2s^{-1} (sandstones) as given in Kappelmeyer and Haenel (1974). This range of diffusivity causes no significant difference in temperature, only a time lag of a few thousand years in the attainment of the same temperatures. The assumption of uniform diffusivity has no deleterious consequences, and in our calculations we have used a value of 1 x 10^{-6} m^2s^{-1} for the thermal diffusivity.

The heat transferred from the intrusion into the surrounding rocks comprises heat lost through cooling of the intrusion from intrusion temperature to background geothermal temperatures, plus the latent heat of crystallization. Latent heat release was simulated with an appropriately higher intrusion temperature (see Jaeger, 1959, for more details). In our computations we use T_i = 1,200 °C.

Intrusion of an individual sill releases an amount of heat proportional to its thickness. Subsequently the thermal diffusivity of the surrounding rocks controls the rate of conductive heat transfer, and any site within proximity of a few sill thicknesses will experience an increase in temperature to some maximum value roughly inversely proportional to the distance of the point of interest to the intrusive body. Then temperatures at this site will decrease gradually until background geothermal gradient temperatures are reestablished.

The temperature history for a site affected by simultaneous multiple intrusions can be much more complex than the case discussed above. On the one hand, sills at different relative distances to a given location may cause this site to experience several increases and falls of temperature as the 'thermal front' emanating from each sill reaches it. On the other hand, the composite effect of multiple sill intrusions to the thermal history of a site may be a single extended period of high temperatures as the thermal front of each sill reaches the site before the previous

front has had time to fully dissipate. In the following section we discuss the results of modeling the intrusion/extrusion history experienced at the borehole AO-1-RS. This borehole is used later in a study of the igneous effects on clay mineral composition and was chosen because continuous cores were available through the section of interest.

3.3 Temperature history due to cooling of multiple igneous bodies

Figure 5.2 shows the geographic location and Figure 5.3 a stratigraphic column for the chosen example site, AO. This borehole penetrated about 860 m of flood basalt cover and intercepted at depths of 1,900 to 2,200 m 10 sills of thicknesses ranging between 1 and 12 m before reaching the basement at 2,251 m depth. We have mentioned that the extrusion of the flood basalts is considered to be a rapid event in geologic time, perhaps taking less than 1 Myr to accumulate a thickness of 1 km of basalt. It is a very short-lived thermal event compared to the characteristic time scale of ca. 100 Myr for the effects of the geothermal gradient over the history of subsidence. In the modeling process we have examined two extrusion histories in order to assess the effects of the flood basalts: (1) the total thickness of the basalt cap is extruded instantaneously at the time of sill emplacement and (2) the flood basalts are assumed to comprise individual flows extruded sequentially over an interval of 1 Myr; the results from the first case portray the maximum thermal effect that the present-day volume of igneous rock could impart. The thermal effect would be less if the sills and flows were emplaced sequentially, i.e. the intrusion/extrusion was distributed over time as in the second case above, allowing the loss of heat and the reduction of temperatures during the intervals between the emplacement of individual basalt flows/sill intrusions. The modeling of sequential sill intrusion is complicated by the fact that the sequence at which they are emplaced is unknown and they vary in thickness by an order of magnitude; by considering the sills intruded simultaneously their combined effect will be maximized.

We begin by discussing the results of thermal modeling for the case in which all sills are intruded at the time of extrusion of the total thickness of flood basalt. As we will show, two periods of peak temperatures occur, each creating an extended period of temperatures above 100 °C. Figure 5.4(a) illustrates the thermal history of the complete igneous/sedimentary column of the site at different times between 1 yr and 200 kyr after the igneous event. Each curve corresponds to the temperature as a function of depth, at indicated times after intrusion. One year after intrusion, the thermal signature of individual sills can be clearly recognized as high temperature spikes, with a broad high temperature depth interval at the top of the section representing the thick surficial basalt cap. Peak temperatures at sample sites (1.8 km - 2.2 km depth) range from 810 °C to 170 °C and are reached within 1 yr to 300 yr after sill intrusion. The 100 year curve shows that peak temperatures at sill sites decrease rapidly and heat is transferred to the sediments in the

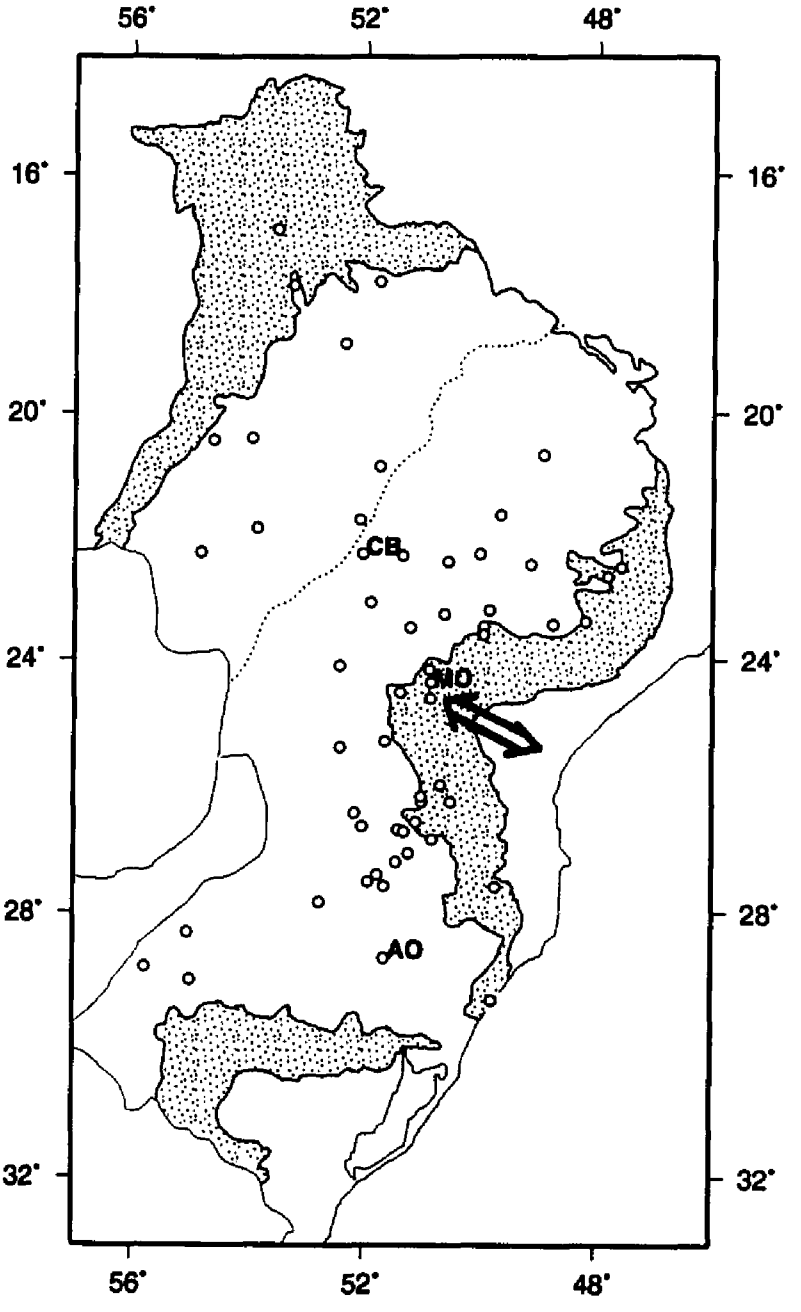

Figure 5.2 Map of the Paraná Basin with sites CB, MO and AO. The arrow indicates the location of the Ponta Grossa Arch. The open circles indicate sites of heat flow determinations presented in Chapter I.

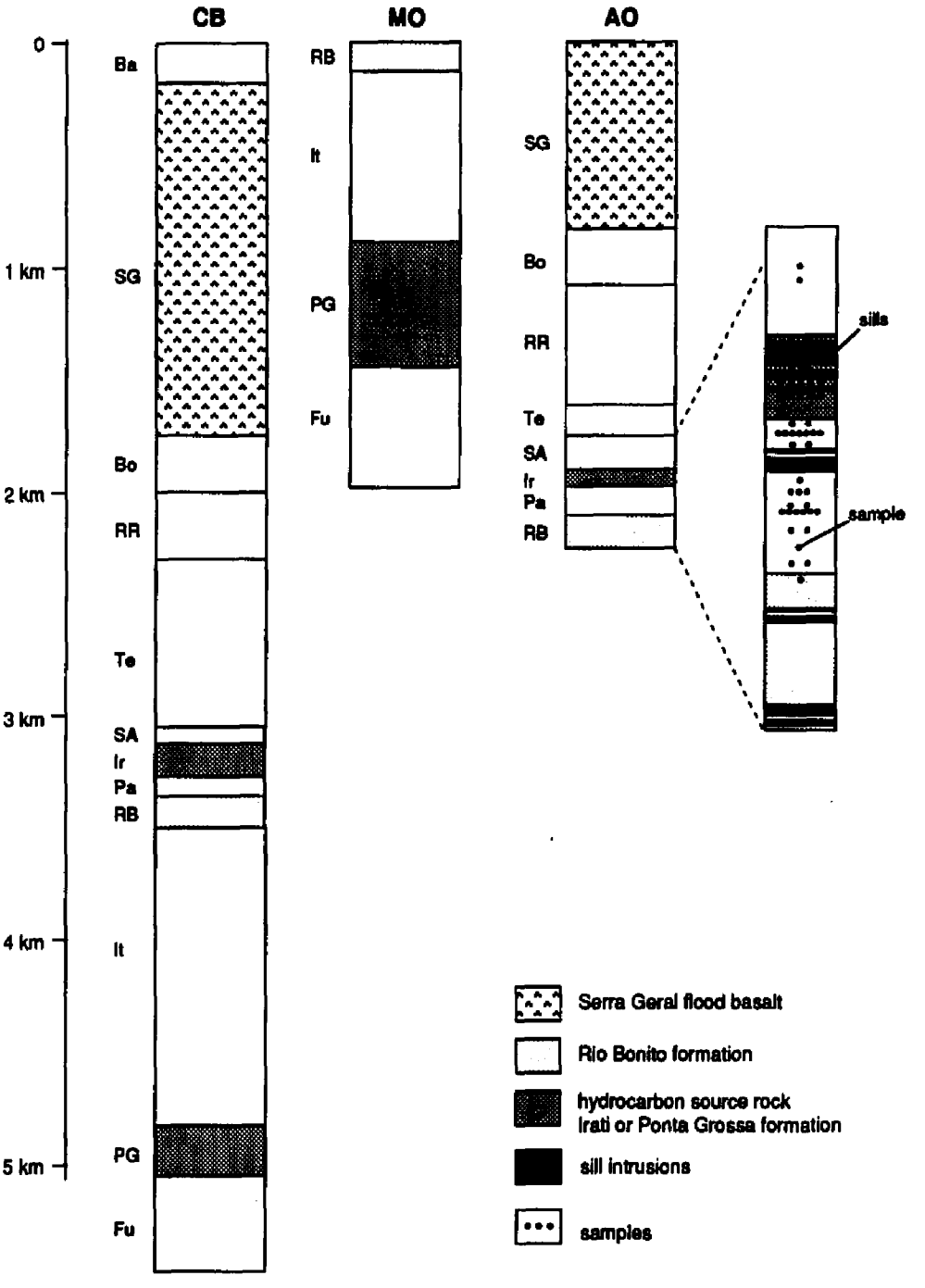

Figure 5.3 Stratigraphic columns for sites CB, MO and AO. The expanded section for site AO shows location and thickness of sill intrusions and approximate sampling sites for I/S determination.

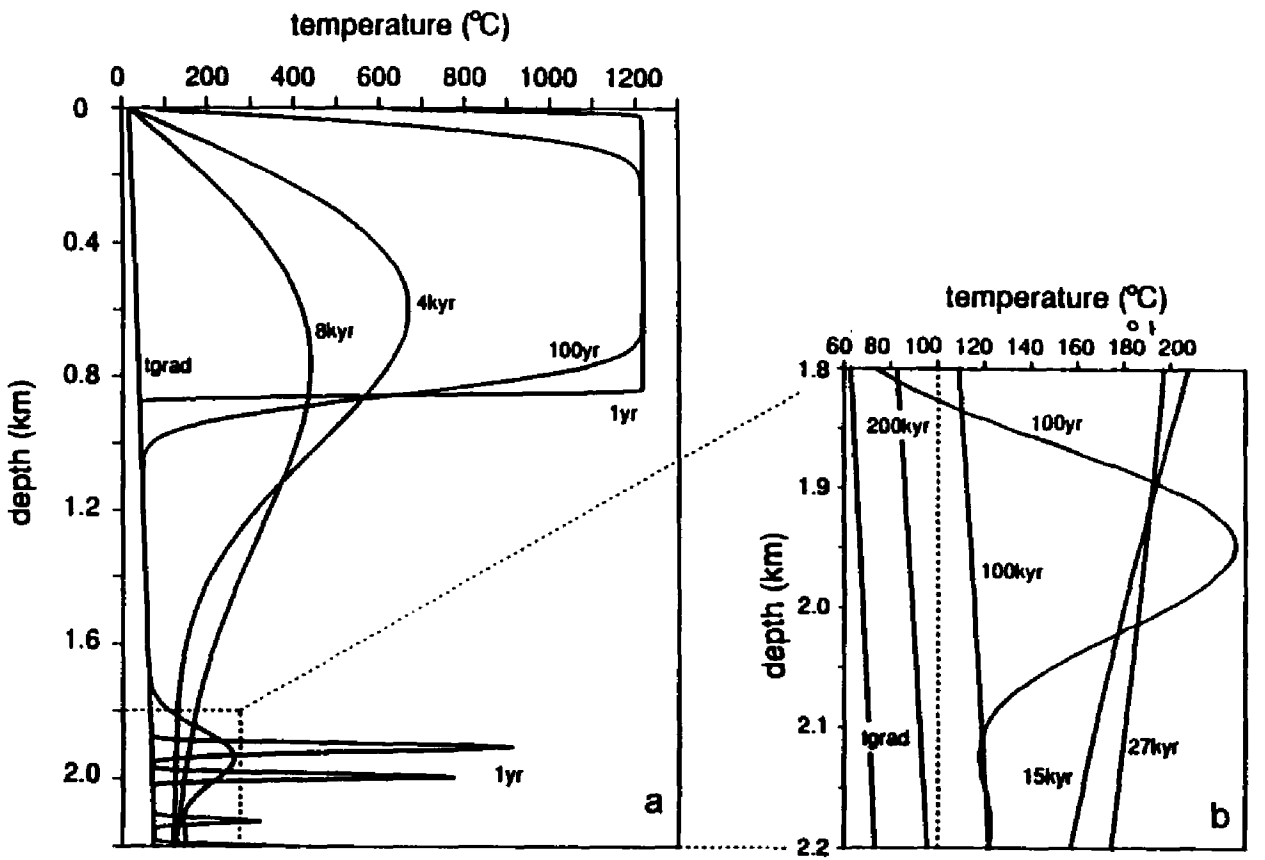

Figure 5.4 (a, left) Calculated temperature evolution due to multiple sill intrusion and simultaneous basalt cap extrusion. Each curve is labeled with the respective time after extrusion/intrusion. (b, right) expanded view of sample interval for later times; 100 yr curve is shown in both (a) and (b), and tgrad shows the temperature due to a geothermal gradient of 26 K km^{-1}.

vicinity of these sills, smoothing out the spikes. The effect of the surficial basalt cap until this time is not yet felt at the depth of the sills. We follow the temperature evolution of this section because we later relate these model results to clay composition from samples within this interval. Temperatures at 4 kyr in the depth interval 1.8 - 2.2 km are rather uniform ranging from 118 °C - 125 °C. Temperatures do not fall below 100 °C before the thermal front from the basalt cap reaches the depth interval of interest sometime around 5 kyr; by 6 kyr the entire section is again warming and the 15 kyr curve in Figure 5.4 (a) shows heating still in progress. Heating continues up to 27 kyr after extrusion/intrusion at which time the shallower part of the depth interval of interest starts to cool while the deeper part is still undergoing warming. Maximum temperatures reached at this second warming range from 185 °C - 210 °C and at 30 kyr the whole interval has practically uniform temperatures of 180 °C - 190 °C. This and the rest of the cooling history can best be observed in Figure 5.4(b), depicting an expanded view of the sediment interval between 1.8 and 2.2 km depth only. This section cools uniformly, and at 100 kyr temperatures are still above 100 °C; it takes 180 kyr for the whole section to fall below 100 °C. Only after 200 kyr is the section within 20 °C of the geothermal gradient background temperatures.

We next discuss the results of thermal modeling for the case in which the basalt is extruded in sequential flows; all sills are assumed to be intruded at the time of extrusion of the first of the series of basalt flows that make up the total basalt thickness at the study site. Although the reported basalt flow thicknesses mentioned earlier span the range from a few meters to 100 m, flows are mostly in the 10 m - 20 m range. In the lack of more specific information about single basalt flows at the study site we assume the first individual basalt flow to be 50 m thick, extruded at the top of the sediment column simultaneously with all sills at depth. Figure 5.5 displays the thermal history of the complete igneous/sedimentary column of this site at different times between 1 yr and 5 kyr since the igneous event in the same format as Figure 5.4. The inset provides an expanded temperature scale for the depth interval of interest. This thermal history proceeds much in the same way as the previous case, but no significant second warming due to the top basalt flow occurs. The maximum effect of this first thin flow upon the deeper section is less than 1 °C and therefore cannot be noticed on Figure 5.5. Therefore a single basalt flow 50 m thick has a negligible contribution to the warming of the section of interest. If we assume that a basalt pile of 1,000 m is made up of individual flows 50 m thick, then 20 such flows are extruded within 1 Myr, which makes an average flow frequency of 1 flow per 50 kyr. The present model suggests that any thermal effect of individual flows 50 m thick will decay within less than 30 kyr, so that an extrusion frequency of 1 flow/50 kyr is not enough to pump heat into the sediments such that a net warming effect may arise. Additionally the more frequent flows in the Paraná Basin are thinner, for which the effect would be even less. Although the sequential extrusion of thin basalt flows adds up to a large amount of heat supplied over geologically short times, this heat is

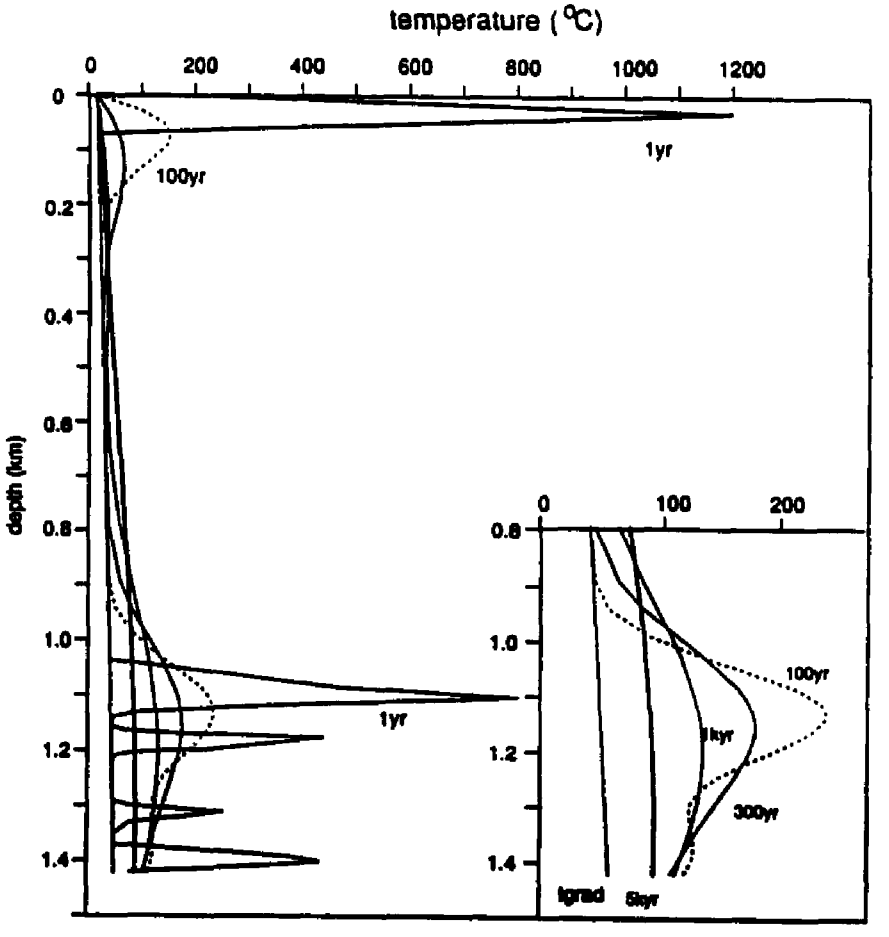

Figure 5.5 Thermal history of multiple sill intrusion and extrusion of a single 50 m thick basalt flow. Each curve corresponds to the temperature profile at the labeled time after extrusion /intrusion. Inset shows expanded temperature scale. The 100 yr curve is dotted in each display; tgrad shows the temperature due to a geothermal gradient of 26 K km^{-1}.

probably diffused away rapidly enough between extrusive events to have negligible influence on sediments at depth.

In summary, the analytical model of sill intrusion/basalt extrusion shows peak temperatures of the order of a few hundred degrees Celsius very nearby sill intrusion, but these are pulses of very short duration. Temperatures exceed 120 °C during about 3.5 kyr and become uniform over the depth interval of interest, cooling uniformly to background temperatures in a few tens of thousand of years. The effects of the extrusion of the flood basalt as a sequence of thin flows is negligible. Only when the extrusion of the total surficial basalt thickness occurs simultaneously with the sills at depth, does the thick basalt cover on the surface provide a second heating event which maintains temperatures above 100 °C uniformly over the whole section for a duration of the order of 150 kyr.

Intervals of time in which temperatures are uniform over the section intruded by sills are of interest because, as will be discussed later, the results from the clay mineral study suggest uniformity of conditions. In the next section we determine the degree of smectite-to-illite conversion in the samples taken from this same borehole, and compare the results to the theoretical histories described above.

3.4 Thermal history recorded by illite/smectite

3.4.1 Introduction

We here address the effects of the flood basalt volcanism and the associated ubiquitous sill intrusions upon the sediments, making use of X-ray powder diffraction (XRD) analysis of clastic sediment samples containing clay minerals. We investigate the progressive conversion of smectite to illite in mixed-layer illite/smectite (I/S) to observe changes in the sediments that may have been induced by the heating of sill intrusion. In the following we shall briefly describe the transformation of smectite to illite in mixed-layer I/S and how these clay minerals relate to the degree of diagenesis and/or very low grade and contact metamorphism in pelitic rocks.

In burial diagenetic environments it is observed that pure smectite gradually disappears with depth. This occurs through the illitization of smectite resulting in the formation of irregular mixed-layer illite/smectite (I/S) with a decreasing percentage of smectite (referred to also as percentage of expandable layers) within the I/S with increasing depth. I/S with a proportion of up to 20% illite/80% smectite layers seems to be relatively stable over considerable depth intervals at shallow levels (Kisch, 1983). When temperatures in the range of 58°C - 92°C (Freed and Peacor, 1989) are encountered the conversion progresses by increasing the proportion of illite layers at the expense of the smectite layers more rapidly. This stage is referred to as the actual onset of the smectite-to-illite conversion. The percentage of smectite continues to decrease with depth to

about 40 % with an associated change in type of interstratification (ordering) of these layers, from random (R0) to ordered IS (R1). Completion of this transformation is considered to have been attained when the proportions of 80% illite/20% smectite are reached. This occurs in the temperature range of 88 °C - 142 °C (Freed and Peacor, 1989). Generally I/S with less than 20 % smectite layers are found to be very stable over large depth intervals. The transition from a random I/S to an ordered I/S has been observed to occur in I/S with more than 60% illite layers (Perry and Hower, 1970) corresponding to a temperature of about 95° C. In some localities the smectite-to-illite conversion has been observed to progress to I/S with less than 15 % smectite with ISII type ordering (R3). In a contact metamorphic environment, Pytte and Reynolds (1989) observe a smooth transition to nearly 100 % illite with proximity to a dyke intrusion.

The measure of the percentage of smectite layers (hereafter % smectite) of I/S has been used in many studies to characterize the effects of burial and contact metamorphism. The investigation of the Tertiary Gulf Coast sequence by Perry and Hower (1970) is the classic example of a burial metamorphic (diagenetic) sequence study. These authors documented the complete smectite-to-illite conversion within a depth interval of 3-4 km. Brusewitz (1986) studied the effects of a diabase intrusion on bentonites in Killekulle, Sweden. She observed a clear monotonic increase in % smectite layers as a function of increasing distance from the intrusive body. Pytte and Reynolds (1989) obtained similar results in their study of the effects of dyke intrusion in the upper Pierre Shale near Walsenburg, Colorado. Nadeau and Reynolds (1981) observed relationships among I/S compositions and proximity to a stock intrusion in the Mancos shale, Southern Rocky Mountains. On the other hand, Smart and Clayton (1985) noted that %smectite and distance to the Whin Sill in northern England were related only very close to the intrusion: the affected region extends for distances about 1.5 times the thickness of the sill, corresponding to temperatures in excess of 250 °C.

Pytte and Reynolds (1989) have described the smectite-to-illite conversion as a kinetic reaction in which the % smectite in I/S is an explicit function of both temperature and time. Based on their study and other data they compiled from the literature, they argue that conversions to 80 %illite at peak temperatures of about 250 °C -150 °C require durations of these thermal conditions from 10 yr to 10 kyr for the contact metamorphic environment. The same degree of conversion in a burial diagenetic environment would, according to Pytte and Reynolds, be accomplished at temperatures of 100 °C - 70 °C existing for intervals of 10 Myr to 100 Myr, respectively.

3.4.2 Sample description and preparation

Our investigation of the effects of sill intrusion on the conversion of smectite to illite comprises detailed examination of core samples from the borehole AO-1-RS, which was used in

the previous section to illustrate the evolution of temperatures as a function of time following sill intrusion and basalt extrusion (see location on map of Figure 5.2). Samples were taken from three Permian formations (Irati, Palermo and Rio Bonito) at varying distances from sills (0.5 to 60 m away from the closest sill) in the depth interval of 1,800 to 2,100 m, as indicated on Figure 5.3. Within the Irati Formation the samples are dark shales which grade to shaly laminated siltstones in the Palermo Formation and to slightly sandier laminated siltstones in the Rio Bonito Formation.

These samples were mechanically disaggregated and the <2 μm fraction separated by centrifugation in 250 ml centrifuge bottles, according to the method of Jackson (1974). Oriented samples were prepared by pipetting a clay slurry of the sediment onto a glass slide. The slides were air dried and then placed in an ethylene glycol atmosphere at ambient temperature for at least 24 hours prior to XRD analysis.

3.4.3 Analytical methods

To establish the proportions of smectite and illite in mixed-layer I/S, we used Method I of Srodon (1980). This method uses the difference in °2θ of the two reflections in the range 42° - 48° 2θ (Δd_2 value) as a measure of the percentage of smectite layers present. The kind of interstratification and degree of perfection of the ordering of I/S also necessary to this procedure is given by inspection of XRD patterns in the range of 5.2° to 10.4° 2θ. For further details on this procedure we refer to Srodon (1980). The samples were scanned in the ranges 4° - 13° 2θ and 41°- 49° 2θ. XRD patterns were recorded using CuKα radiation, and the data were collected automatically by step-scanning at 0.01° 2θ intervals with 1 s counting time.

3.4.4 XRD results

Figure 5.6 presents three representative XRD patterns (samples 23, 36 and 40). The presence of a smectite component in our samples can be readily seen in the characteristic asymmetric and broadened 10 Å peak of the ethylene glycol treated sample. Table 5.1 contains the results of the analysis in terms of % smectite present for the 39 samples.

Practically all samples show perfect IS type interstratification except sample 11 (random) and samples 2, 5 and 13 (partial IS). The mean %smectite is 38.4 ± 2.1 (standard deviation about the mean), so the overall variability is of the order of about 6 % with respect to the mean value. In Srodon (1980) the errors of the method for determining the % smectite are reported to be within 1-5% of the % smectite determination. Due to the fact that some of the peaks in this analysis are quite broad and plateau like, therefore making peak position difficult to determine with precision, we assess our error to be of the order of 5%. This signifies that the variability among our samples is close to the analytical error and thus despite some lithologic variability the composition of I/S should be considered uniform over the depth interval investigated. In Figure 5.7 these results are

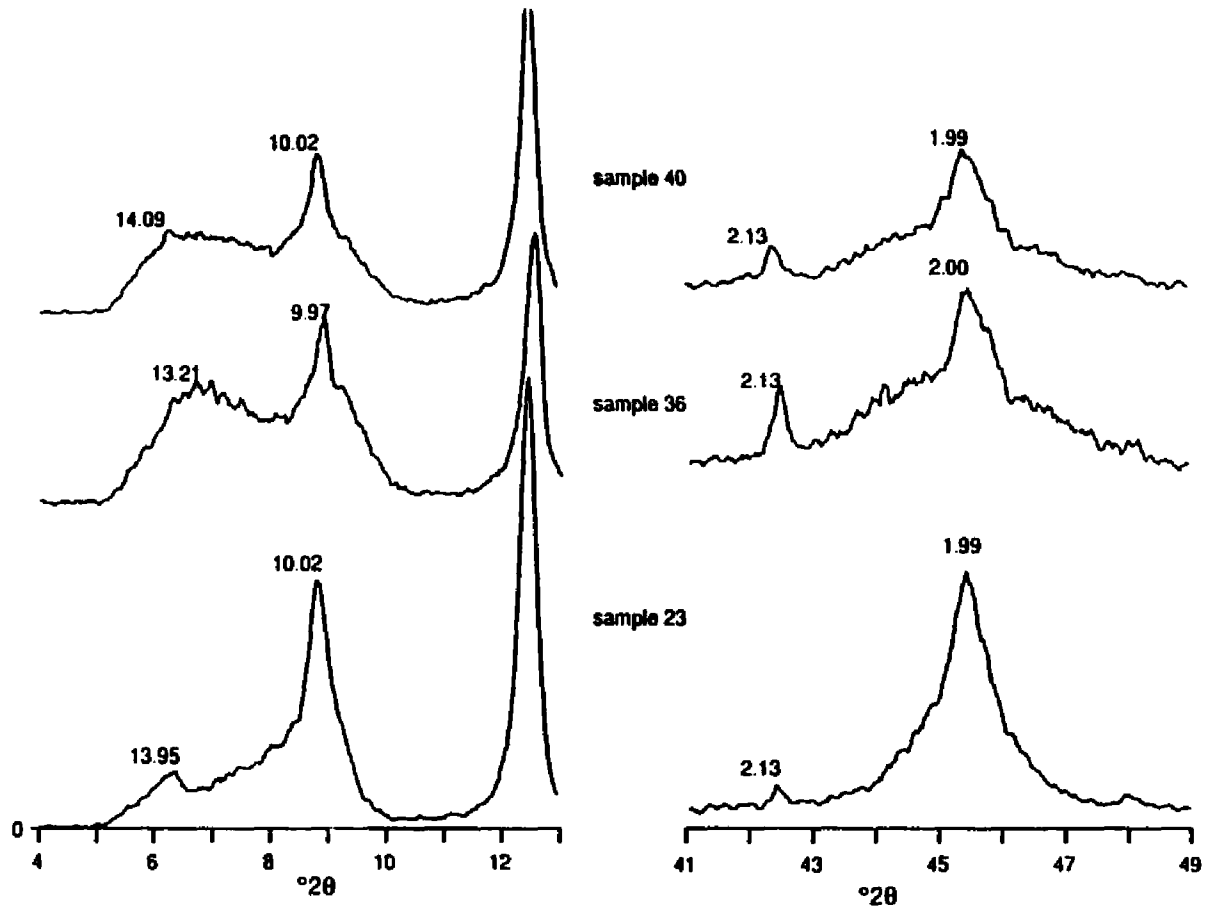

Figure 5.6 XRD patterns for representative samples (ethylene glycol treated). The d-value is shown above the respective peak.

TABLE 5.1 XRD results for illite/smectite

Sample number	Depth (m)		Distance from the next sill (m) above	below	Percent smectite in I/S
1	1835.5			60.5	38.6
2	1844.5			51.6	40.7
4	1893.8			2.2	32.3
	1896.0	* sill 1			
	1908.0	(12 m)			
	1909.0	sill 2			
	1911.0	(2 m)			
5	1911.5		0.5	2.5	38.2
7	1912.0		1.0	2.0	41.4
	1914.0	sill 3			
	1920.0	(6 m)			
8	1921.5		1.5	7.5	41.4
10	1922.1		2.1	6.9	43.6
11	1922.5		2.5	6.5	41.8
13	1928.1		8.1	0.9	39.6
	1929.0	sill 4			
	1931.0	(2 m)			
15	1939.5		8.5	46.5	43.2
16	1939.9		8.9	46.2	41.4
18	1948.1		17.1	37.9	39.5
19	1965.5		34.5	20.5	39.1
20	1966.5		35.5	19.5	39.5
21	1972.5		41.5	13.5	36.4
22	1975.5		44.5	10.5	37.3
23	1976.2		45.2	9.8	38.2
24	1976.4		45.4	9.6	36.4
25	1977.5		46.5	87.5	36.8
26	1977.7		46.7	8.4	38.4
27	1978.0		47.0	8.1	36.8
29	1984.2		53.2	1.8	35.9
	1986.0	sill 5			
	1989.0	(3 m)			
	1990.0	sill 6			
	2000.0	(1.5 m)			
31	2007.2		7.2	114.9	36.8
32	2007.8		7.8	114.3	38.2
33	2009.1		9.1	112.9	36.4
34	2010.0		10.0	112.0	37.3
35	2012.0		12.0	110.0	38.2
36	2012.5		12.5	109.6	35.9
37	2012.7		12.7	109.3	38.2
38	2016.0		16.0	106.0	38.2

continued on the following page

TABLE 5.1 XRD results for illite/smectite (continued)

Sample number	Depth (m)	Distance from the next sill (m) above	Distance from the next sill (m) below	Percent smectite in I/S
39	2016.3	16.3	105.7	38.2
40	2016.5	16.5	105.6	38.2
41	2017.0	17.0	105.0	40.5
42	2018.0	18.0	104.0	38.2
43	2018.6	18.6	103.4	38.2
44	2034.3	34.3	87.8	38.2
46	2052.9	52.9	69.1	38.2
48	2071.0	71.0	51.0	36.8
49	2097.6	97.6	24.4	37.3
	2122.0 2123.0	sill 7 (1 m)		
	2124.0 2127.0	sill 8 (3 m)		
	2200.0 2205.0	sill 9 (5 m)		
	2213.0 2217.0	sill 10 (4 m)		

* given are depths of top and bottom of sill

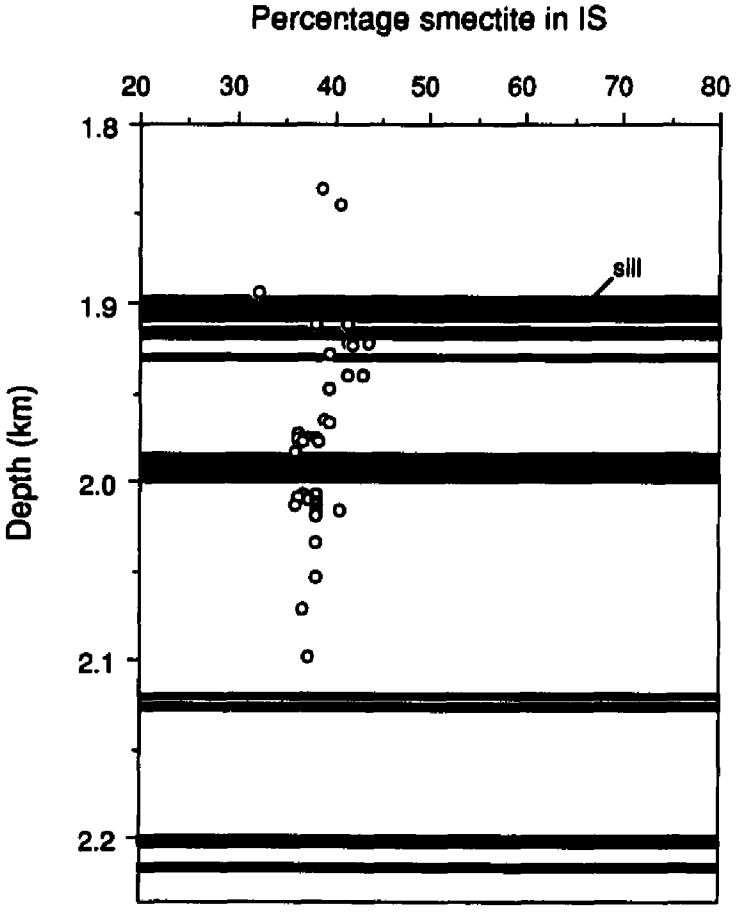

Figure 5.7 Percentage smectite in I/S as a function of depth, with shaded areas showing location and thickness of sill intrusions.

plotted as a function of depth with sill positions marked. The percent smectite scale brackets the whole range in variation from the beginning of smectite to illite conversion at 80 % smectite to its completion at 20 % smectite. No apparent relationship between sill and sample site configuration and I/S composition is observed and the conversion of smectite to illite is incomplete.

3.4.5 Discussion

Previous studies in contact metamorphic environments (Brusewitz, 1986; Pytte and Reynolds, 1989; Nadeau and Reynolds, 1981) have shown a clear relationship of % smectite and type of ordering with distance from intrusive body; generally a monotonic increase of %smectite with increasing distance. These studies, however, have investigated the effects of the presence of individual intrusions, whereas in our case the effects are made more complex by multiple bodies.

Our results for the proportion of smectite layers within mixed-layer I/S differ from those cited above. The % smectite for our samples has a small variability around 38% smectite/62% illite, so despite some lithologic variation, mixed-layer I/S is overall quite uniform. The onset of conversion is recorded (practically all samples have >60% illite layers with IS type ordering), but the conversion has not gone to completion. As mentioned above Figure 5.7 shows no apparent relation between I/S composition and sill proximity.

The uniformity of %smectite indicates an uniformity of conditions at all sample sites. This uniformity suggests that peak temperatures alone do not control the smectite-to-illite conversion, because if they did samples closest to sills would show higher degrees of conversion than samples at greater distances. Hence, duration of thermal conditions (and perhaps other factors) must also be an important factor. The thermal model of the igneous event shows two time intervals in which an overall uniformity in temperatures over the sample depth range is attained: (a) an early interval due to the intrusion of sills in which temperatures are uniform at an average of 154 °C after about 500 yr and remain essentially uniform across the sample depth range (although diminishing with time) as the section cools: at 4 kyr temperatures are in the range 118 °C - 125 °C, and temperatures remain above 120 °C for about 3.5 kyr; (b) a second warming occurs for the case where the basalt is extruded all at once, increasing temperatures at sample sites to between 185 °C and 210 °C. In this case, at 30 kyr temperatures are uniform between 180 °C and 190 °C and remain above 100 °C to 180 kyr, such that uniform temperature conditions above 100 °C occur during a 150 kyr interval. The second warming is absent when the basalt is accumulated by sequential flows over a 1 Myr interval. Figure 5.8 shows the ranges of temperatures for onset and completion of the smectite-to-illite conversion as compiled by Freed and Peacor (1989) from case studies. Temperatures from the thermal model within the range for completion of the smectite-to-illite conversion occur during 3.5 to 150 kyr. The data, however, indicate incomplete conversion,

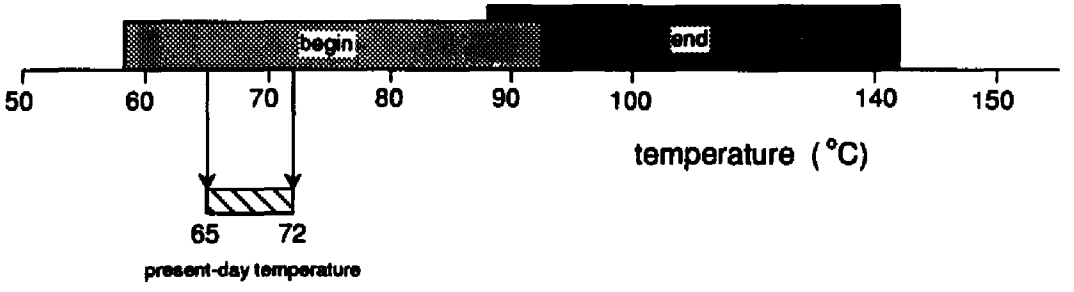

Figure 5.8 Ranges of temperature for onset and completion of the smectite-to-illite conversion as compiled by Freed and Peacor (1989). The present-day temperature range for the sample site is indicated.

thus suggesting that intervals of time of this order are insufficient to promote the conversion to completion, or alternatively that such high temperatures as predicted by the conductive model have not been attained. Model calculations assuming conductive heat transfer only yield the maximum thermal effect from the igneous event; any convective heat transfer will redistribute heat more efficiently and yield lower temperatures. The igneous rocks are intruded into wet and porous sediments and may have promoted a pulse of convective flow which may have removed heat and aided in reducing temperatures rapidly within the sediments.

The present-day geothermal gradient at this site is 26 K km^{-1} and exposes this section to temperatures of 65 - 72 °C, within the range needed for the onset of the smectite-to-illite conversion as indicated on Figure 5.8. In this context the extrusion of this thick basalt cap, of the order of 1 km, may have contributed to bringing the underlying sediments within smectite-to-illite conversion temperatures through burial alone, moving the underlying sedimentary section to greater and warmer depths. Considering subsidence at the study site of the same order as the present-day basalt thickness (860 m) the sample depth interval would have been shifted from a region of background temperatures of the order of 43 °C - 49 °C to deeper levels of 65 °C - 72 °C at about 130 Ma. We show this effect in describing the results of modeling thermal histories for another two other boreholes later in Section 4.

Thus, within the context of strictly thermal models, there exist two possibilities to explain the uniform observed % smectite composition in terms of thermal phenomena: (1) uniform temperatures of about 100 °C over the section attained from multiple intrusions over times ranging up to 150 kyr, caused by igneous activity, with incomplete conversion perhaps due to the short duration of these higher temperature conditions, or (2) the geothermal gradient has brought the section to its present composition, but higher temperatures of longer duration are apparently necessary to complete the conversion.

Even though thermal controls on I/S predominate in the literature, other possibilities may also explain the observed I/S data. The uniformity of I/S suggests that homogenization within the sampled depth interval may have occurred. This may perhaps be accomplished by a fluid flow event. If a fluid flow pulse related to the intrusion into wet porous sediments occurred, heat could have been removed rapidly by advection, preventing the sediments from experiencing high temperatures. Another possibility is that the smectite to illite conversion may have at one time been completed, producing an uniform I/S ratio of about 80 %, and that later retrograde activity within the sediments caused illite layers to be 'reconverted' to smectite. Detailed examination of these alternatives are beyond the scope of this dissertation.

3.5 Summary

A thermal model of multiple sill intrusion has been derived and applied to the extrusion/intrusion geometry of the study site at borehole AO-1-RS: 860 m of flood basalt at the surface and 10 sills intruded in the depth interval of 1.8 km - 2.2 km. The maximum thermal effect of this volume of igneous rock has been assessed by assuming that the total surficial thickness of basalt and the sills at depth were intruded simultaneously. The sedimentary section close to the sill intrusion region experiences peak model temperatures of 150 °C to 800 °C attained within a few hundred years. As this heat due to the sill intrusion is diffused over the section of interest temperatures become uniform above 120 °C for a time period of 3.5 kyr. The effect of extruding the total thickness of the surface basalt flow produces a second warming that peaks at about 27 kyr with temperatures of 185°C - 210 °C and yields uniform model temperatures above 100 °C during 150 kyr. Alternatively if the flood basalts are modeled as thin individual flows extruded sequentially, the thermal calculations suggest these to have an insignificant effect on temperatures within the sampled region.

The results of the determination of %smectite in I/S show uniform values of about 38 % smectite over the whole sampling interval between 1.8 and 2.2 km depth, showing that the smectite-to-illite conversion was initiated, but not completed. There is no relationship between observed %smectite in I/S and sill position and thickness. Three hypotheses can explain the uniform 38 % smectite in I/S data. (1) I/S is in agreement with the present-day thermal conditions controlled by the long term geothermal gradient, with temperatures sufficient to initiate but not to complete the smectite-to-illite conversion; the igneous event, although providing high temperature conditions, was too short-lived to influence the rate of smectite-to-illite conversion and its principal thermal effect was depositional, shifting the sample interval at about 130 Ma to its present-day depth and temperature range (this is in agreement with the results of the modeling of thermal histories in Section 4). (2) The igneous event provided sufficiently high temperatures for full S-I conversion but insufficient time, the conversion being suppressed by kinetic effects. (3) The smectite-to-illite conversion may have been completed during the igneous event, but retrograde activity has reconverted part of the illite to smectite or a fluid flow event has prevented the sediments from experiencing high temperatures or has obliterated any thermal imprint on the clay minerals (either geothermal gradient or igneous) producing a homogenized section with uniform I/S that reflects the characteristics of the fluid.

It is likely that the overall thermal effect of the cooling of igneous rocks has been minor in promoting clay diagenesis in the study site and although substantial amounts of heat were released in this igneous event, most of it was able to be redistributed rapidly. However, the extruded volume of lava has contributed to a loading of the Paraná Basin with on average of 600 m

of basalt, which has contributed to the subsidence of the basin. The consequence of this event is the shifting of the sedimentary column downward to its present-day temperature range of 65 °C - 72 °C, a range compatible with the geologically recorded onset of the smectite-to-illite conversion in other locations. In addition to thermal affects, geological, chemical and hydrological factors may also influence the I/S ratio under certain circumstances. Our discussion in this study, however has focused principally on the effects of the thermal conditions and their duration.

4. A COMPARISON OF THE THERMAL HISTORY OF TWO SITES

We now develop detailed thermal histories that integrate the effects of subsidence, uplift and Mesozoic thermal events. Oliveira (1987) analyzed the subsidence history of the Paraná Basin, finding three major depositional phases (Silurian-Devonian, Permo-Carboniferous and Jurassic-Cretaceous). The first two Oliveira arbitrarily attributed to extensional events and the third to the depositional load of the Serra Geral flood basalts. Heat flow was considered uniform over the whole basin, with two high heat flow events corresponding to the extensional events. In the present study, we use numerical modeling to investigate the effects of subsidence, uplift and erosion, including the effects of variable heat flow with time. The variation of heat flow includes an initial period of high heat flow which could be attributed to a basin-initiating thermal event, and the effects of the Serra Geral igneous event with an increase in heat flow due to the cooling of an underplate and the effects of heat diversion due to a thickened zone of lithosphere underneath the central part of the Paraná Basin.

We address the thermal histories of two contrasting sites within the Paraná Basin: one located in the central and deepest part, and second on the eastern margin of the basin. Location of these two sites, CB and MO, is shown in Figure 5.2, and their stratigraphy in Figure 5.3. The depositional history of these two sites differs markedly. CB is the deepest borehole in the basin: it penetrates over 1,500 m of flood basalt and encounters the basement at a depth of 5,500 m. In contrast, MO lies on the Ponta Grossa Arch, uplifted in the Late Jurassic and later again in the Late Cretaceous/Tertiary. As a consequence, the stratigraphic section younger than Middle Permian has been stripped off at site MO. With respect to site CB this corresponds to a section over 3,000 m thick. The present-day heat flow at CB is 48 mW m^{-2}, while at MO it is 58 mW m^{-2}. Figure 5.9 shows temperature profiles for both sites computed from the best fit temperature field obtained from the inversion of BHT data for the whole basin (see Chapter IV); CB has higher temperatures than MO at equivalent depths, even though its heat flow is lower.

To model this thermal evolution we have used a numerical model (GOTHIC: Gas, Oil and Thermal History Integrated Code) developed by Deming and Chapman (1989) that solves the one-dimensional time-dependent conductive heat transfer equation including solid-state advection (subsidence and uplift), time-dependent heat flow from the basement, heterogeneous

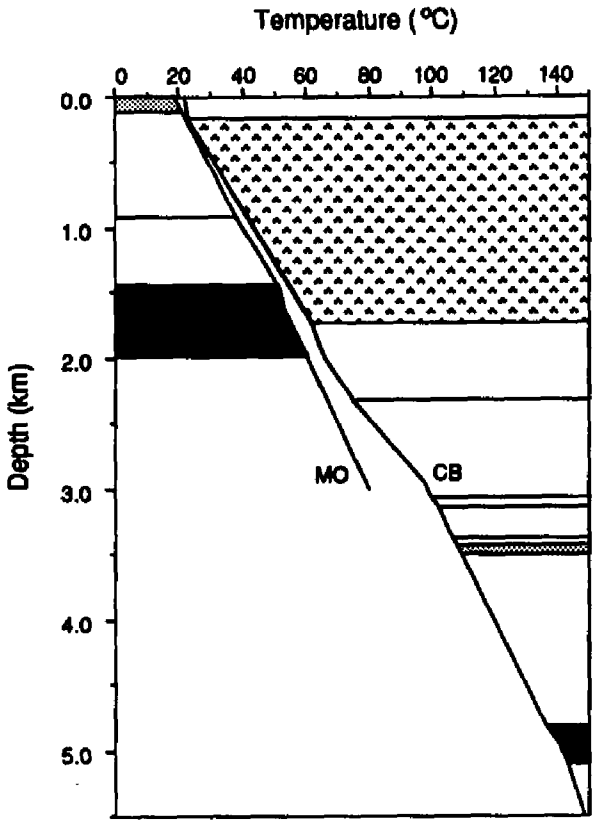

Figure 5.9 Temperature profiles for sites CB and MO. The dark shaded interval denotes the Furnas formation and the light shading the Rio Bonito formation at both sites. The patterned interval shows the Serra Geral flood basalt thickness at site CB.

temperature dependent thermal conductivity, sediment compaction, and radiogenic heat production (for a detailed discussion see Deming and Chapman, 1989). We use the present-day thermal state at these sites to constrain the results of modeling the thermal history. The timing of basin stratigraphic and igneous events has been taken from Oliveira (1987) and is shown in Table 5.2 below. The Serra Geral igneous event is considered here principally as deposition of another stratigraphic unit; the heat content associated with this event was considered and discussed in section 3. However, we have included the contributions of increased heat flow from the cooling of the underplate and the redistribution of heat flow following the Serra Geral igneous event due the diversion of heat by a thickened lithosphere beneath the Paraná Basin.

The model output yields the depth and temperature of a chosen horizon, and surface heat flow at the site as a function of time. The effect of subsidence is to depress cold rocks into the subsurface causing a transient decrease in the temperature gradient and surface heat flow, while erosion brings warmer rocks closer to the surface, causing a transient increase in geothermal gradient and surface heat flow (discussion of the thermal effects of uplift and erosion was presented in Chapter III).

Table 5.2 Chronology of the Paraná Basin (Oliveira, 1987)

Event/Formation		Time interval (Ma)	Duration (Ma)
unconformity		0 - 65	65
Baurú	Ba	65 - 119	54
Serra Geral (igneous)	SG	119 - 144	25
Botucatú	Bo	144 - 188	44
unconformity		188 - 248	60
Rio do Rasto	RR	248 - 251	3
Teresina	Te	251 - 253	2
Serra Alta + Irati	SA + Ir	253 - 255	2
Palermo	Pa	255 - 258	3
Rio Bonito	RB	258 - 261	3
Itararé	It	261 - 296	35
unconformity		296 - 367	71
Ponta Grossa	PG	367 - 394	27
unconformity		394 - 401	7
Furnas	Fu	401 - 414	13

Uncertainties in the results are associated with the uncertainties in the model parameters (initial porosities, rates of compaction, matrix thermal conductivities, matrix thicknesses, radiogenic heat production, surface temperature as a function of time). The results are not significantly affected by changing the initial porosities and compaction rates, and mean thermal conductivities

are well constrained (see Chapter II). The formation thicknesses included the sill thicknesses intruded into these formations, such that the formation thicknesses of units older than the igneous event have been overestimated for the history preceding the igneous event, with the consequence that the resulting temperature history for any given formation older than the Serra Geral formation will be an upper limit. The time intervals spanning basin wide unconformities are treated in general as non-depositional intervals, as estimates of the amount of uplift and erosion are highly speculative. However we have modeled a case in which erosion within a period of unconformity was included. The effect on surface heat flow is small (less than 2 mW m^{-2}) and the transient effect decays within a few million years.

Figure 5.10 shows the resulting total subsidence curves for each stratigraphic interval for site CB. Immediately apparent are the three major depositional events described earlier in section 2.1: Silurian-Devonian (414 - 367 Ma), Carboniferous-Permian (296 - 248 Ma) and Jurassic-Cretaceous (144 - 119 Ma) and shown in Table 5.2. An estimate of the mean total subsidence rate for each stratigraphic interval of Table 5.2 for this site is given in Figure 5.11 and emphasizes the episodic aspect of basin evolution. Although subsidence rates for the same interval may vary across the basin, they show that the subsidence rate for the Carboniferous-Permian deposition is higher by an order of magnitude than the other depositional epochs, amounting to hundreds of meters per million year. With exception of the deposition of the Serra Geral flood basalts subsidence rates were small during the Jurassic-Cretaceous, less than tens of meters per million year.

Figure 5.12 shows the surface heat flow history obtained from the GOTHIC model for a variable basal heat flow with higher heat flow accompanying the Paleozoic initiation of the basin and the Mesozoic Serra Geral event, following this last event heat flow decreases at this site due to diversion of heat from beneath the central part of the basin to the eastern margin. Surface heat flow is temporarily depressed at the beginning of each depositional interval, with the magnitude of the decrease larger for higher sedimentation rates. Subsequently heat flow increases towards a new 'equilibrium' value, slightly higher than before the last depositional event because of the radiogenic heat production of the sediments deposited in that interval. Within the long history of the Paraná Basin, all transient effects of sedimentation decay within a few million years. The depositional effect of the flood basalt event (144 - 119 Ma) decreases heat flow from 144 Ma to 63 Ma. However, the inclusion of a basal heat flow increase associated with the plume impingement and flood basalt production and extrusion offsets nearly entirely the depositional effect. Following the Serra Geral event heat flow decreases due to heat diversion to a new steady state at the present-day heat flow value. Furthermore, the results in Figure 5.12 show that an initial high heat flow event decays within less than 50 Myrs, in agreement with the effect predicted by the McKenzie (1978) model.

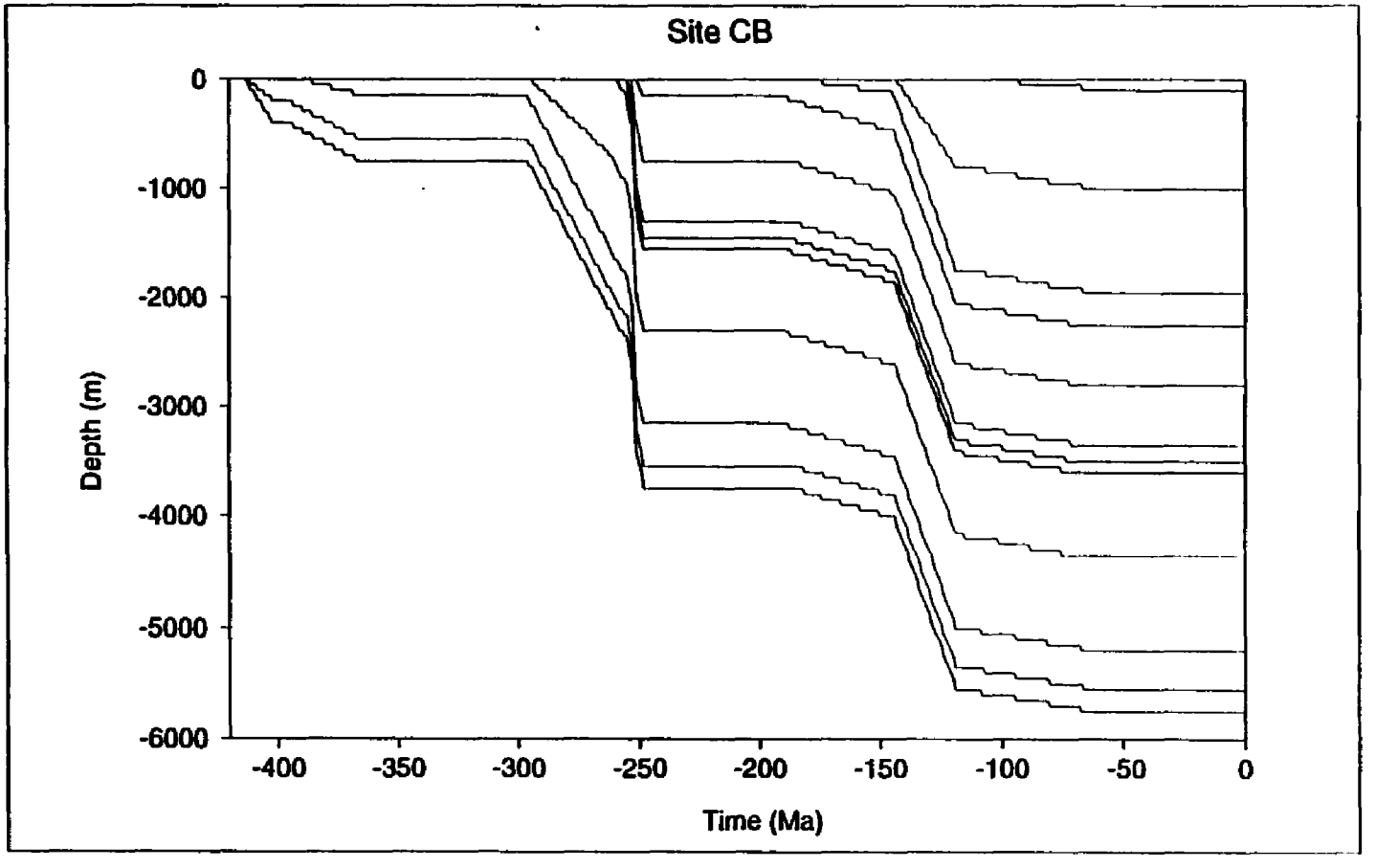

Figure 5.10 Subsidence curves for site CB including all formations; at the present-day (time=0) the stratigraphic column in Figure 5.2 is matched.

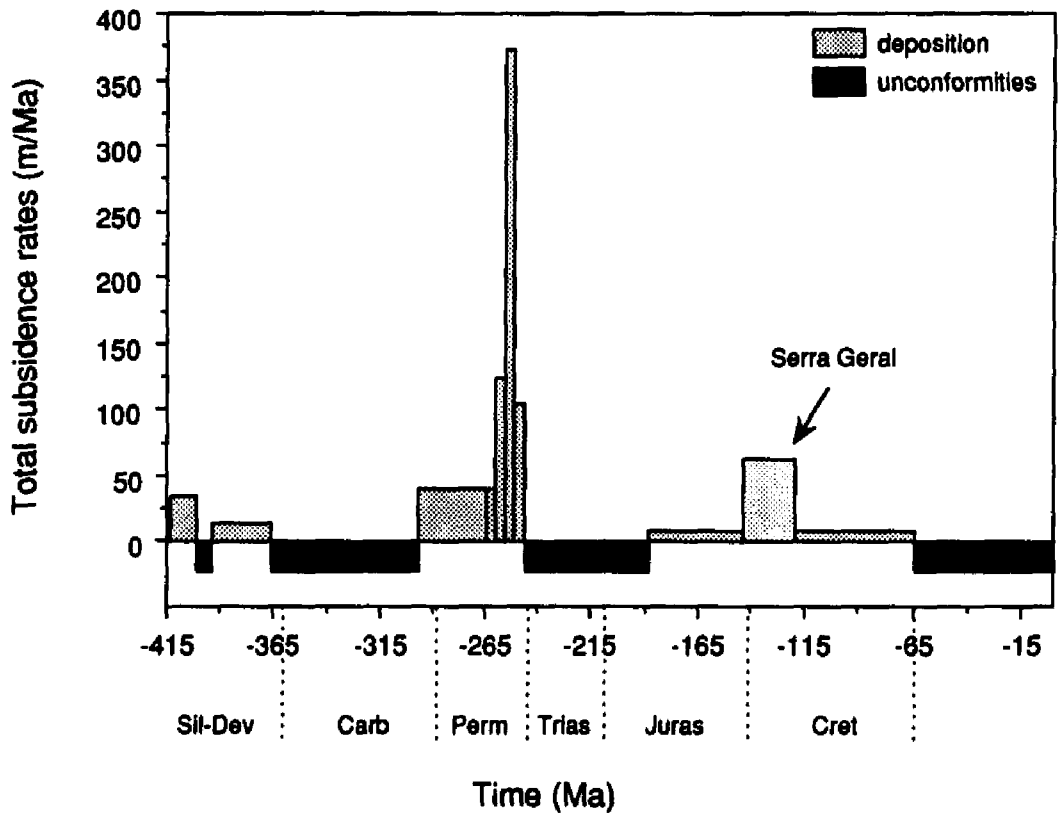

Figure 5.11 Estimated maximum subsidence rates at site CB.

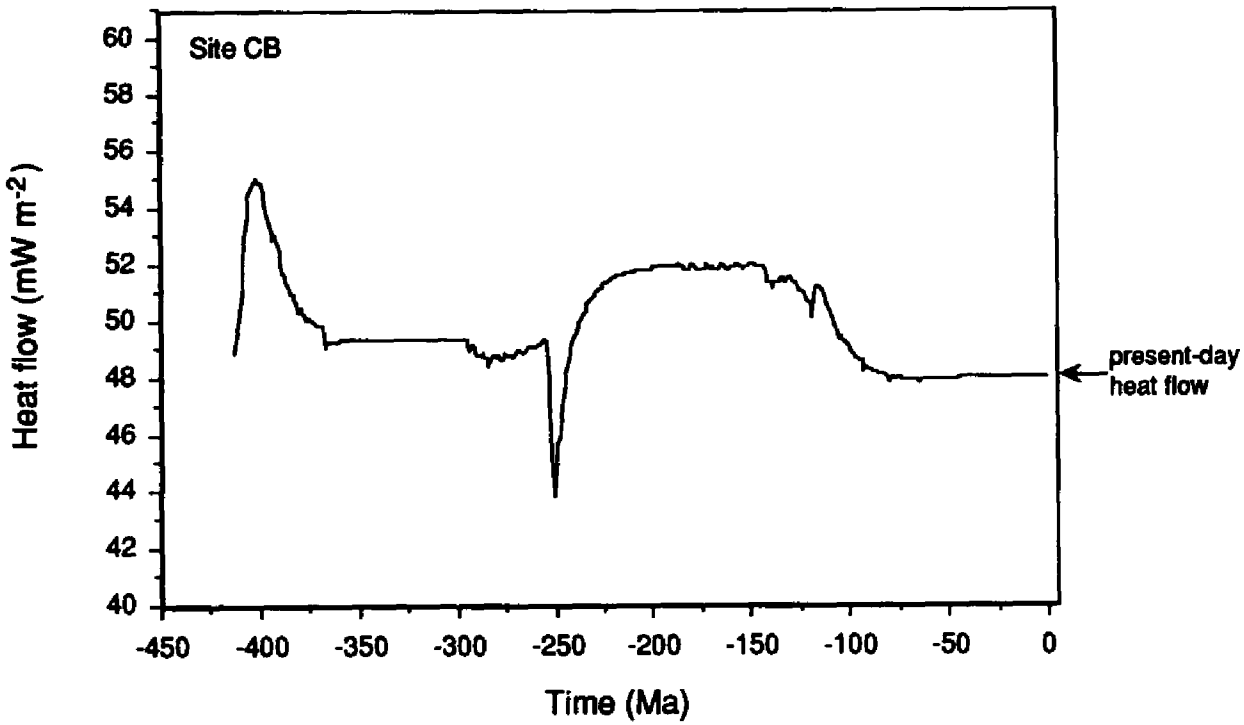

Figure 5.12 Surface heat flow vs. time for site CB. An initial high basal heat flow event, high heat flow due to the Serra Geral event (144 - 119 Ma) and subsequently a decrease in heat flow due to heat diversion under the thickened lithosphere were included in the model.

We have plotted the temperature history of the top of the basement in Figure 5.13. The effect of initial high basal heat flow is less than 1 °C, and cannot be perceived at the scale of the figure. In Chapter III we have shown that increased temperatures in the basin due to the cooling of flood basalts are very short-lived: within less than 2 Myr temperature increments are less than 5 °C at the top of the basement. Also we showed that cooling of an underplate produced increased heat flow of up to 6 mW m^{-2}, with maximum increments of temperatures of about 7 °C, decaying to one half this magnitude within 20 Myrs. The contribution of such episodes of increased heat flow upon the time-temperature-integral (the area under the curve in Figure 5.13) is very small. The largest effect of the Serra Geral event that can be observed in Figure 5.13, is the depositional effect of the flood basalt thickness at the CB site. This alone is responsible for increasing the temperatures at the base of the basin by about 40 °C and has consequences for the maturation of hydrocarbons as we discuss below.

The Irati formation is a source rock for some of the oil plays in the Paraná Basin (Zalán et al., 1991), hence its thermal evolution is of relevance to the maturation of hydrocarbons. To illustrate the effect of the Serra Geral igneous event upon the maturation of source rocks for hydrocarbons, we include the temperature history within the Irati formation in Figure 5.13. The depositional effect is responsible for the largest increase in temperature, of the order of 40 °C. The increased heat flow due to the Mesozoic igneous event causes only a small blip in the temperature history; the effect of the decrease in heat flow due to the diversion of heat is larger. The GOTHIC model also computes an estimate of the percentage of organic matter which has been converted to oil. Figure 5.14 shows the percent of organic matter converted to oil as a function of time. Oil generation begins approximately at 125 Ma, reaching a conversion of 36 % of the organic matter at the present-day. Higher heat flow from the Serra Geral event caused the rate of conversion to increase early in the oil generation process, and as heat flow decreases the rate of conversion slows down. The Irati formation is also characterized by hosting sill intrusions in much greater numbers than the other formations in this basin (Zalán et al., 1991). The temperature history in the sediments due to the proximity of sill intrusions was addressed in the previous section 3. Sill intrusions of up to tens of meters thick, such as in the example of site AO discussed in section 3.3, maintain high temperatures for time intervals only of the order of thousands of years. The effect of intrusions of hundreds of meters last only hundreds of thousands of years. These short-lived effects make a very small contribution to the time-temperature-integral (TTI).

We next use the same model and approach to investigate the thermal history of site MO, and compare the results to those obtained for site CB. Site MO is situated at the eastern margin of the basin, upon the Ponta Grossa Arch, which was uplifted at first before and again after the flood basalt extrusion. This site at the present-day has higher heat flow than the first site CB. We have

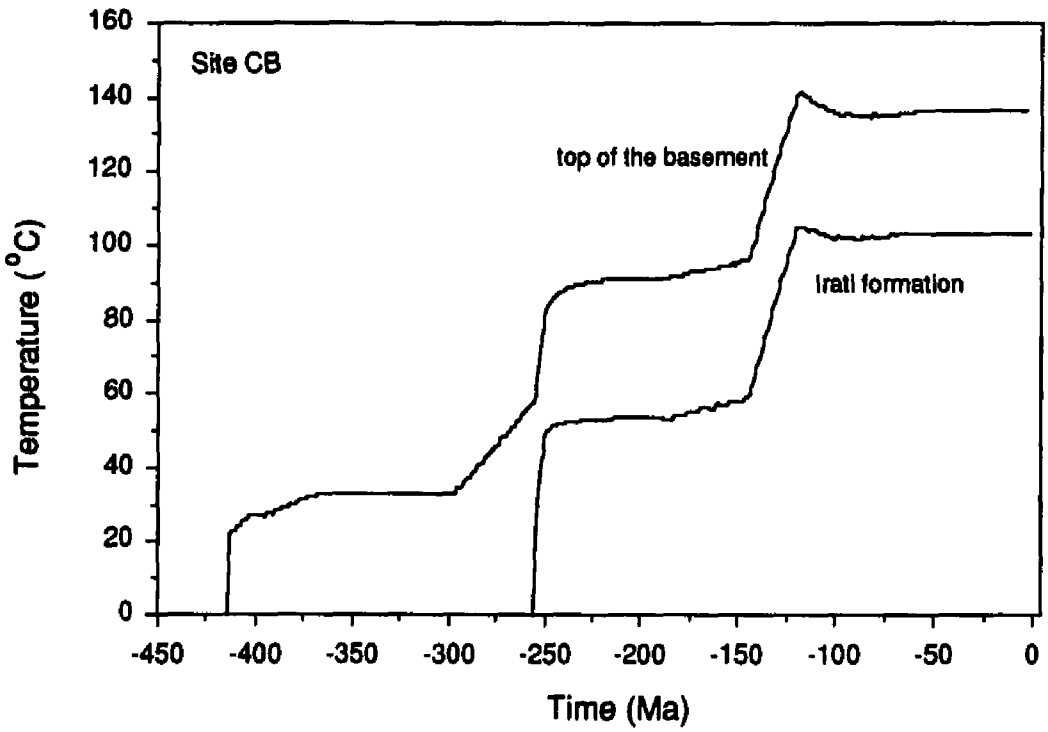

Figure 5.13 Temperature vs. time at the top of the basement and in the Irati formation at site CB. Variable basal heat flow is the same as for Figure 5.12.

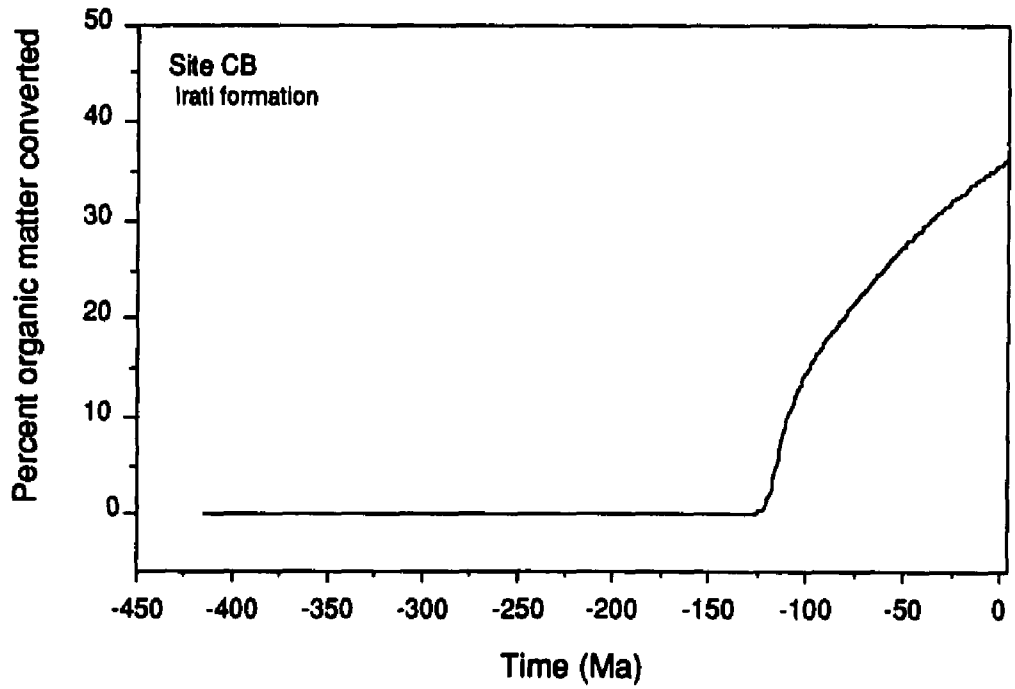

Figure 5.14 Percentage of organic matter converted to oil as a function of time in the Irati formation. Variable basal heat flow is the same as for Figure 5.12.

investigated the effects of two end-member histories testing the effects of a period of unconformity: the first case (a) illustrates deposition beginning with the Furnas formation at about 414 Ma and ending with the end of sedimentation of the Rio Bonito formation at 260 Ma; subsequently neither deposition nor erosion occurs to the present-day; and in the second case(b) all stratigraphic units present at basin-center site CB are deposited, but later the units younger than the Rio Bonito are eroded continuously from 65 Ma to the present day. For both cases the same variation in basal heat flow through time was assumed: initially a period of high heat flow (414 Ma) then the effects of the Mesozoic igneous event with increased heat flow due to cooling of extrusion/intrusions in the same amount as for site CB, and finally an increase in heat flow due to the additional heat that was diverted from the central part of the basin (in the same amount as the corresponding decrease in heat flow for site CB). The subsidence curves shown in Figure 5.15 include examples for both histories. In case b (deposition and erosion) the thicknesses of the presently missing stratigraphic units were estimated from isopach maps from Ferreira (1982). The evolution of heat flow through time for both histories is depicted in Figure 5.16. For the erosional case (b), heat flow increases from about 250 Ma due to the deposition of the 'missing' section and is produced by radiogenic heat production in the sediments. Subsequent erosion of this section increases heat flow temporarily, but this transient effect decays rapidly to the equilibrium surface heat flow.Generally the two histories yield very similar surface heat flow, which suggests that all transient effects due to deposition and uplift have enough time to decay to insignificance. The significant change in heat flow for both cases is an increase associated with the diversion effect subsequent to the Serra Geral event (144-119 Ma).

The temperature history of the two depositional histories at site MO is depicted in Figure 5.17 for the top of the basement. Temperatures for the erosional case (b) reach higher values than in case (a) due to the deposition of the missing section. These higher temperatures are fairly long-lived (tens of millions of years) and therefore contribute significantly to the time-temperature-integral, which is relevant to hydrocarbon generation. At site MO the Irati formation, a hydrocarbon source rock is missing, having been stripped off by erosion. The other possibility of a source rock for this site would be the Ponta Grossa formation. We followed its thermal evolution with the GOTHIC model for both cases of depositional histories; only minor conversion of organic matter occurs in the erosional case (about 1 %) and none in the non-depositional case (a).

In comparing the thermal histories of sites CB and MO we note the following: the evolution of surface heat flow at both sites follow a similar history up to the Serra Geral igneous event. Subsequently heat flow decreases at CB due to the diversion of heat towards the margin of the basin where site MO is located and heat flow increases. The sedimentary section at site MO probably never attained depths as large as site CB. This is due to the fact that the flood basalt thickness, if present at this site, would have been less than at site CB in the center of the basin,

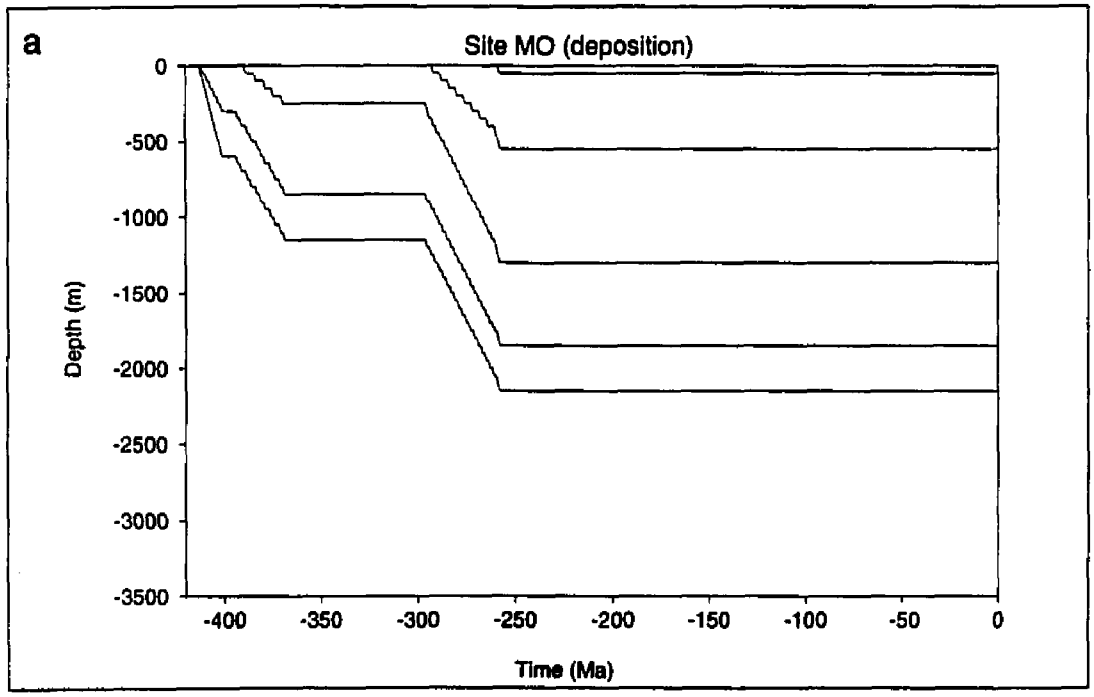

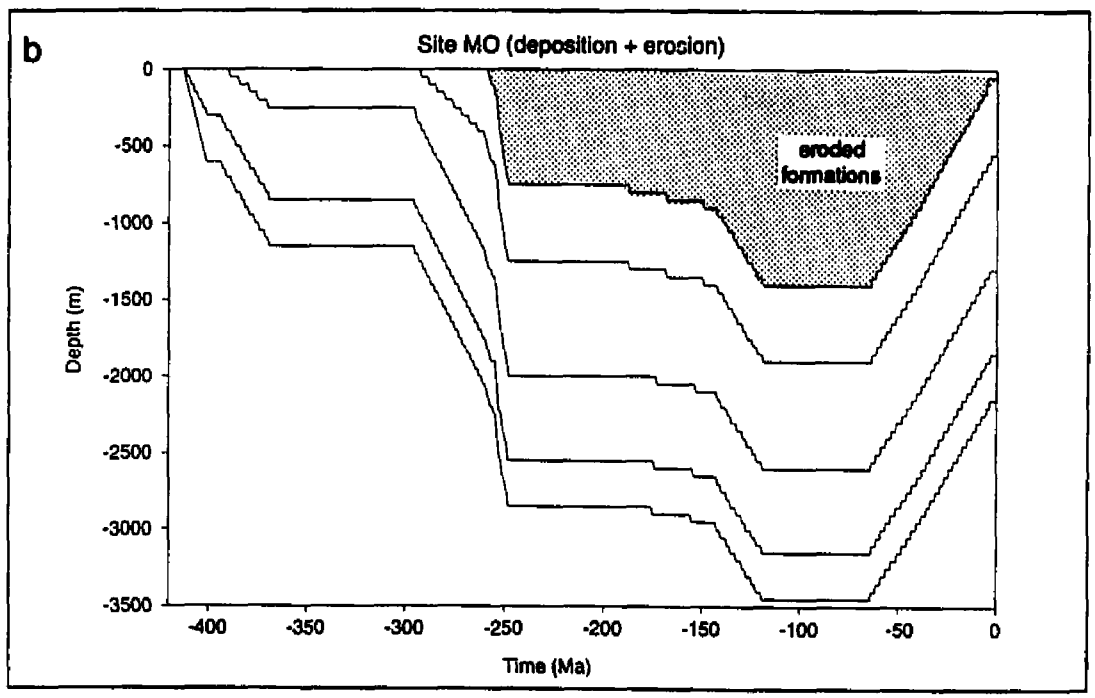

Figure 5.15 Subsidence curves for site MO. (a) represents a history of deposition only and (b) includes continuous erosion from 65 Ma to the present-day, such that in both cases the stratigraphic column of Figure 5.2 is matched at the present-day.

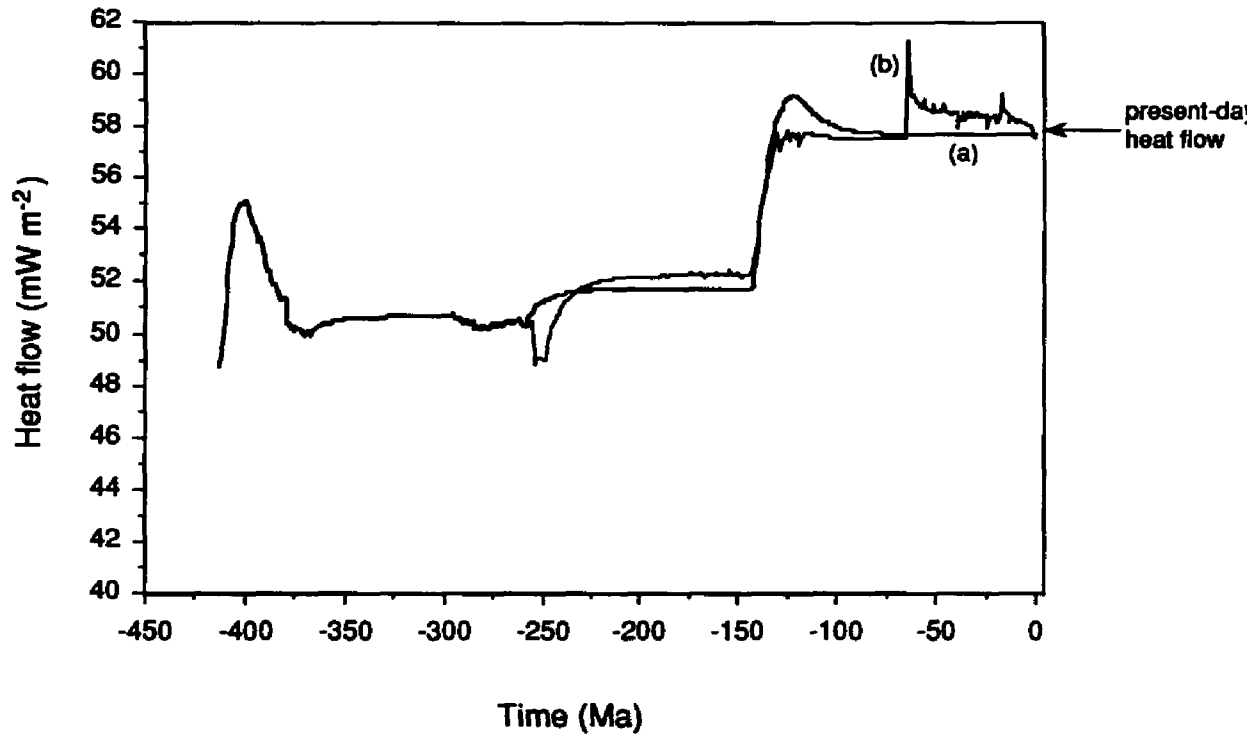

Figure 5.16 Surface heat flow vs. time for site MO. Curve (a) assumes depositional events only with no deposition nor erosion since 260 Ma, and curve (b) includes deposition up to 65 Ma and then continuous erosion to the present day.

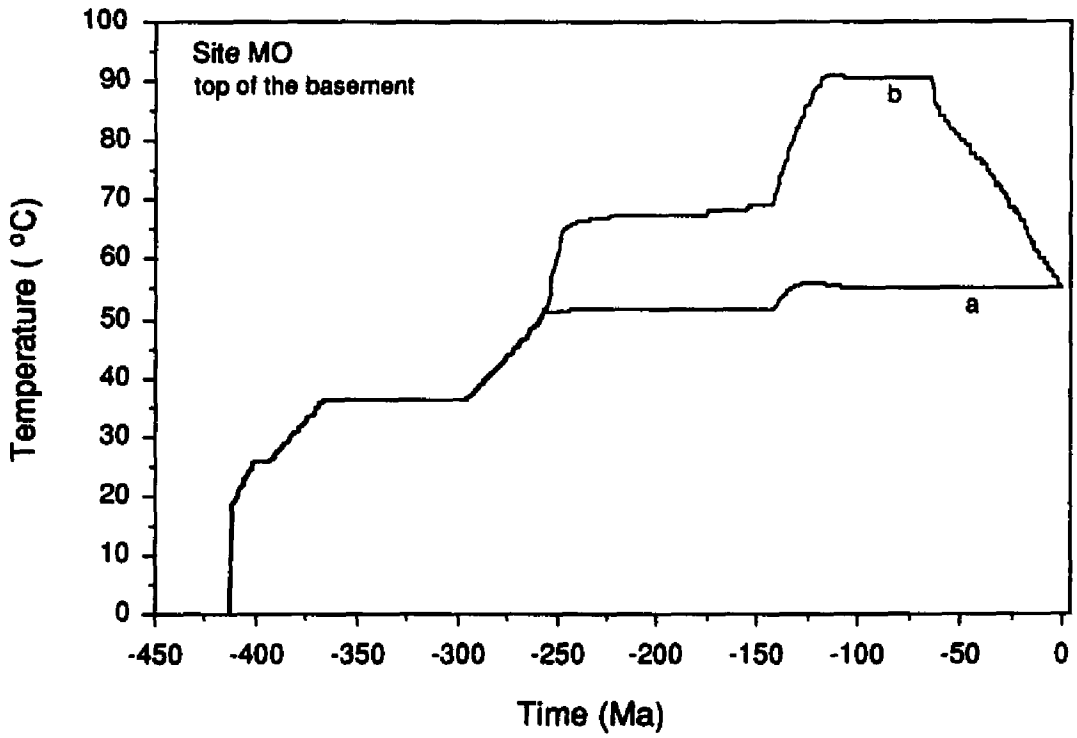

Figure 5.17 Temperature vs. depth for the top of the basement in site MO. Curve (a) assumes depositional events only with no deposition nor erosion since 260 Ma; curve (b) includes deposition up to 65 Ma and then continuous erosion to the present day.

and also due to erosion following the Ponta Grossa Arch uplift, which did not affect site CB. Potential hydrocarbon source rocks in the Paraná Basin include the Irati and the Ponta Grossa formations. At site CB both formations have met conditions for hydrocarbon generation. At site MO, however, the Irati formation was removed by erosion and the Ponta Grossa formation generates only small amounts of hydrocarbons. The higher heat flow at this site since the Serra Geral event was not capable of offsetting the thermal effect of a shallower position of this source rock when compared to its situation at site CB.

In summary, the significant effect of the Serra Geral igneous activity was the deposition of the thick flood basalts, which increased the temperatures of the sediments by about 40 °C in the center of the basin. Modeling of the thermal history due to subsidence and uplift showed that transient effects of deposition and erosion decay within a few million years. Episodes of higher heat flow associated with an Early Paleozoic basin-initiating event and the Mesozoic Serra Geral igneous event also decay within tens of millions of years and do not contribute significantly to the thermal maturation of the sediments. It is the Serra Geral depositional event that is responsible for initiating the conversion of organic matter to oil in the Irati formation. A comparison of two sites located respectively in the center and at the uplifted margin of the basin, shows similar evolution in surface heat flow up to the Serra Geral event. Subsequently the heat flow at the center decreases while increasing at the margin due to the diversion of deep heat caused by a zone of thickened lithosphere underneath the central part of the basin. Total subsidence at the margin has been less and the total depths reached by the sediments have been diminished by erosion. Consequently hydrocarbon maturation levels at the margin are incipient, whereas in the basin center the potential for significant generation exists.

5. DISCUSSION AND CONCLUSION

The thermal history of the Paraná Basin may or not have been initiated with a period of high heat flow more than 400 Ma ago. Modeling results suggest that this thermal event would have been of little consequence to any but the earliest sediments. Subsequently the history has been predominantly one of subsidence, perhaps interrupted by regional uplift. Three major phases of subsidence occurred during the Silurian-Devonian, Carboniferous-Permian and Jurassic-Cretaceous resulting in the accumulation of over 6 km of sedimentary and igneous rocks in the basin center. The last depositional event is related to the Mesozoic Serra Geral igneous activity in which flood basalts were extruded at 135-130 Ma over most of the basin surface with associated intrusions in the sediments. At the present-day the igneous rocks comprise up to 30 % of the basin fill by volume. Their low thermal conductivity compared to the generally siliciclastic sediments of the basin changed the thermal conductivity structure of the basin after this event. Furthermore the deposition of flood basalts accounts for up to 2 km of subsidence in the basin

center within a few million years, increasing the temperatures within the sediments by up to 40 °C. The distribution and range of 'illite crystallinity' data seem to reflect the combined effects of increasing temperature and time with burial. Modeling the effects of the cooling of the igneous rocks and the effects of higher heat flow during the Serra Geral event showed that the greatest thermal effect derives from the depositional (subsidence) as opposed to the transient high temperature thermal effects of the flood basalts. The I/S ratio of mixed-layer illite smectite measured on core samples taken in proximity to sill intrusions is compatible with the present-day temperatures controlled by the geothermal gradient and suggests that short-lived high temperatures associated with the Serra Geral igneous activity do not affect significantly the I/S ratio. A result of a comparison of the thermal history of two sites of different subsidence/uplift histories suggests that the differences in present-day surface heat flow arise from differences in basal heat flow into the basin, and this in turn is likely related to differences in lithospheric structure and history across the basin.

CHAPTER VI

SUMMARY AND CONCLUSION

In this dissertation I have investigated the heat flow, thermal structure and thermal evolution of the Paraná Basin in southern Brazil. I address the temperature evolution of this basin due to subsidence and uplift and to the Mesozoic Serra Geral igneous event with its consequences for the lithospheric structure of this region. The observational bases for this study are temperature measurements in deep exploration wells, thermal conductivity measurements on core samples, regional and local stratigraphic data, and characteristics of clay minerals in the sediments.

Mean thermal conductivities obtained from measurements on numerous core samples vary from 3.1 to 1.8 W $m^{-1}K^{-1}$ from the eastern basin margin to the center as a function of the thickening of the Serra Geral flood basalt cap. BHT data from 79 boreholes in the Paraná Basin yielded 187 temperature values that after correction for drilling disturbances and combined with surface temperatures were used to compute mean geothermal gradients at 56 sites. These range mostly between 20 and 30 K km^{-1}. Geothermal gradients and thermal conductivities combine to yield 56 new heat flow values for the Paraná Basin, in the range 40 to 75 mW m^{-2}. This variation has a coherent geographic expression: higher heat flow occurs more frequently along the eastern basin margin, diminishing and becoming more uniform towards the central axial region of the basin, the region of greatest basalt cover.

In order to interpret the heat flow pattern in the Paraná Basin I have investigated factors and processes that may influence heat flow in this setting. Attempts were made to evaluate the magnitude of two kinds of factors: steady state thermal effects produced by topography, large scale thermal conductivity and heat production contrasts, variation of crustal and lithospheric thickness, and subsurface fluid flow; and transient effects due to igneous activity, uplift, erosion and sedimentation, and surface temperature history. Transient effects due to uplift and erosion of the eastern basin margin related to the opening of the South Atlantic may contribute to the present-day heat flow, but insufficiently to explain the magnitude of the observed variation; the rapid 'deposition' of the Serra Geral flood basalts has no influence upon the present-day heat flow. A two-part hypothesis to explain the pattern of heat flow variation in the Paraná Basin relates to the crustal/lithospheric structure and history of the basement underlying the basin: (1)

underplating associated with the extrusion of the Serra Geral flood basalts could provide a region of low thermal conductivity and low radiogenic heat production in the lower crust beneath the central region of the Paraná Basin and (2) the existence of thickened lithosphere generated as a consequence of basalt depletion underlying the central part of the basin may divert deep mantle heat away from the central region into the thinner lithosphere underlying the basin margin and surrounding folded belts. The thermal effects of flood basalts at the surface and underplating in the lower crust due to the combination of thermal conductivity contrast and radiogenic heat production contrast yield differences of the order of 10 % of the mean heat flow. An underplate alone can account for only part of the observed heat flow variation. The modelling of heat diversion by a zone of thickened lithosphere generated through basalt depletion suggests that this mechanism can provide a heat flow contrast at the surface of the appropriate amount or larger. The same effect can be achieved by thinning the lithosphere at the eastern margin of the basin. It appears that crustal and shallow processes and structures alone cannot explain the large scale heat flow pattern across the Paraná Basin. Deeper causes must be invoked; variation in lithosphere thickness (thickening beneath the basin center or thinning beneath the basin margin) can easily provide the observed contrasts in heat flow.

I investigate in more detail the temperature field in the Paraná Basin by applying a least squares inversion to the temperature and stratigraphic data. This analysis yields best fitting geothermal gradients for 14 representative formations and from these a best fit thermal field for the Paraná Basin was computed. The thermal field across the basin at several depths was analyzed by mapping the deviations of the expected temperatures with respect to the mean expected temperature at a given depth. At all depths the deviations showed a spatially coherent pattern with above average temperatures for a given depth found beneath the thick basalt flows, and below average temperatures beneath the eastern margin of the basin. Finite difference modeling of a purely conductive regime produced similar temperatures and deviations as observed from the best fit temperature field. Advective heat transport models suggest that subsurface fluid flow does not alter the regional heat flow pattern significantly. The conductive and advective heat transport model results suggest that the temperature and heat flow pattern in the Paraná Basin is dominantly a conductive regime. The effects of advective heat transport through fluid flow are likely to be small and restricted to areas of limited extent within the principal recharge and discharge areas.

I also address the thermal evolution of the sedimentary fill of the Paraná Basin. Numerical models are used to obtain temperature histories and the evolution of surface heat flow through time. The thermal history of the Paraná Basin may or not have been initiated with a period of high heat flow more than 400 Ma ago. Modeling results suggest that this thermal event would have been of little consequence in but the earliest sediments. Subsequently the history has been

predominantly one of subsidence, interrupted by regional uplift. Three major phases of subsidence occurred during the Silurian-Devonian, Carboniferous-Permian and Jurassic-Cretaceous resulting in the accumulation of over 6 km of sedimentary and igneous rocks in the basin center. The last depositional event is related to the Mesozoic Serra Geral igneous activity in which flood basalts were extruded at 135 - 130 Ma over most of the basin surface with associated intrusions in the sediments. At the present-day the igneous rocks comprise up to 30 % of the basin fill by volume. Their low thermal conductivity compared to the generally siliciclastic sediments of the basin, changed the thermal conductivity structure of the basin after this event. Furthermore the deposition of flood basalts accounts for up to 2 km of subsidence in the basin center within a few million years, increasing the temperatures within the sediments by up to 40 °C. The distribution and range of 'illite crystallinity' data seem to reflect the combined effects of increasing temperature and time with burial. Modeling the effects of the cooling of the igneous rocks and the effects of higher heat flow during the Serra Geral event showed that the greatest thermal effect derives from the depositional (subsidence) effects as opposed to the transient high temperature thermal effects of the flood basalts. The I/S ratio of mixed-layer illite smectite measured on core samples taken in proximity to sill intrusions is compatible with the present-day temperatures controlled by the geothermal gradient and suggests that short-lived high temperatures associated with the Serra Geral igneous activity did not affect significantly the I/S ratio. A result of a comparison of the thermal history of two sites of different subsidence/uplift histories suggests that the differences in present-day surface heat flow arise from differences in basal heat flow into the basin, and this in turn is likely related to differences in lithospheric structure and history across the basin.

APPENDICES

APPENDIX A

BOTTOM HOLE TEMPERATURE DATA

Borehole	Depth (m)	T_o (°C)	Uncorrected BHT (°C)	Corrected BHT (°C)
AA1SP	1193	21	50.6	54.1
AA1SP	2488	21	71.7	80.7
AA1SP	2939	21	80.0	91.0
AA1SP	2966	21	78.9	90.0
AG1MT	1947	22	65.6	72.9
AL1RS	2041	19	48.9	54.0
AL1SC	1637	16	56.1	61.2
AL1SC	2469	16	60.0	68.6
AL1SC	2710	16	65.6	75.2
AL1SC	3545	16	83.0	95.7
AL1SC	3876	16	92.5	106.4
AM1MT	1430	21	37.8	42.3
AM1MT	3329	21	103.3	115.7
AO1RS	1254	16	48.9	53.1
AO1RS	2251	16	64.4	73.4
AP1PR	2183	20	64.4	71.2
AP1PR	2787	20	72.2	81.3
AP1PR	4040	20	90.0	103.3
AP1PR	4300	20	93.3	107.8
AR1SP	1425	22	61.7	66.3
AR1SP	2731	22	71.1	81.6
AS1SP	1335	20	47.8	51.9
AT1SP	1259	20	40.0	42.9
AV1PR	2787	21	97.8	111.9
BN1SC	962	18	48.3	51.9
BN1SC	1101	18	44.4	48.7
BN2SC	702	18	40.6	43.0
CA1PR	275	19	28.3	29.0
CA1PR	797	19	30.6	33.0
CA1PR	1797	19	46.1	52.9
CA2PR	1888	19	60.0	68.2
CA3PR	1055	19	56.1	59.5
CA3PR	1586	19	71.1	76.9
CA3PR	2674	19	79.4	90.5
CA1SC	1935	16	70.0	79.0
CB1DASP	4556	22	110.6	128.0
CB1DASP	4639	22	115.0	132.7
CB1DASP	4659	22	115.6	133.4
CB1DASP	4804	22	122.2	140.5
CB2SP	3102	22	89.4	101.2
CB2SP	4553	22	119.5	154.8
CB2SP	4600	22	116.7	134.2
CB2SP	4651	22	123.3	141.0
CB2SP	4706	22	117.8	135.7
CB2SP	5197	22	132.2	152.0
CB2SP	5299	22	133.3	153.5

continued on the following page

Bottom Hole Temperature Data (continued)

Borehole	Depth (m)	To (°C)	Uncorrected BHT (°C)	Corrected BHT (°C)
CB3SP	3044	22	90.6	102.2
CB3SP	4425	22	120.0	136.9
CB3SP	4481	22	107.8	124.9
CB3SP	4551	22	114.4	131.8
CB3SP	4985	22	120.6	139.6
CB3SP	5531	22	132.0	153.1
CB4SP	2472	22	73.9	83.0
CB4SP	3240	22	90.0	102.4
CB4SP	4332	22	102.8	119.3
CB4SP	4355	22	102.8	119.4
CB4SP	4816	22	117.2	135.6
CG1MT	1557	22	46.1	50.1
CG1MT	2524	22	64.4	71.8
CM1PR	3192	19	85.0	96.6
CM1PR	4240	19	98.9	114.3
CN1SC	1034	16	37.8	40.9
CN1SC	1775	16	55.0	61.2
CP1SP	990	20	70.4	75.3
CP1SP	1545	20	65.0	73.7
DO1MT	1833	21	51.7	58.0
DO1MT	2916	21	86.7	97.8
DO1MT	4160	21	114.4	130.3
DO3MT	1037	21	43.3	46.3
DO3MT	2227	21	65.6	73.7
DO4MT	1001	21	43.3	46.2
DO4MT	1330	21	48.9	53.1
DO4MT	1993	21	60.0	67.0
GP1PR	2600	17	81.1	92.4
GP1PR	3638	17	103.3	119.5
GU3SP	981	20	37.8	40.3
GU4SP	901	20	37.8	40.0
HV1SC	2700	16	79.4	90.9
IT1RS	625	20	37.8	39.2
IT1RS	1679	20	50.0	54.9
IT1RS	2516	20	64.4	72.6
J1PR	1995	20	65.0	72.6
JA1GO	2107	22	65.6	73.0
JT1PR	121	20	32.2	32.4
JT1PR	1164	20	38.9	42.0
JT1PR	2334	20	60.0	67.6
LA1SC	118	16	32.2	32.6
LA1SC	775	16	38.9	42.5
LA1SC	1343	16	62.5	69.5
LI1SP	1429	22	60.0	64.1
LI1SP	1941	22	60.0	66.1
LI1SP	3460	22	76.7	88.6
LS1PR	2316	16	63.3	72.0
LS1PR	2768	16	75.0	85.8

continued on the following page

Bottom Hole Temperature Data (continued)

Borehole	Depth (m)	T_o (°C)	Uncorrected BHT (°C)	Corrected BHT (°C)
LS1PR	3962	16	101.7	117.3
LV1PR	826	16	43.3	45.8
LV1PR	2362	16	56.7	66.1
M1APR	741	16	46.1	48.6
M1APR	1557	16	51.7	58.1
M1APR	1861	16	65.6	73.6
MA1RS	2715	17	81.1	92.8
MC1PR	1967	16	62.8	70.6
MO1PR	2017	18	53.3	59.3
MO2PR	1992	18	53.9	59.8
MR1RS	1522	17	54.4	60.2
MR1RS	2292	17	71.1	80.8
MR1RS	2589	17	81.1	92.4
O1PR	2025	19	66.5	74.5
OL1SP	1165	22	43.3	46.7
OL1SP	2040	22	65.6	72.6
OL1SP	2568	22	73.3	82.6
PA1SC	1126	17	46.1	50.1
PA1SP	436	21	40.0	41.0
PA1SP	1494	21	51.1	55.7
PA1SP	2105	21	60.0	67.2
PE1SP	2388	22	78.9	87.5
PE1SP	2939	22	75.6	86.6
PE1SP	2954	22	82.2	93.2
PE1SP	3850	22	98.9	113.3
PG1SP	191	20	32.2	32.8
PG1SP	959	20	44.4	48.3
PG1SP	1228	20	60.0	65.3
PI1SC	1719	17	51.7	57.7
PI1SC	2163	17	62.8	70.8
PI1SC	2271	17	68.3	76.8
PN1SP	158	20	31.7	32.1
PN1SP	776	20	39.4	41.7
PN1SP	1669	20	53.9	60.1
PN1SP	1683	20	53.3	59.5
PP1SP	1960	21	54.4	59.7
PP1SP	3663	21	77.8	88.6
PU1SC	1244	16	35.0	38.4
PU1SC	2326	16	62.8	70.3
QT1PR	1386	20	43.3	46.8
R1PR	115	18	36.7	37.0
R1PR	1028	18	46.1	49.6
R1PR	1830	18	54.4	61.7
R1PR	1909	18	57.2	64.9
RA1MS	865	22	49.4	51.2
RA1MS	2173	22	55.3	61.3
RA1MS	3474	22	72.2	82.4
RC1PR	1517	16	51.1	56.4

continued on the following page

Bottom Hole Temperature Data (continued)

Borehole	Depth (m)	T_o (°C)	Uncorrected BHT (°C)	Corrected BHT (°C)
RC1PR	1999	16	61.1	68.7
RCH1SC	3183	16	83.3	95.8
RD1RS	1504	18	48.9	53.1
RD1RS	3418	18	74.4	85.6
RI1RS	1638	20	46.1	50.4
RI1RS	2401	20	60.0	66.9
RP1MT	1840	22	83.9	94.0
SD1MT	980	20	48.9	52.1
SD1MT	1919	20	65.6	73.2
SD1MT	2997	20	87.8	100.8
SJ1PR	1212	20	42.8	46.7
SJ1PR	2232	20	68.3	76.8
SJ1PR	2346	20	73.9	82.9
TB1SP	1519	22	61.7	66.1
TB1SP	1869	22	62.2	68.0
TB1SP	2998	22	78.9	89.2
TB1SP	3514	22	83.3	95.4
TB1SP	4600	22	107.8	123.6
TB1SP	4696	22	108.9	125.1
TB1SP	4783	22	107.8	124.3
TB1SP	4945	22	109.0	126.0
TG1SC	973	16	41.1	44.7
TG1SC	1554	16	62.8	69.3
TG1SC	1690	16	65.6	72.8
TG1SC	2305	16	74.4	85.1
TG1SC	2431	16	76.7	88.1
TL1MT	2547	22	83.3	92.1
TL1MT	4582	22	98.9	115.2
TO1RS	990	19	46.7	50.4
TP1SC	2337	16	54.4	61.0
TP1SC	2998	16	62.8	71.6
TQ1MT	2017	22	58.9	65.1
TV1SC	1950	16	65.0	72.3
TV1SC	2011	16	63.9	71.5
TV1SC	2235	16	67.2	75.9
TV2SC	1967	16	63.3	70.7
TV2SC	1988	16	55.6	63.1
TV2SC	2110	16	59.4	67.4
TV2SC	2966	16	72.2	84.3
TV3SC	1986	16	63.9	71.3
TV3SC	2094	16	66.1	74.1
TV4SC	1957	16	60.0	67.3
TV4SC	2071	16	61.1	69.0
UV1PR	1110	16	38.9	42.2
UV1PR	2162	16	62.2	70.0

APPENDIX B

THERMAL CONDUCTIVITY MEASUREMENTS

Borehole Name	Formation	Lithology	Depth (m)	Thermal conductivity ($W\ m^{-1}\ K^{-1}$)
AB1SP	Pa	siltstone	213.5	1.74
AB1SP	RB	sandstone	242.0	2.40
AB1SP	It	siltstone	285.8	3.01
AL1RS	RR	siltstone	876.6	1.70
AL1RS	RR	sandstone	951.6	3.65
AL1RS	Pa	siltstone	1535.7	1.96
AL1RS	It	glacial mudstone	1821.8	2.57
AL1RS	It	shale	1963.2	1.17
AO1RS	RB	sandstone	2125.3	3.63
AS1SP	It	sandstone	130.6	3.21
AS1SP	It	glacial mudstone	222.5	2.93
AS1SP	It	siltstone	300.3	2.79
AS1SP	It	siltstone	301.5	2.23
AS1SP	It	sandstone	511.3	2.93
AS1SP	It	siltstone	846.9	2.02
AS1SP	It	sandstone	1156.0	3.24
BN1SC	RB	shale	335.3	1.47
BN2SC	RB	shale	200.0	1.51
BN2SC	RB	siltstone	205.5	3.03
BN2SC	RB	siltstone	206.0	2.92
BN2SC	RB	sandstone	336.0	4.05
BN2SC	RB	siltstone	365.5	2.17
CA1PR	Te	siltstone	222.5	2.20
CA1PR	SA	siltstone	652.6	1.62
CA1PR	Pa	siltstone	786.0	1.85
CA1PR	It	siltstone	1200.0	2.68
CA1PR	It	siltstone	1308.0	3.55
CA1PR	It	siltstone	1419.5	2.41
CA1PR	PG	shale	1676.0	2.34
CA1PR	PG	shale	2146.0	1.57
CA1PR	Fu	shale	2604.0	1.98
CA1PR	Fu	sandstone	2739.0	5.82
CA1SC	Bo	sandstone	631.0	2.62
CA1SC	RR	siltstone	720.0	1.53
CA1SC	RR	siltstone	962.5	1.78
CA1SC	RR	siltstone	1061.2	2.27
CA1SC	Te	siltstone	1260.5	2.03
CA1SC	Pa	siltstone	1558.5	1.78
CA1SC	RB	sandstone	1694.0	3.27
CA1SC	It	shale	1911.3	1.83
CB1DASP	sill	diabase	4476.8	2.27
CB1DASP	sill	diabase	4608.8	2.33
CB1SP	Te	siltstone	2818.7	2.90
CB1SP	Te	shale	3006.1	3.06
CB1SP	It	glacial mudstone	3615.7	2.82
CB1SP	It	conglomerate	3784.4	4.38

continued on the following page

Thermal conductivity measurements (continued)

Borehole Name	Formation	Lithology	Depth (m)	Thermal conductivity ($W m^{-1} K^{-1}$)
CB2SP	lt	siltstone	4460.0	3.59
CB2SP	PG	shale	4930.7	3.25
CB3SP	lr	shale	3144.8	1.93
CB3SP	lt	sandstone	4543.9	5.54
CB4SP	SA	siltstone	3164.5	2.41
CB4SP	SA	siltstone	3165.5	2.51
CM1PR	SG	basalt	571.5	2.03
CM1PR	RR	sandstone	1526.5	2.64
CM1PR	RR	siltstone	1729.8	1.99
CM1PR	RR	sandstone	1930.9	3.43
CM1PR	RR	siltstone	2032.5	2.23
CM1PR	Te	siltstone	2229.0	2.31
CM1PR	Te	siltstone	2332.7	2.56
CM1PR	SA	siltstone	2575.3	2.15
CM1PR	lr	shale	2672.0	2.83
CM1PR	Pa	siltstone	2692.5	2.85
CM1PR	RB ab	siltstone	2894.3	3.17
CM1PR	RB	siltstone	3082.5	2.73
CM1PR	lt	siltstone	3180.5	3.49
CM1PR	lt	glacial mudstone	3404.5	3.68
CM1PR	lt	sandstone	3600.6	3.90
CM1PR	lt ab	shale	3842.7	1.76
DO1MT	SG	basalt	299.0	1.45
DO1MT	RR	siltstone	812.3	2.73
DO1MT	RR	sandstone	909.7	2.87
DO1MT	Te	siltstone	1162.4	2.46
DO1MT	Te	siltstone	1358.3	3.03
DO1MT	SA	siltstone	1683.5	2.61
DO1MT	lr	shale	1836.0	1.99
DO1MT	Pa	sandstone	1859.0	5.81
DO1MT	RB	sandstone	1940.5	4.52
DO1MT	RB	sandstone	2145.5	4.42
DO1MT	RB	sandstone	2415.7	2.93
DO1MT	lt	siltstone	2519.0	1.85
DO1MT	lt	glacial mudstone	2605.8	3.18
DO1MT	lt	sandstone	3194.0	6.21
DO1MT	lt	sandstone	3321.5	4.70
DO1MT	lt	sandstone	3366.0	4.73
DO1MT	lt	sandstone	3685.0	5.26
DO1MT	Fu	sandstone	4115.0	5.72
JT1PR	RB	sandstone	157.0	2.25
JT1PR	lt	sandstone	240.5	2.84
JT1PR	lt	glacial mudstone	335.7	3.49
JT1PR	lt	sandstone	635.0	2.85
JT1PR	lt	sandstone	1035.0	3.35
JT1PR	lt	glacial mudstone	1233.0	3.85
JT1PR	lt	sandstone	1330.0	5.28
JT1PR	PG	shale	1574.0	2.05

continued on the following page

Thermal conductivity measurements (continued)

Borehole Name	Formation	Lithology	Depth (m)	Thermal conductivity ($W\ m^{-1}\ K^{-1}$)
JT1PR	Fu	sandstone	2032.0	5.26
JT1PR	Fu	sandstone	2198.5	5.36
JT1PR	lt la	glacial mudstone	2286.0	3.67
LA1SC	Te	shale	192.6	2.29
LA1SC	Te	sandstone	194.0	4.02
LA1SC	Ir	shale	575.7	1.74
LA1SC	Pa	siltstone	679.4	2.56
LA1SC	RB	siltstone	836.5	3.27
LA1SC	lt	shale	1011.8	2.71
LI1SP	RR	siltstone	1213.3	2.15
LI1SP	RR	siltstone	1318.0	1.97
LI1SP	RR	siltsiltstoneone	1411.0	2.30
LI1SP	RR	siltstone	1425.5	1.53
LI1SP	RR	sandstone	1518.0	2.93
LI1SP	Te	siltstone	1605.5	2.25
LI1SP	Ir	halite	1694.0	4.87
LI1SP	lt	glacial mudstone	1808.8	3.35
LI1SP	lt	glacial mudstone	1852.8	2.56
LI1SP	lt	sandstone	1874.3	3.96
LI1SP	lt	siltstone	2048.2	2.80
LI1SP	lt	siltstone	2138.0	2.66
LI1SP	lt	sandstone	2142.0	3.37
LI1SP	lt	sandstone	2226.0	3.56
LI1SP	lt	sandstone	2400.5	3.79
LI1SP	lt	sandstone	2816.3	4.06
LI1SP	lt	glacial mudstone	2933.0	3.45
LI1SP	lt	sandstone	3181.2	3.75
LI1SP	lt	conglomerate	3275.7	3.47
LI1SP	Fu	sandstone	3375.5	5.38
MO1PR	PG	siltstone	824.5	1.94
MO1PR	PG	shale	1095.0	1.82
MO1PR	PG	sandstone	1414.5	3.64
MO1PR	Fu	sandstone	1481.5	6.44
MO1PR	sill	diabase	1913.2	2.42
OL1SP	Te	siltstone	1338.1	2.68
OL1SP	Te	siltstone	1338.2	2.52
OL1SP	SA	siltstone	1429.0	1.74
OL1SP	Pa	sandstone	1490.5	4.72
OL1SP	lt	glacial mudstone	1629.0	2.29
OL1SP	lt	sandstone	1740.5	2.39
OL1SP	lt	conglomerate	1826.0	3.78
OL1SP	lt	sandstone	2122.0	3.57
OL1SP	lt	siltstone	2149.4	3.52
OL1SP	lt	siltstone	2265.0	2.56
OL1SP	lt	sandstone	2372.0	4.70
PP1SP	SG	basalt	134.0	2.02
PP1SP	SG	basalt	510.5	2.01
PP1SP	SG	basalt	820.0	1.48

continued on the following page

Thermal conductivity measurements (continued)

Borehole Name	Formation	Lithology	Depth (m)	Thermal conductivity ($W m^{-1} K^{-1}$)
PP1SP	Bo	sandstone	1254.0	2.50
PP1SP	RR	sandstone	1362.0	2.33
PP1SP	RR	siltstone	1465.0	2.34
PP1SP	RR	siltstone	1499.0	2.38
PP1SP	RR	siltstone	1739.0	2.44
PP1SP	Te	siltstone	1859.0	2.17
PP1SP	Pa	sandstone	2053.0	2.01
PP1SP	RB	siltstone	2153.5	2.62
RC1PR	Te	siltstone	190.5	1.74
RC1PR	Te	siltstone	304.0	1.83
RC1PR	RB	sandstone	696.0	3.23
RC1PR	It	siltstone	888.6	1.82
RC1PR	It	siltstone	981.8	3.45
RC1PR	It	siltstone	1050.3	2.54
RC1PR	It	siltstone	1336.0	3.84
RC1PR	PG	siltstone	1590.0	2.15
RC1PR	Fu	sandstone	1810.0	5.94
RC1PR	Fu	sandstone	1918.9	5.81
RI1RS	RR	siltstone	1170.7	2.69
RI1RS	Te	siltstone	1301.3	1.88
RI1RS	Te	siltstone	1301.6	1.68
RI1RS	Pa	siltstone	1937.5	2.05
RI1RS	Pa	siltstone	1938.0	2.20
RI1RS	It	shale	2154.6	1.53
SD1MT	SG	basalt	138.0	2.07
SD1MT	Bo	sandstone	1192.5	2.65
SD1MT	Bo	sandstone	1395.9	2.14
SD1MT	RR	siltstone	1566.3	2.27
SD1MT	Te	sandstone	1741.3	3.39
SD1MT	SA	shale	2421.3	1.97
SD1MT	RB	sandstone	2830.0	3.31
SD1MT	RB	sandstone	2927.5	3.63
SD1MT	It	siltstone	3001.5	3.07
SJ1PR	RR	siltstone	214.0	2.01
SJ1PR	RR	sandstone	419.0	2.13
SJ1PR	Te	siltstone	520.0	2.25
SJ1PR	Te	siltstone	696.0	2.46
SJ1PR	SA	siltstone	795.0	2.24
SJ1PR	RB	siltstone	1085.0	2.07
SJ1PR	RB	siltstone	1138.2	2.00
SJ1PR	It	glacial mudstone	1188.2	2.46
SJ1PR	It	sandstone	1443.5	4.61
SJ1PR	It	sandstone	1783.0	3.88
SJ1PR	PG	siltstone	2124.5	2.67
SJ1PR	PG	shale	2191.6	2.30
TB1SP	Ir	shale	2619.8	1.20
TB1SP	Ir	shale	2628.0	1.17
TB1SP	RB	siltstone	2732.7	2.16

continued on the following page

Thermal conductivity measurements (continued)

Borehole Name	Formation	Lithology	Depth (m)	Thermal conductivity ($W\ m^{-1}\ K^{-1}$)
TB1SP	It	glacial mudstone	2831.9	2.92
TB1SP	It	sandstone	3002.6	5.26
TB1SP	It	shale	3701.0	2.79
TB1SP	Fu	sandstone	4494.3	5.89
TL1MT	SG	basalt	395.6	1.93
TL1MT	RR	siltstone	1276.4	1.85
TL1MT	Te	siltstone	1409.0	2.51
TL1MT	Te	siltstone	1521.6	2.04
TL1MT	Te	siltstone	1881.0	1.74
TL1MT	Te	shale	2196.5	1.04
TL1MT	RB	sandstone	2603.7	2.57
TL1MT	It	glacial mudstone	2651.0	2.87
TL1MT	It	shale	2798.6	1.88
TL1MT	It	conglomerate	3145.0	4.73
TL1MT	It	glacial mudstone	3293.3	3.20
TL1MT	It	siltstone	3445.7	4.23
TL1MT	It	conglomerate	3681.0	4.76
TL1MT	It	glacial mudstone	3681.8	5.20
TL1MT	PG	sandstone	3736.3	4.73
TL1MT	PG	siltstone	3877.0	2.34
TL1MT	sill	diabase	4080.0	2.20
TL1MT	Fu	sandstone	4212.0	5.33
TL1MT	Fu	sandstone	4415.0	3.32
TL1MT	Fu	sandstone	4523.0	3.25
TO1RS	Bo	sandstone	168.4	3.88
TO1RS	RR	sandstone	219.0	2.85
TO1RS	RR	siltstone	382.3	1.78
TO1RS	RR	siltstone	430.0	2.81
TO1RS	RR	siltstone	493.0	1.89
TO1RS	Te	siltstone	540.6	1.19
TO1RS	SA	shale	620.0	1.02
TO1RS	Ir	shale	724.0	1.47
TO1RS	Ir	siltstone	760.5	2.45
TO1RS	RB	siltstone	853.0	2.99
TO1RS	RB	coal	903.5	0.33
TO1RS	RB	siltstone	904.0	2.69
TO1RS	RB	sandstone	938.0	3.78
TP1SC	sill	diabase	126.0	1.72
TP1SC	RR	sandstone	905.3	2.12
TP1SC	RR	siltstone	1110.0	2.01
TP1SC	RR	siltstone	1110.5	1.72
TP1SC	RR	siltstone	1294.5	1.73
TP1SC	RR	siltstone	1395.0	2.08
TP1SC	Te	siltstone	1645.0	2.66
TP1SC	SA	siltstone	1939.4	2.39
TP1SC	SA	shale	1942.2	1.83

continued on the following page

Thermal conductivity measurements (continued)

Borehole Name	Formation	Lithology	Depth (m)	Thermal conductivity ($W\ m^{-1}\ K^{-1}$)
TP1SC	lr	shale	2050.5	2.35
TP1SC	Pa	shale	2141.0	1.84
TP1SC	RB	siltstone	2190.0	3.46
TP1SC	RB	siltstone	2294.8	3.46
TP1SC	lt	glacial mudstone	2510.8	2.99
TP1SC	lt	sandstone	2613.5	4.27
TP1SC	lt	glacial mudstone	2759.0	2.76
TP1SC	lt	conglomerate	2870.0	4.81
TP1SC	Fu	sandstone	2928.4	5.49
TP1SC	Fu	sandstone	2956.0	6.26

BIBLIOGRAPHY

BIBLIOGRAPHY

Am. Assn. Petr. Geol. (AAPG), 1976. Basic data file from AAPG Geothermal Survey of North America: Univ. of Oklahoma, Norman.

Bachu, S., 1985. Influence of lithology and fluid flow on the temperature distribution in a sedimentary basin: a case study from the Cold Lake area, Alberta, Canada, *Tectonophysics, 120*, 257-284.

Bachu, S., 1988. Analysis of heat transfer processes and geothermal pattern in the Alberta basin, Canada, *J. Geophys. Res., 93*, 7767-7781.

Bachu, S. and Burwash, R.A., 1991. Regional-scale analysis of the geothermal regime in the Western Canada sedimentary basin, *Geothermics, 20(5/6)*, 387-407.

Ballard, S., 1987. Terrestrial heat flow and thermal structure of the lithosphere in southern Africa, PhD thesis, The University of Michigan, Ann Arbor, 140 pp.

Ballard, S. and Pollack, H.N., 1987. Diversion of heat by Archean cratons: a model for southern Africa, *Earth Planet. Sci. Lett., 85*, 253-264.

Ballard, S., Pollack, H.N. and Skinner, N.J., 1987. Terrestrial heat flow in Botswane and Namibia, *J. Geophys. Res., 92*, 6291-6300.

Basaltic Volcanism Study Project, 1981. *Basaltic volcanism on the terrestrial planets*. Pergamon Press, Inc., New York, 1286 pp.

Bazanow, E.A., Pritula, Yu. A. and Zabaluev, V.V., 1976. Development of main sturctures of the Siberian Platform: history and dynamics, *Tectonophysics, 36*, 289-300.

Birch, F., 1950. Flow of heat in the Front Range, Colorado. *Geol. Soc. Amer. Bull., 61*, 567-630.

Bons, A. J., 1989. Very low-grade metamorphism of the Seo Formation in the Orri Dome, South-Central Pyrenees, *Geologie en Mijnbouw, 68*, 303-312.

Boyd, F.R. and Gurney, J. J., 1986. Diamonds and the African lithosphere, *Science, 232*, 472-477.

Brigaud, F., Chapman, D.S. & Le Douaran, S., 1990. Thermal conductivity in sedimentary basins using lithologic data and geophysical well logs, *AAPG Bull., 74(9)*, 1459-1477..

Brusewitz, A.M., 1986. Chemical and physical properties of Paleozoic potassium bentonites form Kinnekulle, Sweden, *Clays and Clay Miner., 34(4)*, 442-454.

Bullard, A., 1947. The time taken for a borehole to attain temperature equilibrium, *Month. Not. Roy. Astr. Soc. Geophys. Suppl., 5*, 127-130.

Cao, S., Lerche, I., and Hermanrud, C., 1988. Formation temperature estimation by inversion of borehole measurements, *Geophysics, 53*, 979-988.

Carslaw, H.S. and Jaeger, J.C., 1959. *Conduction of heat in solids*, Oxford University Press, 2nd edition, p 388.

Carvalho, H. d. S. & Vacquier, V., 1977. Method for determining terrestrial heat flow in oil fields, *Geophysics, 42(3)*, 584-593.

Chapman, D.S., Keho, T.H., Bauer, M.S. and Picard, M.D., 1984. Heat flow in the Uinta Basin determined from bottom hole temperature (BHT) data, *Geophysics, 49(4)*, 435-466.

Combs, J.B. and Simmons, G., 1973. Terrestrial heat flow determinations in the north central United States, *J. Geophys. Res., 78*, 441-461.

Cordani, U.G. & Vandoros, P., 1967. Basaltic rocks of the Paraná Basin. In: *Problems in Brazilian Gondwana Geology*, J.J. Bigarella, R.D. Becker & I.D. Pinto (eds), Curitiba, 207-231.

Cordani, U.G., Neves, B.B.B., Fuck, R.A., Porto, R., Filho,A.T. and Cunha, F.M.B., 1984. Estudo preliminar de integração do Pré-Cambriano com os eventos tectônicos das bacias sedimentares brasileiras, *Bol. Ciência-Técnica-Petróleo, publ n. 15*, PETROBRÁS-CENPES-CINTEP, 70p.

Cox, K.G., 1988. The Karroo Province, in: *Continental Flood Basalts*, J.D. Macdougall (ed), Kluwer Academic Publishers, 239-271.

Deming, D. & Chapman, D.S., 1988a. Heat flow in the Utah-Wyoming thrust belt from analysis of bottom-hole temperature data measured in oil and gas wells, *J. Geophys. Res.*, 93, 13657-13672.

Deming, D. and Chapman, D.S., 1988b. Inversion of bottom-hole temperature data: The Pineview field, Utah-Wyoming thrust belt, *Geophysics, Vol. 53, No. 5*, 707-720.

Deming, D. and Chapman, D.S., 1989. Thermal histories and hydrocarbon generation: example from Utah-Wyoming thrust belt, *AAPG Bull., 73(12)*, 1455-1471.

Deming, D., Sass, J. H., Lachenbruch, A. H. and De Rito, R. F., 1992. Heat flow and subsurface temperature as evidence for basin-scale ground-water flow, North Slope of Alaska, *Geol. Soc. Amer. Bull., 104(5)*, 528-542.

Duchkov, A.D., 1991. Review of Siberian heat flow data, in: *Terrestrial Heat Flow and the Lithosphere Structure*, Cermak, V. and Rybach, L. (eds), Springer-Verlag, 426-443.

Erlank, A.J.(ed), 1984. Petrogenesis of the volcanic rocks of the Karroo province, *Geological Society of South Africa Spec. Publ. No. 13*, 395 pp.

Ernesto, M. & Pacca, I.G., 1988. Paleomagnetism of the Paraná basin flood volcanism, southern Brazil. In : *The Mesozoic flood volcanism of the Paraná basin: petrogenesis and geophysical aspects*, Piccirillo, E.M. and Melfi, A.J., Instituto Astronômico e Geofísico, University of São Paulo, Brazil, 229-255.

Ferreira, F.J.F., 1982. Intergração de dados aeromagnéticos e geológicos: configuração e evolução tectônica do arco de Ponta Grossa, M. Sc. thesis, University of São Paulo, Brazil, 169 pp.

Freed, R.L. & Peacor, D.R., 1989. Variability in temperature of the smectite/illite reaction in Gulf Coast sediments, *Clay Minerals, 24*, 171-180.

Frey, M., 1986. Very low-grade metamorphism of the alps - an introduction, *Schweiz. mineral. petrogr. Mitt., 66*, 13-27.

Frey, M., 1987. Very low-grade metamorphism of clastic sedimentary rocks, in: *Low temperature metamorphism*, M. Frey (ed), Backie, Chapman and Hall, New York, 9-58.

Furlong K.P. & Fountain, D.M., 1986. Continental-crustal underplating: thermal considerations and seismic-petrologic consequences, *J. Geophys. Res.,91(B8)*, 8285-8294.

Gable,R., 1979. Draft of a geothermal flux map of France, in: *Terrestrial Heat Flow in Europe*, Cermak V. and Rybach, L. (eds), Springer-Verlag, 179-185.

Giedskehang, A., Creer, K.M. & Mitchell, J.G., 1975. Paleomagnetism and K-Ar ages of the south-west African basalts and their bearing on the time of initial rifting of the South Atlantic Ocean. *Geophys. J. R. astr. Soc., 42*, 1-20.

Grand, S.P., 1987. Tomographic inversion for shear velocity beneath the North American plate, J. Geophys. Res., 92(B13), 14,065-14,090.

Gupta, M.L., 1982. Heat flow in the Indian Peninsula - its geological and geophysical implications, *Tectonophysics, 83*, 71-90.

Gupta, M.L. and Gaur, V.K., 1984. Surface heat flow and probable evolution of Deccan volcanism, *Tectonophysics, 105*, 309-318.

Gupta, M.L., Sharma, S.R. and Sundar, A., 1991. Heat flow pattern and lithospheric thickness of peninsular India, in: *Terrestrial Heat Flow and the Lithosphere Structure*, Cermak, V. and Rybach, L. (eds), Springer-Verlag, 283-292.

Gurnis, M., 1988. Large-scale mantle convection and the aggregation and dispersal of supercontinents, *Nature, 332*, 695-699.

Hamza, V.M and Eston, S.M., 1983. Assessment of geothermal resources of Brazil - 1981. *Zbl. Geol. Palaeont. Teil I, H. 1/2*,128-155.

Hamza, V.M., Eston, S.M., Araujo, R., Vitorello, I. and Ussami, N. ,1978. Coleção Brasileira de dados geotérmicos, *publ. IPT (Instituto de PesquisasTecnológicas do Estado de São Paulo) nº 1109*, 315 pp.

Harry, D.L. and Sawyer, D.S., 1992. Basaltic volcanism, mantle plumes, and the mechanics of rifting: the Paraná flood basalt province of South America, *Geology, 20*, 207-210.

Haxby, W.F., Turcotte, D.L. and Bird, J.M., 1976. Thermal and mechanical evolution of the Michigan Basin, *Tectonophysics, 36*, 57-75.

Henry, S.G. and Pollack, H.N., 1988. Terrestrial heat flow above the Andean Subduction Zone in Bolivia and Peru, *J. Geophys. Res., 93(B12)*, 15153-15162.

Hermanrud, C. Cao, S. and Lerche, I., 1990. Estimates of virgin rock temperature derived from BHT measurements: Bias and error, *Geophysics, 55(7)*, 924-931.

Herz,N., 1977. Timing of spreading in the South Atlantic: information from Brazilian alkalic rocks, *Geol. Soc. Am. Bull., 88*, 101- 112.

Howell, P.D. and van der Pluijm, B. A., 1990. Early history of the Michigan Basin: subsidence and Appalachian tectonics, *Geology, 18*, 1195-1198.

Hurter, S.J., 1987. Aplicação de geotermômetros químicos em águas de fontes brasileiras na determinação do fluxo geotérmico, MSc thesis, University of São Paulo, Brazil, 189 pp.

Hurter, S.J., 1988. The use of chemical geothermometry and heat loss models in estimating terrestrial heat flow for low-temperature hydrothermal systems, *Rev. Bras. Geof., 6(2)*, 33-42.

Hurter, S.J., Eston, S.M. and Hamza, V.M., 1983. Coleção brasileira de dados geotérmicos. Série 2 - fontes termais, *Publ. IPT (Instituto de Pesquisas Tecnológicas do Estado de São Paulo), nº 1233*, 111 pp.

Ingersoll, R. V., 1988. Tectonics of sedimentary basins, *Geol. Soc. Am. Bull., 100,* 1704-1719.

Jackson, M.L.,1975. Soil chemical analysis - advanced course, 2nd edition, published by the author, Madison , Wisconsin.

Jaeger, J.C., 1959. Application of the theory of heat conduction to geothermal measurements. In: *Terrestrial heat flow,* Lee (ed), 7-23.

Jones, M.Q.W., 1981. Heat flow and heat production studies in the Namaqua mobile belt and Kaapvaal craton, PhD. thesis, Univ. of the Witswatersrand, Johannesburg, 319 pp.

Jones, M.Q.W., 1987. Heat flow and heat production in the Namaqua mobile belt, South Africa, *J. Geophys. Res., 92,* 6273-6289.

Jordan, T.H., 1978. Composition and development of the continental tectosphere, *Nature, 274,* 544-548.

Jordan, T.H., 1981. Continents as a chemical boundary layer, *Phil. Trans. R. Soc. London, A301,* 359-373.

Jordan, T.H., 1988. Structure and formation of the continental tectosphere, *J. Petrol.,* Spec. Lithosphere Issue, 11-37.

Judge, A.S. and Beck, A.E.,1973. Analysis of heat flow data - several boreholes in a sedimentary basin, *Can. J. Earth Sci., 10,* 1424-1507.

Kaila, K.L., Rao, I.B.P., Koteswara Rao, P., Madhava Rao, N., Krishna, V.G. and Sridhar, A.R., 1989. DSS studies over Deccan Traps along the Thuadara-Sendhwa-Sindad profile, across Narmada-Son Lineament, India, in :*Properties and Processes of Earth's Lower Crust, AGU Geophysical Monograph 51, IUGG Vol. 6,* 127-141.

Kappelmeyer, O. & Haenel, R., *Geothermics with special reference to application,* Geoexploration Monographs, Series 1- No. 4, O. Rosenbach and C. Morelli (eds), Geopublication Associates, Gebrueder Borntraeger, 238p., 1974.

Kisch, H.J., 1983. Mineralogy and petrology of burial diagenesis (burial metamorphism) and incipient metamorphism in clastic rocks, in: *Diagenesis in sediments and sedimentary rocks,* 2, Developments in sedimentology 25B, G. Larsen and G.V. Chilinger (eds), Elsevier, 289-493.

Kish, H. J., 1987. Correlation between indicators of very low-grade metamorphism, in: *Low temperature metamorphism,* Frey, M. (ed), Chapman and Hall, New York, 227-300.

Lees, C.H., 1910. On the isotherms under mountain ranges in radioactive districts, *Proc. Roy. Soc., A, 83,* 339-346.

Lucas, J., Camez, Th. and Millot, G., 1959. Détermination pratique aux rayons X des minéraux argileux simples et interstratifiés, *Bull. Serv. Carte Geol. Als. Lorr., 12(2),* 21-31.

Lucazeau, F., Lesquer, A. and Vasseur, G., 1991. Trends of heat flow density from West Africa, in: *Terrestrial Heat Flow and the Lithosphere Structure,* Cermak, V. and Rybach, L. (eds), Springer-Verlag, 417-425.

Luheshi, M. N., 1983. Estimation of formation temperatures from boreholes measurements, *Geophys. J. Roy. Astr. Soc., 39,* 319-333.

Mahoney, J.J., 1988. Deccan Traps, in: *Continental Flood Basalts*, J.D. Macdougall (ed), Kluwer Academic Publishers, 151-194.

Majorowicz, J.A. and Jessop, A.M., 1981(a). Regional heat flow patterns in the Western Canadian sedimentary basin, *Tectonophysics, 74, 3/4*, 209-238.

Majorowicz, J.A. and Jessop, A.M., 1981(b). Present heat flow and a preliminary paleogeothermal history of the Central Prairies basin, Canada. *Geothermics, 10, 2*, 81-93.

Majorowicz, J.A., Jones, F.W. and Jessop, A.M., 1986. Geothermics of the Williston basin in Canada in relation to hydrodynamics and hydrocarbon occurrences, *Geophysics, 51, 3*, 767-779.

Majorowicz, J.A., Rahman, M. Jones, F.W. and McMillan, N.J., 1985. The paleogeothermal and present thermal regimes of the Alberta Basin and their significance for petroleum occurrences, *Canadian Petroleum Geology, 33, 1*, 12-21.

McCord, J., Reiter, M. and Phillips, F., 1992. Heat flow data suggest large ground-water fluxes through Fruitland coals of the northern San Juan basin, Colorado-New Mexico, *Geology, 20*, 419-422.

McKenzie, D., 1978. Some remarks on the development of sedimentary basins, *Earth Planet. Sci. Lett., 40*, 25-32.

McKenzie, D. and Bickle, M.J., 1988. The volume and composition of melt generated by extension of the lithosphere, *J. Petrol., 29, 3*, 625-679.

Meister, E.M., 1973. Gradientes geotérmicos nas bacias sedimentares brasileiras. *Bol. Tec. PETROBRÁS, 16, 4*, 221-232.

Melfi, A.J., Piccirillo, E.M. and Nardy, A.J.R., 1988. Geological and magmatic aspects of the Paraná Basin - an introduction. In : The Mesozoic flood volcanism of the Paraná basin: petrogenesis and geophysical aspects, Piccirillo, E.M. and Melfi, A.J., Instituto Astronômico e Geofísico, University of São Paulo, Brazil, 1-13.

Melfi, A.J., 1967. Potassium-argon ages for core samples of basaltic rocks from Southern Brazil. *Geochim. Cosmochim. Acta, 31*, 1079-1089.

Menke, W., *Geophysical data analysis: discrete inverse theory*. International Geophysics Series 45, revised ed, Academic Press, Inc., 285 pp., 1989.

Molina, E.C., Ussami, N. Sá, N.C. de and Blitzkow, D., 1989. Interpretação dos dados gravimétricos da parte norte da Bacia do Paraná, *Rev. Bras. Geoc., 19, 2*, 187-196.

Montes-Lauar, C.R., Comin-Chiaramonte, P., Ernesto, M., Pacca, I.G. and Piccirillo, E.M., 1987. Análise química e paleomagnética de detalhe de um derrame espesso: implicações vulcanológicas. VI Simpósio Regional de Geologia, abstracts 1, Rio Claro, Brazil.

Mullis, J., 1987. Fluid inclusion studies during very low-grade metamorphism, in: *Low temperature metamorphism*, M. Frey (ed), Chapman and Hall, New York, 162-199.

Nadeau, P.H. and Reynolds, R.C, Jr., Burial and contact metamorphism in the Mancos shale, *Clays & Clay Minerals, 29(4)*: 249-259, 1981.

Neves, B.B.B. and Cordani, U.G., 1991. Tectonic evolution of South America during the Late Proterozoic, *Precambrian Res., 53*, 23-40.

Nyblade, A.A., Pollack, H.N., Jones, D.L., Podmore, F. and Mushayandebvu. M., 1990. Terrestrial heat flow in east and southern Africa, *Jour. Geophys. Res.*, 95, 17,371-17,384.

Nyblade, A.A., 1992. Terrestrial heat flow in east and southern Africa and the thermal structure of Precambrian lithosphere, PhD thesis, The University of Michigan, Ann Arbor, 165 pp.

Oliveira, L.O.A., 1987. Aspectos da evolução termo-mecânica da Bacia do Paraná, MSc. Thesis, Universidade Federal de Ouro Preto, Escola de Minas, 179 pp.

Padilha, A.L., Trivedi, N.B., da Costa, J.M., Vitorello, I., Dupis, A. and Cavoit, C., 1989. Audio-magnetotelluric study in northeast region of Paraná basin, *Geophysics, 54(7)*, 824-831.

Padilha, A.L., Trivedi, N.B., Vitorello, I. and da Costa, J.M., 1992. Upper crustal structure of the northeast Paraná basin , Brazil, determined from integrated magnetotelluric and gravity measurements, *Jour. Geophys. Res., 97(B3)*, 3351-3365.

Peate, D.W., Hawkesworth, C.J., Mantovani, M.S.M. and Shukowsky, W., 1990. Mantle plumes and flood-basalt stratigraphy in the Paraná, South America, *Geology,18*, 1223-1226.

Pereira, R.V., 1969. Atlas climatológico do Brasil (reedição de mapas selecionados), Ministério da Agricultura (ECEPLAN), Escritório de Meteorologia, Rio de Janeiro.

Perry, E. and Hower, J., 1970. Burial diagenesis in Gulf Coast pelitic sediment, *Clays & Clay Minerals, 18*, 165-177.

Piccirillo, E.M. and Melfi, A.J., 1988. *The Mesozoic flood volcanism of the Paraná Basin: petrogenetic and geophysical aspects*, Instituto Astronômico e Geofísico, University of São Paulo, Brazil, 600 pp.

Piccirillo, E.M., Comin-Chiaramonte, P., Melfi, A.J., Stolfa, D. Bellieni, G., Marques, L.S., Giaretta, A., Nardy, A.J.R., Pinese, J.P.P., Raposo, M.I.B. and Roisenberg, A., 1988. Petrochemistry of continental flood basalt-rhyolite suites and related intrusives from the Paraná Basin, Brazil, In : *The Mesozoic flood volcanism of the Paraná basin: petrogenesis and geophysical aspects*, Piccirillo, E.M. and Melfi, A.J., Instituto Astronômico e Geofísico, University of São Paulo, Brazil, 105-156.

Pollack, H. N., 1986. Cratonization and thermal evolution of the mantle, *Earth Planet. Sci. Lett., 80*, 175-182.

Pomerol, Ch., Debelmas, J., Mirouse, R., Rat, P. and Rousset, C., 1980. *Geology of France with twelve itineraries*, Masson, Paris.

Powell, W. G., Chapman, D.S., Balling, N. and Beck, A. E., 1989. Continental Heat-Flow Density, in *Handbook of Terrestrial Heat-Flow Density Determination*, Haenel, R., Rybach, L. & Stegena, L. (eds), Kluwer Academic Publishers, 167-222.

Pytte, A.M. and Reynolds, R.C., The thermal transformation of smectite to illite. In: *Thermal history of sedimentary basins, methods and case histories*, Naeser, N.D. & Mc Culloh, T.H. (eds), Springer Verlag : 133-140, 1989.

Rabinowitz, P.D. and LaBreque, J., 1979. The Mesozoic South Atlantic Ocean and evolution of its continental margins, *J. geophys. Res., 84(B11)*, 5973-6002.

Ramos, A. N. and Formoso, L., 1975. Argilominerais das rochas sedimentares da Bacia do Paraná, *Ciência-Técnica-Petróleo, PATROBRÁS, 9*, 46pp.

Rao, G.V., Rao, R.U.M.and Narain, H., 1979. Geothermal regime of Gondwana basins of Peninsular India, In: Laskar, B., Raja Rao, C.S. (eds) 4-th Int. Gondwana Symp., Hindustan Publ. Corp., Delhi, pp II, 850-857.

Rebouças, A. C., 1976. Recursos hídricos subterrâneos da Bacia do Paraná, Thesis (Livre Docência), University of São Paulo, 143 pp.

Rocha Campos, A.C., Cordani, U.G., Kawashita, K., Sonoki, H.M. and Sonoki, I.K., Age of the Paraná flood volcanism. In : *The Mesozoic flood volcanism of the Paraná basin: petrogenesis and geophysical aspects*, Piccirillo, E.M. and Melfi, A.J., Instituto Astronômico e Geofísico, University of São Paulo, Brazil, 25-45, 1988.

Rybach, L., 1989. Determination of heat production rate, in: *Handbook of Terrestrial Heat-Flow Density Determination*, Haenel, R., Rybach, L. & Stegena, L. (eds), Kluwer Academic Publishers, 125-142.

Santos, J. , 1986. Densidade de fluxo térmico na Bacia do Paraná - Estado de São Paulo, MSc. thesis, University of São Paulo, Brazil, 101 pp.

Setzer, J., 1966. Atlas climático e ecológico do Estado de São Paulo. Comissão Interestadual da Bacia do Paraná-Uruguai e CESP.

Shen, P.Y. and Beck, A.E., 1986. Stabilization of bottom hole temperature with finite circulation time and fluid flow, *Geophys. J. Roy. Astr. Soc., 86*, 63-90.

Sleep, N.H. and Snell, N.S., 1976.Thermal contraction and flexure of mid-continent and Atlantic marginal basins, *Geophys. J. Roy. Astr. Soc., 45*,125-154.

Smart, G. and Clayton, T., 1985. The progressive illitization of interstratified illite-smectite from Carboniferous sediments of northern England and its relationship to organic maturity indicators, *Clay Minerals, 20*, 455-466.

Smith, L. and Chapman, D.S., 1983. On the thermal effects of groundwater flow, 1. Regional scale systems, *J. Geophys. Res., 88(B1)*, 593-608.

Speece, M.A., Bowen, T.D. Folcik, J.L. and Pollack, H.N., 1985. Analysis of temperatures in sedimentary basins: the Michigan Basin. *Geophysics, 50(8)*, 1318-1334.

Srodon, J., 1980. Precise identification of illite/smectite interstratifications by x-ray powder diffraction, *Clays & Clay Minerals, 28(6)*, 401-411.

Stanley, W.D., Saad, A. R. and Ohofugi, W., 1985. Regional magnetotelluric surveys in hydrocarbon exploration, Paraná basin, Brazil, *AAPG Bull., 69(3)*, 346-360.

Tóth, J., 1962. A theory of groundwater motion in small drainige basins in Central Alberta, Canada, *J. Geophys. Res., 67(11)*, 4375-4387.

Turcotte, D.L. and Schubert, G., 1982. *Geodynamics, applications of continuum physics to geological problems*, John Wiley & Sons, 450 pp.

Uyeda, S. and Watanabe, T., 1970. Preliminary report of terrestrial heat flow study in the South American continent: distribution of geothermal gradients. *Tectonophysics, 10*, 234-242.

Vitorello, I., 1978. Heat flow and radiogenic heat production in Brazil, with implications for thermal evolution of continents. PhD dissertation, 145 pp., Univ. of Mich., Ann Arbor, USA.

Vitorello, I. and Pollack, H.N., 1980. On the variation with age of continental heat flow and the thermal evolution of continents. *Jour. Geophys. Res., 85*, 983-996.

Vitorello, I., Hamza, V.M. and Pollack, H.N., 1978. Terrestrial heat flow in the Brazilian Highlands. *Jour. Geophys. Res., 85, B7*, 3778-3788.

Vitorello, I. Hamza, V.M., Pollack, H.N. and Araujo, R.C.L., 1980. Geothermal investigations in Brazil. *Rev. Bras. Geoc., 8*, 71-89.

Von Herzen, R. P. and Uyeda, S., 1963. Heat flow through the Eastern Pacific Floor, *Jour. Geophys. Res., 68, 14*, 4234-4240.

White, R. S., 1989. Volcanism and igneous underplating in sedimentary basins and at rifted continental margins, in Origin and evolution of sedimentary basins and their energy and mineral resources, Price, R.A. (ed), *AGU Geophysical monograph 48, IUGG volume 3*, 125-127.

White, R.S. and McKenzie, D., 1989 a. Volcanism at rifts, Scientific American, July 1989, 62-71.

White, R.S. and McKenzie, D., 1989 b. Magmatism at rift zones: the generation of volcanic continental margins and flood basalts, *Jour. Geophys. Res.*,94, B6, 7685-7730.

Willett,S. D. & Chapman, D.S., 1987. On the use of thermal data to resolve and delineate hydrologic flow systems in sedimentary basins: an example from the Uinta Basin, Utah, in: *Proceedings, Third Canadian/American Conference on Hydrogeology of Sedimentary Basins : Applications to Exploration and Exploitation*, Hitchon, B., Bachu, S. & Seuveplane, C. (eds), Dublin, Ohio, 159-168.

Willett, S.D. and Chapman, D.S., 1989. Temperatures, fluid flow and heat transfer mechanisms in the Uinta Basin, in: *Hydrogeological regimes and their subsurface thermal effects*, Beck, A.E., Garven, G. and Stegena, L. (eds), *AGU Geophysical Monograph 47, IUGG Series vol 2*, 29-33.

Yoder, H.S. Jr., 1976. *Generation of basaltic magma*, National Academy of Sciences, 265 pp.

Zalán, P.V., Conceição, J.C., Wolff, S., Astolfi, M.A., Vieira, I.S., , Appi, V.T., Neto, E.V.S., Cerqueira, J.R. , Zanotto, O.A., Paumer, M.L. & Marques, A., 1986. Análise da Bacia do Paraná, Internal Report of PETROBRÁS/DEPEX/CENPES/1035-5765, Rio de Janeiro, 5 volumes.

Zalán, P.V., Wolff, S., Astolfi, M.A., Vieira, I.S., Conceição, J.C., Appi, V.T., Neto, E.V.S., Cerqueira, J.R. and Marques, A., 1991. The Paraná Basin, Brazil, in: *Interior cratonic basins*, Leighton, M.W., Kolata, D.R., Olts, D.F., Eidel, J.J. (eds), *AAPG Memoir 51*, 681-708.

Zolotukhin, V.V. and Al'mukhamedov, A.I., 1988. Traps of the Siberian Platform, in: *Continental Flood Basalts*, J.D. Macdougall (ed), Kluwer Academic Publishers, 273-310.